Improving Understanding of Lithium–Oxygen Batteries Using Atomistic Simulations

by

Emily Crabb

B.S. Physics and B.S.E. Computer Engineering, University of Pittsburgh (2016)

Submitted to the Department of Physics in Partial Fulfillment of the Requirements for the Degree
of
Doctor of Philosophy
at the
Massachusetts Institute of Technology
May 2022

Signature of Author _____

Department of Physics
May 6, 2022

Certified by _____

Jeffrey C. Grossman
Professor of Materials Science and Engineering
Thesis Supervisor

Certified by _____

Leonid S. Levitov
Professor of Physics
Thesis Co-Supervisor

Accepted by _____

Deepto Chakrabarty
Professor of Physics
Associate Department Head of Physics

Improving Understanding of Lithium–Oxygen Batteries Using Atomistic Simulations

by

Emily Crabb

Submitted to the Department of Physics on May 6, 2022 in Partial Fulfillment of the Requirements for the Degree of Doctor of Philosophy in Physics

Abstract

Developing novel battery technologies is required to electrify hard to decarbonize industries. One such novel technology, lithium–oxygen batteries, has great potential for electric aviation but is hampered by our lack of detailed knowledge of the processes occurring inside the batteries. Thus, the projects in this thesis work to further our fundamental understanding of these battery systems using atomistic simulations.

In the first project, I explored one simulation methodology, *ab initio* molecular dynamics, commonly used to model battery systems. I examined the coordination environment of lithium ions in different solvents and compared the computational results to experimental data. The result was that the computationally calculated properties were heavily dependent on the starting configuration of the system, which illustrates the importance of both equilibration method and sufficient independent sampling for extracting experimentally relevant quantities from *ab initio* molecular dynamics simulations. Such details are often poorly documented or not justified in the literature, so this work indicates a need for increased attention to these details to ensure *ab initio* molecular dynamics studies are reproducible and physically accurate and thus useful.

In the second project, I utilized classical molecular dynamics to explore a wider range of properties for systems of lithium salts in twelve different solvents. This work combined a dedication to accuracy, as I compared the results from the computations to experimental data, with innovative ways of measuring ionic transport. I examined how solvent metrics combining different properties such as solvent donor number and viscosity that are relatively easy to measure experimentally correlate with the atomistic lithium transport mechanisms that are quite difficult to measure experimentally but readily accessible computationally, with the goal of eventually enabling the prediction of these transport mechanisms and thus a deeper understanding of the system on an atomistic scale from a few simple experiments. To my knowledge, this is the first time such solvent metrics have been examined with relation to ionic transport mechanisms in small molecule liquid solvent systems.

Thesis Supervisor: Jeffrey C. Grossman
Title: Professor of Materials Science and Engineering

Thesis Co-Supervisor: Leonid S. Levitov
Title: Professor of Physics

Acknowledgements

Contents

List of Figures

List of Tables

1 Introduction

There is increasing demand for "green" energy technologies in both power generation and transportation.[1–3] However, these technologies rely heavily on the ability to store large quantities of energy for significant lengths of time. Renewable energy sources like solar, wind, and hydropower are intermittent, so energy storage is critical for them to be viable replacements for coal and natural gas. Electric vehicles must be able to transport enough energy to power themselves for hundreds of miles, while electric planes would need ranges of well over a thousand miles to fully decarbonize aviation. This has resulted in a huge increase in the demand for batteries[3] and in the amount of research focused on improving battery technology.[4,5] This battery research encompasses everything from developing new electrolytes for lithium-ion batteries[6] to exploring novel battery technologies like lithium– or sodium–air batteries,[7–9] and as computers become more powerful[10] and computational methods become more sophisticated,[11,12] computational techniques have become an important part of battery research.

Computational battery research is diverse in both methods and goals, from using Monte Carlo simulations to predict battery lifetimes[13] to using machine learning to determine cathode properties.[14] However, there is a unified goal in much of this work: to enable the faster and cheaper design of better batteries. High throughput studies can be significantly easier, cheaper, and faster to perform computationally than experimentally, enabling, for example, the screening of billions of candidate molecules for solar heat batteries.[15] Simulations can also probe the dynamics of processes that can be difficult or expensive to directly observe experimentally, such as solid electrolyte interphase formation (the growth of passivation layers on the electrodes of a battery due to decomposition of the electrolyte).[16]

One long-term and ongoing area of focus has been to better understand physical processes occurring inside batteries, ranging from the mechanisms governing solid electrolyte interphase formation to how ions are transported through the bulk electrolyte, on an atomistic level using molecular dynamics simulations.[17–23] As mentioned above, these processes can be hard to directly observe experimentally, but they also be important for understanding battery performance. For example, the growth of a solid electrolyte interphase on the anode of a battery prevents further electrolyte decomposition but can also cause the battery capacity to fade, so investigating the mechanics of solid electrolyte interphase formation via atomistic simulations is key to furthering our understanding of battery degradation.[16] For ionic transport, examining the transport mechanisms is again difficult experimentally but possible computationally, and improving our knowledge of transport mechanisms can allow the design of novel electrolytes with targeted properties such as low viscosity and high ionic diffusivity.[24]

Prior to the mid-2000s, most simulations aimed at capturing dynamical properties such as diffusion and viscosity were performed using classical molecular dynamics (MD), and this remains the primary method used to compute such properties that require relatively large systems and long timescales.[19,23,25] However, thanks to great advances in both algorithmic efficiency and computational power over the past several decades, simulating battery materials on the atomistic level using *ab initio* molecular dynamics (AIMD) with forces from density functional theory (DFT – a quantum mechanical method to calculate the electronic structure of many-body systems such as atoms, molecules, liquids, and solids) calculations has become more common.[17,18,20–22,26–28] AIMD has some limitations compared to classical MD, primarily simulation length and system size. However, it also has significant advantages when simulating atomistic behavior, as AIMD calculates the behavior using quantum mechanical methods rather

10

than empirical force fields as in classical MD and is thus more transferable and better suited to capture reactions and describe properties such as partial charges and charge transfer.[18,21] Due to these advantages, AIMD has gained popularity in battery research, especially for examining properties that may depend on charge transfer such as lithium-ion solvation in different electrolytes, which is important because the solvation environment of lithium ions influences how lithium is transported in the system.[17,18,21] However, most AIMD studies in the literature rely on the assumption that even small, short simulations can obtain physically accurate results.

1.1 Overview

The work in this thesis examines how lithium ions are transported in different small molecule liquid solvents using both classical MD and AIMD. Lithium transport is an important process to understand, as it is closely tied to ionic conductivity and thus battery properties such as the charging and discharging rates. Enabling fast charging is especially important for applications such as electric cars and airplanes, as the user does not want to wait hours for the battery to recharge.[29] Therefore, better understanding what factors govern lithium transport can enable us to design higher performing batteries. The atomistic transport mechanisms are difficult to directly examine experimentally but can be extracted from simulations, making this problem an ideal candidate for computational study.

My research in this thesis includes two projects with different goals. The first, detailed in the *Ab Initio* Molecular Dynamics Methodology Study section, is primarily a methodology study. I examine how equilibration and sampling methodology affect the results of AIMD simulations by investigating how lithium ions are coordinated with solvent molecules and counter anions in several common lithium–air battery systems, and I show the importance of both equilibration

method and sufficient independent sampling for extracting experimentally relevant quantities from AIMD simulations, which have often been neglected in the literature. The second, detailed in the Lithium Transport Mechanisms section, focuses on using classical MD simulations to obtain physical insights to guide battery design. I develop solvent metrics by combining different properties that can be measured experimentally and investigate how these metrics relate to atomistic scale lithium transport mechanisms in a variety of small molecule liquid solvents, and the results suggest novel methods for predicting transport properties and designing new solvents.

I will now give some background information on batteries and the different molecular dynamics methods and some motivation as to why my research is relevant and important.

1.2 Batteries

The fundamental concept of a battery is a device that stores chemical energy and then provides power by converting that chemical energy to electrical energy. Batteries are critical to many different aspects of our society, with applications ranging from pacemakers to personal electronics such as phones and laptops to "green" transportation in the form of electric cars, buses, and planes. This last category is especially interesting, as electric transportation is critical to decarbonization. There has been immense progress in the past decade on improving electric cars, with innovations in battery technology and battery manufacturing resulting in the median range of an electric vehicle for sale in the United States jumping from 68 miles in 2011 to 259 miles in 2020 and similar improvements in other markets.[30,31] However, incremental improvement is not sufficient for electric aviation, as electrifying even a typical regional airplane, designed to travel ~500 miles and hold 30–75 passengers, would require batteries with specific energies (energy per unit mass) several times higher than those of current commercial

lithium-ion batteries.[32,33] I will return to electric transportation in the discussion of lithium-ion and lithium–oxygen batteries in the following sections.

1.2.1 Lithium-Ion Batteries

Lithium-ion batteries are one of the dominant commercial battery technologies today, used in most portable consumer electronic devices and most electric vehicles.[34] A schematic of a typical lithium-ion battery during the discharge cycle is shown in Figure 1. During discharge, lithium ions carry current from the carbon (commonly graphite) anode through the electrolyte to the lithium-metal oxide cathode. During charging, an external current is applied to the battery, forcing the lithium ions to travel from the cathode through the electrolyte to the anode, where intercalation (lithium ions being reversibly inserted into the porous anode material) occurs. Graphite is the dominant commercial anode material and has been for decades because it is cheap, electrically conductive, and allows for lithium intercalation with only modest volume expansion.[35,36] Limiting volume expansion is especially important because large changes in the anode volume during intercalation can cause the solid electrolyte interphase to crack during each cycle and thus cause further electrolyte degradation, passivation, and capacity fade to occur.[37]

Li-Ion battery during discharge
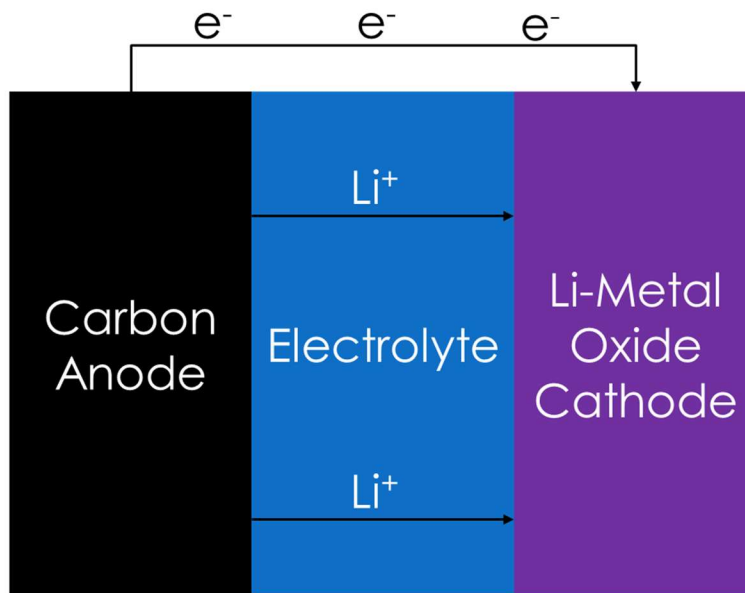
Figure 1: Schematic of lithium-ion battery during discharge.

Lithium-ion batteries have become dominant for several reasons. They have high specific energies compared to older battery technologies such as lead–acid batteries, with high-quality commercial batteries reaching specific energies of ~0.9 MJ/kg for lithium-ion batteries versus ~0.2 MJ/kg for lead–acid batteries.[38–40] Lithium-ion batteries also have high coulombic efficiencies (the ratio of the total charge extracted from the battery to the total charge put into the battery), with efficiencies that can exceed 99% in ideal charging conditions compared to efficiencies of ~90% for lead–acid batteries;[41] can withstand more cycles at high temperatures than lead–acid batteries;[42] and have the potential for many of their components to be recyclable, though this is not always cost-efficient industrially.[34]

One major area of continuing research and development for lithium-ion batteries is on developing and improving the electrolyte through which the lithium ions travel.[43–45] The

electrolyte consists primarily of solvent molecules, plus lithium ions, counter anions, and any additives or contaminants. Commercial lithium-ion batteries most commonly utilize a small molecule liquid solvent such as ethylene carbonate.[44] However, the choice of solvent can have a huge impact. Most obviously, the solvent affects the dynamic lithium transport processes occurring during the charging and discharging stages, thus affecting properties such as the battery charging and discharging rates that would be critical to electric aviation, as batteries would need to recharge quickly while a plane is being unloaded and reloaded. Additionally, different solvents have different rates of thermal decomposition, and this decomposition can lead to gas generation which both degrades the battery performance, thus reducing the battery lifetime, and can result in safety concerns, as the gases generated may be flammable, which would be of obvious concern in airplanes.[44,46] Different solvents may also have different optimum operating temperatures, making them better or less suited for different applications. Finally, there are more direct commercial considerations such as the cost of the solvents, though this may be of less importance for aviation with its generally high equipment and operating costs than for an application such as large battery storage power plant. As such, there is much research geared at finding new solvents or combinations of solvents that could be used for various applications and understanding what specific properties of solvents are most critical for their performance in lithium-ion batteries.[43,45,47,48] While my research is primarily focused on lithium–air applications, the second project on lithium transport mechanisms in different solvents is also relevant to lithium-ion applications as many of the same solvents are used in the two types of batteries.

Despite their widespread usage and continuing research, there are fundamental limitations to lithium-ion batteries that are relevant for potential applications such as electric aviation. The

most fundamental limitation is the specific energy. While lithium-ion batteries may have a specific energy several times higher than older technologies such as lead–acid batteries, it is still insufficient for most electric aviation applications. In the past few years, there have been many news articles about companies developing electric aircraft,[49–51] but the technologies fall into a few categories: (1) using lithium-ion batteries to transport ~10–20 passengers up to around 500 miles,[52–54] (2) using lithium-ion batteries in hybrid planes that electrify only some aspects of the flight such as electric takeoff and landing,[55,56] and (3) using novel technologies still being developed (such as hydrogen fuel cells or batteries with chemistries other than lithium-ion) to power larger planes for longer distances.[57–59] Furthermore, in a recent study, Bills et al. estimated that the minimum specific energy threshold for a commercially viable electric regional airplane designed to hold 30–75 passengers would be ~1.8 MJ/kg, though this would only achieve around a quarter of the current average range for such aircraft.[32] This is about twice as high as the specific energies of the best commercial lithium-ion batteries available today,[33] and it is also higher than the theoretical maximum specific energy of ~1.6 MJ/kg for a lithium-ion battery.[60] Furthermore, in a similar study, Schäfer et al. estimated that traveling 2,000 km without stopping to recharge would require a specific energy of at least ~6 MJ/kg,[33] and intercontinental flights between the US and Europe are over 5,000 km. To give a point of comparison, the specific energy for jet fuel is 43 MJ/kg.[61] With the growing focus on the importance of aviation in decarbonization efforts,[62,63] the limitations of lithium-ion batteries have led to a resurgence of interest in other battery technologies, as evidenced by the companies investigating novel technologies such as hydrogen fuel cells[57–59] and beyond lithium-ion battery technologies such as lithium–sulfur[64] and lithium–air batteries.[65]

1.2.2 Lithium–Oxygen Batteries

One such technology that has emerged as a promising possibility for electric aviation is lithium–oxygen batteries. The promise lies in the specific energy, with experimentally realized batteries achieving specific energies on the order of what is required for short-range electric aircraft and a theoretical maximum comparable to jet fuel.[33,40,66] A schematic of a lithium–oxygen battery during the discharge cycle is shown in Figure 2. During discharge, lithium ions are released from the lithium-metal anode through oxidation. They carry current as they pass through the electrolyte to the porous cathode and then react with oxygen that has entered the electrolyte through the porous cathode, ultimately forming a lithium oxide discharge product on the cathode surface. During charging, the lithium oxides are decomposed into oxygen which diffuses back through the cathode and out of the battery and lithium ions which travel through the electrolyte to be deposited at the anode.[66] The porous cathode is often carbon-based.[66]

The reason for the high specific energy of lithium–oxygen batteries relates to how the energy is stored in lithium–oxygen battery compared to in lithium-ion batteries. While a lithium–oxygen battery is in a charged state but before discharge occurs, its energy is stored in the form of bonds in the lithium-metal anode. This contrasts with energy being stored via intercalation of lithium ions into the anode in lithium-ion batteries.[67] The anode in a lithium-ion battery has a maximum ratio of lithium to anode material with the specific ratio depending on the composition of the anode, while there is no such limit for the lithium-metal anode in a lithium–oxygen battery. This enables a higher specific energy.

One important note is that lithium–oxygen strictly refers to using pure oxygen as the gas input for the battery. Lithium–oxygen batteries are commonly used in laboratory settings, as using pure oxygen as the gas input is controlled and reproducible. However, most real-world

17

applications would instead require lithium–air batteries, with ambient air used as the input gas. This could lead to other side reactions, as water, carbon dioxide, and nitrogen could enter the battery in addition to the oxygen.[68] For example, it has been shown that even water content of 500 parts per million in the electrolyte can have a signficant effect on the morphology of the lithium oxide discharge on the cathode in a lithium–oxygen battery.[69] This reduced control over the battery chemistry is one complication in studying and designing lithium–air batteries.

Li-O_2 battery during discharge
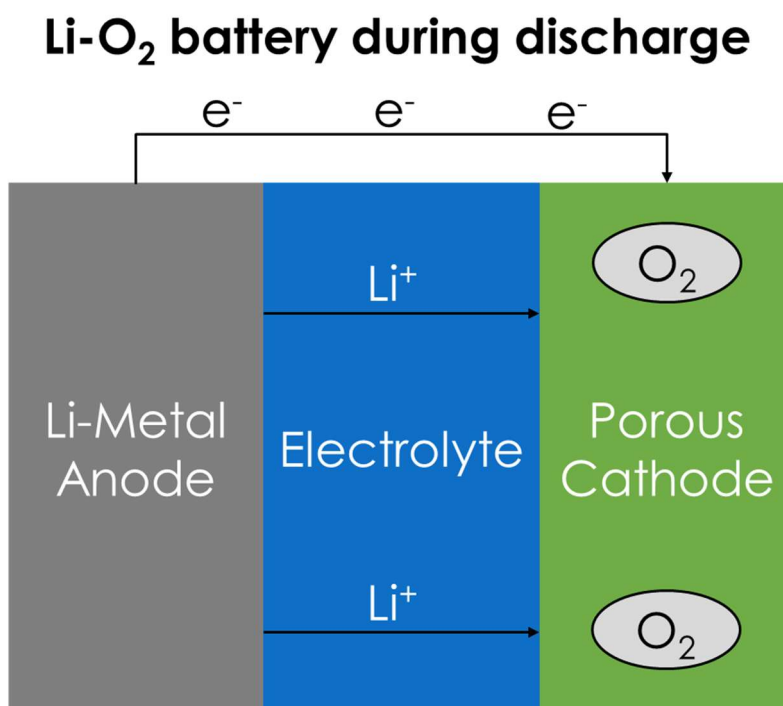
Figure 2: Schematic of lithium–oxygen battery during discharge.

As with lithium-ion batteries, the choice of solvent plays a large role in the behavior of lithium–oxygen batteries. My research focuses on non-aqueous, small molecule liquid solvents, which are widely used in lithium–oxygen battery studies,[9,69,70] though there are several other classes of

electrolytes including aqueous, polymer, and ceramic. The overarching goals of my research are to improve the simulation techniques for modeling how lithium ions are transported in different candidate solvents and then use physically relevant quantities extracted from these simulations to enable better battery design. In pursuit of these goals, I have focused on bulk electrolyte systems without electrodes or external electric fields. These systems are much more accessible computationally, not requiring nearly as large of systems as would be needed to accurately model electrodes, while also still giving valuable insights into ionic transport mechanisms.

Despite the promise of lithium–oxygen or lithium–air batteries, they are not used commercially today for several reasons. Solvents are a particular area of interest for the reasons discussed above in the lithium-ion battery section, mainly that many of the key battery properties such as performance, lifetime, safety, and cost are greatly affected by the choice of solvent. For example, many early lithium–air batteries used aqueous solvents, but parasitic reactions between the lithium metal and the water could create hydrogen gas and lithium hydroxide.[66] This was a safety concern, so much recent research instead utilizes non-aqueous solvents. Another combined safety, lifetime, and performance concern is the growth of dendrites from the lithium-metal anode, which can eventually cause the battery to short circuit.[68] Thus, there is research to find solvents that can suppress dendrite growth.[71] The work in this thesis will focus on how the choice of solvent affects transport properties, as transport properties such as ionic conductivity are one key measure of battery performance.[72–74]

1.3 Molecular Dynamics

At its most fundamental, molecular dynamics is a method to simulate the movement of particles over time. The simulated particles can be atoms or pseudo-atoms. Pseudo-atoms are used to

approximate groups of atoms and are used in coarse-grained molecular dynamics; an example would be using one simulation particle to represent an entire molecule or even group of molecules rather than an individual atom. This technique enables larger simulations but sacrifices accuracy and atomistic-level detail. The work in this thesis solely used all-atom molecular dynamics simulations, as the research probes atomistic properties and phenomena.

The dynamics part of molecular dynamics refers to modeling the interactions between the different particles in the system by numerically solving Newton's equations of motion. The fundamental concept relies on only freshman-level physics equations: $\vec{a} = \vec{F}/m$ and $\vec{F} = -\nabla U$. Given initial positions and velocities for the particles, various well-established computational techniques can be used to integrate to find velocities and positions at a later time once the forces are known.[75] Thus, the primary question in molecular dynamics simulations is how to obtain the forces or, equivalently, the potential energies. The method of obtaining the forces defines the different types of molecular dynamics, and two such types will now be discussed: classical molecular dynamics and *ab initio* molecular dynamics.

1.3.1 Classical Molecular Dynamics

The key concept of classical molecular dynamics is using force fields to describe particle interactions. A force field is a collection of functional forms and parameters used to calculate the potential energy of the system. An example is modeling a bond in a molecule as a spring with a spring constant and equilibrium length. As a result, classical molecular dynamics has many fixed quantities. Molecules are explicitly defined, with fixed bonds and fixed charges on each atom in the molecule. Parameters such as atomic charges and bond lengths and angles may come directly from experimental data, from more accurate but more expensive computational methods such as

density functional theory calculations, or from iterative optimization for desired properties such as density or viscosity. The functional forms, such as modeling bonds as springs, can come directly from physical insights or from trial-and-error. One important note is that traditional force fields such as AMBER, CHARMM, and GROMOS do not allow bonds to break or form.[76–78] There are newer reactive force fields, perhaps the most well-known being ReaxFF, that allow bond breaking and formation,[79] but the work in this thesis uses traditional force fields that have fixed bonds and charges, as these force fields are parametrized for the solvent and salt molecules used in the study.

Classical molecular dynamics simulations have many strengths. Simulations of thousands of small molecules for tens of nanoseconds take only a few days to run on one or two nodes of a cluster or supercomputer, and larger systems and longer runtimes are accessible with more time and computing power. One of the most widely used classical molecular dynamics codes, LAMMPS, scales very efficiently with system size using parallelization.[80] While simulating thousands of molecules for tens of nanoseconds may not compare to the scale of experimental studies, these simulations are large and long enough to extract many physically relevant quantities, ranging from the equilibrium density of a liquid solvent to the ion transport mechanisms in a polymer electrolyte. In this thesis, I calculate different dynamic properties such as viscosities, densities, and diffusion coefficients for classical molecular dynamics simulations of liquid systems. Since my simulations explicitly model all atoms, I can also extract atomic scale properties such as the coordination environment of a lithium ion in a given solvent.

However, classical molecular dynamics also has limitations. One was previously mentioned: that bonds and atomic charges are typically fixed. Thus, traditional classical molecular dynamics simulations cannot model chemical reactions or processes that rely heavily on charge transfer.

Another major limitation is the force fields. Force fields need to be parametrized for each molecule being simulated, and parametrizing a force field can be a time-consuming task. Additionally, a force field that is well parametrized for one application may be poorly parametrized for another, even for the same molecule, and it is thus important to validate results from classical molecular dynamics with experimental data or more accurate but more expensive computational methods. To illustrate this, I will briefly discuss the two force fields used in this thesis: PCFF+ and OPLS.

PCFF+ is an extension of PCFF (Polymer Consistent Force Field), parametrized for additional molecules. Many of the PCFF parameters are derived from more accurate and more computationally intensive computational methods, while others are derived by fitting to molecular crystal data.[81,82] However, past work has shown PCFF is generally ill-suited for molecular dynamics simulations at finite temperatures, often finding the densities of systems to be too low compared to experimental data.[82] Additionally, the original focus for the parametrization was largely polymeric systems, rather than small molecule liquid systems.[81] As such, PCFF+ is used in this thesis only as a comparison point to test a hypothesis that the initial classical molecular dynamics equilibration method used for *ab initio* molecular dynamics simulations does not affect the final results. More details will be given in the *Ab Initio* Molecular Dynamics Methodology Study section.

OPLS (Optimized Potentials for Liquid Simulations), in contrast, is widely used for simulations of small molecule liquid systems, and there continues to be research into parametrizing new molecules and improving old parametrizations.[83–86] Many OPLS parameters are derived from more accurate and more computationally intensive computational methods, and there has been an emphasis on testing the accuracy of OPLS parameters by comparing properties such as densities

for simulations of liquid systems of pure organic solvents to experimental data.[87] I have continued this emphasis on validation with experimental data but expanded it to new properties and beyond systems of pure organic solvents by comparing densities, viscosities, and ionic conductivities for simulations of solvent–lithium salt systems to experimental data. More details about this validation and the further physical insights obtained from the classical molecular dynamics simulating using the OPLS force field will be discussed in the Lithium Transport Mechanisms section.

1.3.2 *Ab Initio* Molecular Dynamics

Unlike classical molecular dynamics, *ab initio* molecular dynamics does not rely on parametrized force fields to calculate forces. Instead, *ab initio* molecular dynamics uses electronic structure calculations based on quantum mechanics. There are several variations, but the *ab initio* molecular dynamics technique used in this thesis utilizes a density functional theory (DFT) calculation at every time step to calculate the forces. DFT is a theoretically exact method that relies on theorems developed by Hohenberg and Kohn.[88–90] These theorems state that the ground-state properties of any interacting many-particle system are uniquely determined by the electron density as a function of position, and further work has extended this to excited states.[91] However, only in very simple problems would the electron density everywhere in space be known. In order to make DFT useful for chemistry and physics applications, Kohn and Sham developed an approximation. Instead of dealing with the complicated many-body problem of interacting electrons, the system of interacting electrons is treated as a system of noninteracting electrons in an effective potential.[91] Different variants of DFT use different approximations for the effective potential, and the trade-off between accuracy and computational resources for these approximations remains one of the major limitations of DFT.

However, DFT and, by extension, *ab initio* molecular dynamics remain far less parametrized than classical molecular dynamics. There is no need to explicitly define bonds and molecules, which allows *ab initio* molecular dynamics to model chemical reactions and processes involving charge transfer.[92,93] Only one set of parameters is used per atomic species for DFT calculations, in contrast to having possibly two or three different sets of parameters for just carbon in one molecule in classical molecular dynamics. With infinite computing time and power, it is theoretically possible to more accurately model any process accessible with classical molecular dynamics using *ab initio* molecular dynamics. In reality, many properties accessible with classical molecular dynamics are not accessible with *ab initio* molecular dynamics due to limitations on system size and length. DFT calculations are simply much more computationally intensive than the parametrized force field calculations used in classical molecular dynamics, and one such calculation is required per time step. As a result, *ab initio* molecular dynamics is typically limited to simulating hundreds of atoms for tens of picoseconds. Thus, many of the dynamic properties such as viscosities and diffusion coefficients that can be extracted from classical molecular dynamics simulations are not accessible with *ab initio* molecular dynamics. *Ab initio* molecular dynamics studies thus focus on properties such as the coordination environment of lithium ions which are believed to equilibrate quickly. In this thesis, I evaluate the validity of the assumption that *ab initio* molecular dynamics is well suited to study such properties by examining how much effect initial system configurations have on the results of *ab initio* molecular dynamics simulations. This work will be discussed in the *Ab Initio* Molecular Dynamics Methodology Study section.

2 *Ab Initio* Molecular Dynamics Methodology Study

This section is adapted from Crabb et al. (2020)[94] and reprinted with permission from *J. Chem. Theory Comput.* 2020, 16, 12, 7255–7266. Copyright 2020 American Chemical Society.

In this study, I show that equilibration methodology and sampling affect the behavior of *ab initio* molecular dynamics (AIMD) simulations of systems of common solvents and salts found in lithium–oxygen batteries. I compare two equilibration methods: (1) using an AIMD temperature ramp and (2) using a classical MD simulation followed by a short AIMD simulation both at the target simulation temperature of 300 K. I also compare two different classical all-atom force fields: PCFF+ and OPLS. By comparing the simulated association/dissociation behavior of lithium salts in different solvents with the experimental behavior, I find that equilibration with the classical force field that produces more physically accurate behavior in the classical MD simulations, namely OPLS, also results in more physically accurate behavior in the AIMD runs compared to equilibration with PCFF+ or with the AIMD temperature ramp. Equilibration with OPLS outperforms even the pure AIMD equilibration because the classical MD equilibration is much longer than the AIMD equilibration (nanosecond vs. picosecond timescales). These longer classical simulations allow the systems to find a more physically accurate initial configuration, and in the short simulation times available for the AIMD production runs, the initial configuration has a large impact on the system behavior. I also demonstrate the importance of averaging coordination number over multiple starting configurations and Li^+ ions, as the majority of Li^+ ions do not undergo a single association or dissociation event even in a ~40 ps long simulation and thus do not sample a statistically significant portion of the phase space. These results show the importance of both equilibration method and sufficient independent sampling for extracting experimentally relevant quantities from AIMD simulations.

2.1 Introduction

In recent years, increased motivation for high-capacity electrochemical energy storage has led to the use of molecular dynamics (MD) simulations to better understand physicochemical processes that occur inside batteries such as cation solvation[17–19,21–23] and solid electrolyte interphase formation[95,96] on the molecular level. Both classical MD with empirically derived forces and *ab initio* molecular dynamics (AIMD) with forces from density functional theory (DFT) calculations have been employed,[17,18,21,22,26–28,95] with AIMD limited to much smaller timescales (tens of picoseconds for AIMD[21,22] vs. tens to hundreds of nanoseconds for classical MD[19,23]) and system sizes (hundreds of atoms for AIMD[21,22,27] vs. thousands of atoms for classical MD[19,23]). Despite these limitations, AIMD has gained popularity in battery research because of its advantages, including transferability between systems and ability to accurately describe properties such as polarization and charge transfer,[18,21] which are especially important for examining properties such as lithium-ion solvation in different electrolytes.[17,18,21] Classical force fields, on the other hand, are typically parametrized so that specific properties of a given system will match values from experiments or *ab initio* theories such as DFT,[19,82] which can result in limited transferability as well as challenges in accurately modeling polarization, charge transfer effects, and chemical reactions.

Most AIMD studies document many simulation parameters such as time step, simulation length, and temperature,[18,21] in some cases justifying the choice of a specific temperature[21] or energy cutoff.[20] However, I have found that there is less discussion and evaluation of how systems are equilibrated and sampled for AIMD simulations. Typically, the first few picoseconds of a production AIMD simulation are treated as equilibration and discarded from the data collection.[17,18,21,22,26–28,95] Sometimes this is preceded by a classical MD simulation.[17,20,26,28]

When a classical MD simulation is used, there is often minimal evaluation of or justification for the choice of force field. The implicit assumption for many AIMD solvation studies is thus that a 30–50 ps AIMD simulation is long enough that the initial configuration and equilibration method are of minimal importance. Also, many papers use only one or two initial configurations.[20,21,26,27] This methodology of executing only one or two production runs relies on the assumption that the system can sample a significant portion of phase space in the tens of picoseconds of simulation time of an AIMD simulation.

However, recent studies on cation coordination in aqueous solutions have questioned the validity of these assumptions.[97–100] In an AIMD study of highly concentrated LiCl aqueous solutions, the length of the simulation (30 ps) was directly compared to the timescale of the exchange of water from the Li^+-ion coordination shell, which is typically on the order of 30–100 ps;[101,102] the authors therefore deemed the mechanism too slow to observe full reorganization of water in the Li^+ coordination shells in their simulation.[97] As a result, the coordination environments in the study were found to be biased by the classical MD method used for equilibration.[97] However, because the timescale of the Li^+–Cl^- interaction was only ~4.5 ps, chloride exchange was observed in the Li^+ coordination shells, and the study could draw conclusions about the Li^+ coordination environment.[97]

Unfortunately, most AIMD studies do not include such a detailed discussion of the timescales of the ion pairing and solvent reorganization processes present in the systems being examined and how these timescales influence the possible effects of the equilibration methodology. Thus, to evaluate these assumptions for the specific case of lithium dynamics in different environments, I examined two different types of equilibration techniques: (1) an AIMD temperature ramp method with no classical equilibration and (2) classical MD followed by a short AIMD

equilibration step at the target temperature. For the classical MD method, I also compared two classical force fields: PCFF+ and OPLS. To evaluate the effect of the equilibration methods, I examined the lithium solvation environment in several systems with different solvents and lithium salts that are commonly used in lithium–oxygen batteries[8,9,103,104] and compared them to recent experimental work from Leverick et al.[9]

2.2 Methodology

2.2.1 Systems

Each simulation system consisted of 50 solvent molecules and 3 lithium-salt molecules. The solvents were acetonitrile (MeCN), dimethyl sulfoxide (DMSO), and 1,2-dimethoxyethane (DME). The salts were lithium bis(trifluoromethanesulfonyl)imide (LiTFSI), lithium trifluoromethanesulfonate (LiTfO), and lithium trifluoroacetate (LiTFA). These solvents and salts were selected due to their extensive use in lithium–oxygen battery research,[8,9,103,104] allowing for direct comparison with experimental results. The ratio of 3 salt molecules to 50 solvent molecules corresponds to molarities ranging from 0.5 M to 1.1 M for the systems simulated, which is similar to the range of molarities investigated for such systems in the literature.[9,103,104] The initial amorphous configurations were generated using MedeA® (when either pure AIMD or the PCFF+ force field was used for equilibration) or fftool and packmol (when the OPLS force field was used for equilibration),[105–108] and the results for three simulations with different random starting configurations were averaged for each solvent–salt combination. The molecular structure for each solvent and salt molecule is shown in Figure 3.
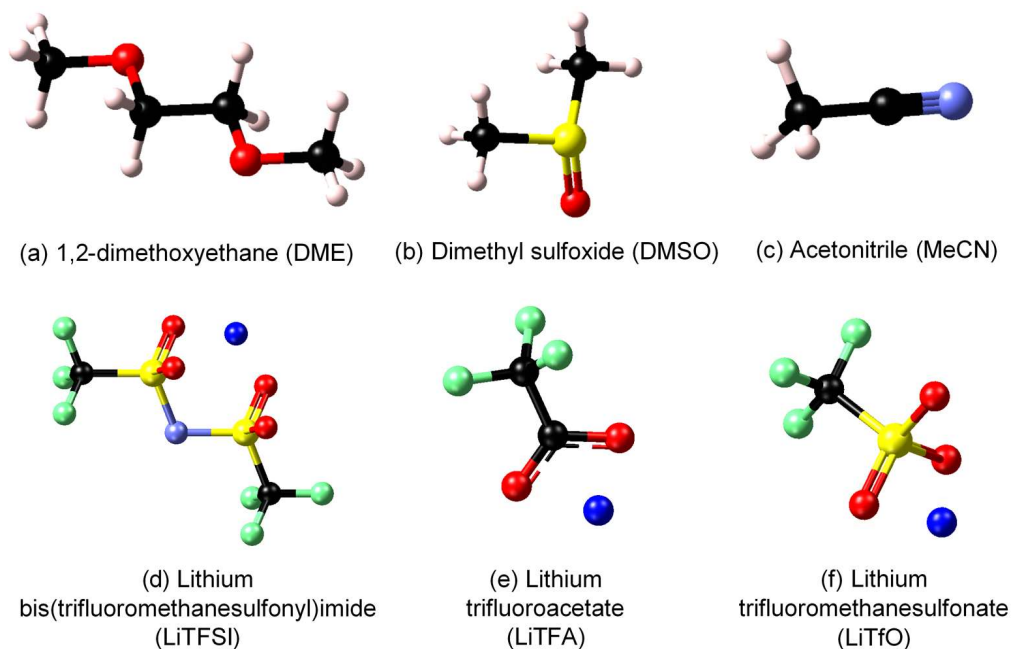
Figure 3: The solvent (a–c) and salt (d–f) molecules used in the simulations. The atomic color code: carbon – black, fluorine – green, hydrogen – white, lithium – blue, nitrogen – purple, oxygen – red, sulfur – yellow

The density of each system was extrapolated from the experimentally known densities of the solvents and salts.[109] Both experiments by my collaborators measuring the density as a function of molarity and data in the literature support the accuracy of this methodology.[110] Densities were calculated this way rather than by performing simulations in the isothermal–isobaric (*NpT*) ensemble for each system because of the prohibitive expense of performing *NpT* simulations with AIMD. Although it would have been possible to use classical simulations in the *NpT* ensemble to find equilibrium densities with each classical force field investigated, this would have impaired a direct comparison between the purely AIMD equilibration and the classical MD equilibration methods. The extrapolated density $\rho_{mixture}$ was calculated using

$$\rho_{mixture} = \frac{V_{salt} * \rho_{salt} + V_{solvent} * \rho_{solvent}}{V_{salt} + V_{solvent}}$$

where ρ_{salt} and $\rho_{solvent}$ are the experimentally known densities of the salt and solvent and V_{salt} and $V_{solvent}$ are the volumes of salt and solvent in the system, given by

$$V_x = \frac{(Molecular\ weight\ of\ x) * (Number\ of\ moles\ of\ x\ in\ system)}{Density\ of\ x}$$

where x represents either the salt or solvent. The same procedure has been used to find "experimental" mass densities for a classical MD study in Molinari et al.[109]

To assess the validity of this approximation, the extrapolated densities were compared to both the equilibrium densities obtained with classical NpT calculations and the experimentally measured densities. For all but one system, the equilibrium densities obtained with classical NpT calculations were within 5% of the extrapolated densities and the experimentally measured densities, as will be discussed in Tables 6 and 7. For further validation, I also performed classical NVT simulations for the solvent–LiTFSI systems and AIMD simulations for the MeCN–LiTFSI system with the density increased or decreased by 10% with respect to the extrapolated value and observed no appreciable change in association/dissociation behavior. More details are included in the Density Study section of the Results and Discussion, but I can conclude that any deviations of the extrapolated densities from the true densities of the systems are unlikely to have an effect on the overall association/dissociation behavior of the systems.

The experimental methodology is included in the Appendix.

2.2.2 *Ab Initio* Molecular Dynamics Methods

Two different AIMD simulation methods for these explicit solvent simulations were investigated in this study: "pure" AIMD and classical MD equilibration + AIMD. All AIMD simulations were performed using the Vienna Ab initio Simulation Package (VASP) with the projector

augmented wave (PAW) method.[111–116] All AIMD simulations used the Perdew–Burke–Ernzerhof (PBE) functional with the zero damping DFT-D3 correction method,[117–119] Γ-point Brillouin zone sampling, a planewave energy cutoff of 400 eV, an energy convergence criterion of 10^{-5} eV, and a time step of 1 fs. I also tested the effect of removing the DFT-D3 correction for two solvent–salt systems and found no significant impact on the overall association/dissociation behavior (as discussed in the Results and Discussion section). All equilibration was performed in the canonical (*NVT*) ensemble using a Nosé–Hoover thermostat with a Nosé frequency of ~834 cm^{-1} corresponding to a period of 40 fs, while all production runs were performed in the microcanonical (*NVE*) ensemble. For the simulations using the MeCN and DMSO solvents, each production run was at least 11 ps with the first picosecond excluded from the final data to allow for further equilibration due to the transition between the *NVT* and *NVE* ensembles. For the DME solvent simulations, each production run was at least 6 ps with the first picosecond excluded from the final data. Because DME is a larger molecule than MeCN or DMSO, the total number of electrons in the DME systems is significantly larger, and thus I could not run for as long a simulation time as for the MeCN and DMSO systems. Though these simulation times are short compared to some AIMD studies that use 25–50 ps simulations,[18,20–22,26] important dynamical information can still be obtained,[17,27,28] and I will show later that the properties considered in this study did not vary significantly even when selected systems were simulated for ~40 ps. Much more important was using multiple independent initial configurations, as will also be discussed in the Results and Discussion section.

2.2.2.1 Pure Ab Initio *Molecular Dynamics Equilibration Method*

For the "pure" AIMD equilibration method, all the equilibration was performed using an AIMD temperature ramp in the *NVT* ensemble, with the temperature of the system initially set at 600 K,

then lowered to 450 K, until finally reaching 300 K. The system was simulated at each of the temperatures for 3 ps, with a separate 0.5 ps simulation used to transition between each pair of temperatures. Thus, the total AIMD *NVT* equilibration simulation time was 10 ps. The high temperatures were used to accelerate relaxation processes, and this temperature ramp method has been used in previous AIMD studies examining the solvation of different cations in water.[120,121] However, care had to be taken in this study because in some cases 600 K and even 450 K are above the boiling points for the solvents and the decomposition temperatures of the salts. Due to the short lengths of the equilibration simulations, this typically was not important. However, I observed an unphysical decomposition of one of the salt counter anions (typically in the form of a dissociation of one or more O or F atoms from the anion) due to the high temperatures in a few of the simulations; these simulations were discarded and replaced with new randomly generated configurations.

2.2.2.2 Classical Molecular Dynamics Equilibration Method

All classical MD simulations were performed with the LAMMPS code.[122] For the classical MD equilibration method, the first equilibration step was a minimization step using conjugate gradients followed by a short 100 ps classical MD simulation within the *NVT* ensemble with a time step of 0.5 fs and the temperature set to 300 K. The cutoff distance for Lennard-Jones and the real-space part of the Coulomb interactions was 9.5 Å, with a simple cutoff used beyond this distance, and tail corrections were applied to the $1/r^6$ term in the potentials. Then, a longer classical MD simulation within the *NVT* ensemble was executed for 100 ns, still with a time step of 0.5 fs and at 300 K. The cutoff distance for Lennard-Jones and the real-space part of the Coulomb interactions was also unchanged at 9.5 Å, and tail corrections were still applied to the $1/r^6$ term in the potentials, but long-range Coulomb interactions were calculated using the

particle–particle–particle–mesh (PPPM) solver with an accuracy of 10^{-5} instead of using a simple cutoff. This longer simulation is the one used for the classical MD analysis in Table 8 in the Results section. After the classical MD simulation, further equilibration was performed by executing a 3 ps AIMD *NVT* simulation at 300 K before executing the AIMD production runs in the *NVE* ensemble, as is common in previous work.[17,18,21,22,26–28,95,123]

2.2.2.3 Classical Force Fields

Using classical MD as an equilibration method for AIMD is a standard practice in the literature,[17,20,26,28] usually with the implicit assumption that details such as the classical force field used will not have a significant impact on the *ab initio* dynamics because an AIMD simulation of 10–50 ps is long enough to obtain a fairly representative sampling of low energy configurations. In order to investigate this, I selected two very different classical force fields for comparison with each other and with the pure AIMD: PCFF+ (an extension of PCFF, Polymer Consistent Force Field) and OPLS (Optimized Potentials for Liquid Simulations).[83,107,108,124–131] The versions of each used in this study are all-atom force fields, but they are otherwise significantly different.

PCFF+ is a force field largely based on the CFF91 force field intended for use with both polymers and organic materials.[82] However, I predicted that PCFF+ would perform poorly for the types of systems in this study (organic electrolytes and lithium salts), as the PCFF/PCFF+ force field was not parametrized for electrolytes.[82] In general, PCFF/PCFF+ does not appear to be extensively used for simulating the types of systems used in this study, namely small lithium-salt molecules in liquid electrolytes. In contrast, OPLS is widely used for modeling the solvents and salts in this study,[84–86,131] and there has been continuing work to improve availability and accuracy of the parameters.[83,108,124–131] As such, I anticipated the classical MD simulations with

33

the OPLS force field would more accurately match experiments than those with the PCFF+ force field would. This difference in accuracy between the two classical force fields helps to gauge the importance of equilibration in AIMD.

2.2.2.4 Classical Molecular Dynamics NpT *Calculations*

To aid in the comparison of the PCFF+ and OPLS classical force fields, *NpT* simulations were also performed on both large pure solvent systems (300 solvent molecules) and production run sized solvent–salt systems (50 solvent molecules and 3 salt molecules). These *NpT* simulations were 5 ns long with a time step of 0.5 fs after a short 100 ps *NVT* equilibration run. Other settings were the same as for the other LAMMPS *NVT* simulations.

2.2.3 Coordination Number Calculations

To compare the different AIMD equilibration methods, I focused on the Li^+-ion solvation environment. Specifically, I calculated the coordination numbers between Li and either N (for MeCN) or O (for DMSO and DME) in the solvent molecules and between Li and O in the salt counter anions. In a few cases, association was observed between Li^+ ions and N in the $TFSI^-$ counter anions, in which case this coordination number was also calculated.

The Li–N and Li–O coordination numbers are defined as the number of N or O atoms within the first solvation shell of the Li^+ ion. The total Li coordination of each system is simply the sum of the Li–N and/or Li–O coordination numbers from the possible Li–solvent and Li–salt interactions (e.g., for the MeCN–LiTFSI system, there can be Li–N coordination with the N in both the MeCN and the $TFSI^-$ counter anions and Li–O coordination with the O in the $TFSI^-$ counter anions; the total Li coordination is the sum of these three contributions). The coordination number was calculated using the radial distribution function (RDF), denoted in

equations by $g(r)$.[132,133] The RDF is the probability of finding another atom of a specific type α in a shell at a distance r and with thickness dr from a reference atom, which in this study is a Li$^+$ ion. In terms of the local density $\rho_\alpha(r)$ of atoms of type α, the partial RDF for species α is given by

$$g_\alpha(r) = \frac{dn_\alpha(r)}{4\pi \, dr \, \rho_\alpha(r)}$$

The coordination number n_α for the first solvation sphere is then defined as the integral of the RDF up to its first minimum r_{min}

$$n_\alpha(r_{min}) = \int_0^{r_{min}} 4\pi r^2 g_\alpha(r) \rho_\alpha(r) dr$$

In practice, the exact location of the first minimum of the RDF could be ill-defined as it was averaged over different time steps and over the three Li$^+$ ions in the simulation. As such, I averaged the RDF values into bins 0.1 Å thick (dr), fitted the RDF for the first solvation shell to a Gaussian function, extracted the mean and standard deviation of the fit, and defined the coordination number as the numerical integral of the RDF at three standard deviations above the mean. The reported data was then averaged over the three simulations performed for each system. The Li–O RDF plots in MeCN–LiTFSI for two different simulations are shown in Figure 4.

In the majority of cases, a Gaussian function was a good fit for the RDF for the solvation shell, and this procedure provided a consistent, unambiguous definition of coordination number (see Figure 4a–b). However, in a few cases (particularly for some of the classical MD simulations using PCFF+), the first solvation shell and therefore the coordination number was ill-defined because multiple Li$^+$ ions and counter anions clustered into one large structure (see Figure 4c–d).
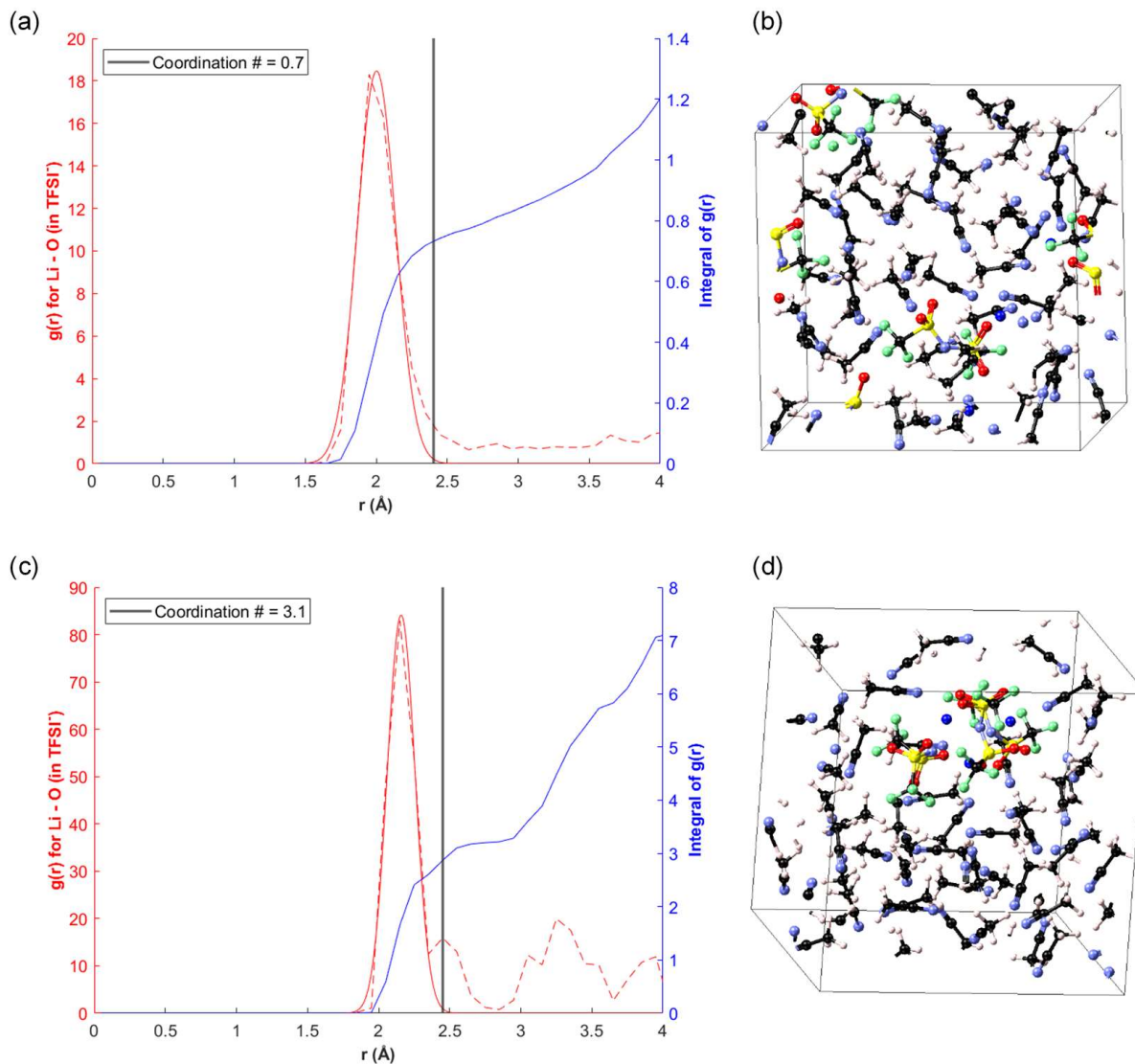
Figure 4: The RDF functions for Li–O (a, c) and system snapshots (b, d) for simulations of MeCN–LiTFSI systems. (a–b) an AIMD simulation using pure AIMD equilibration; (c–d) a classical MD simulation with the PCFF+ force field. The dashed red lines in (a) and (c) are the RDF data with bin widths of 0.1 Å, while the solid lines are the fitted Gaussian function. The grey vertical lines on the RDF plots in (a) and (c) indicate three standard deviations above the mean for the Gaussian function. The integral of the RDF function at this point is defined as the coordination number. In the classical MD simulation, all the Li$^+$ ions and TFSI$^-$ counter anions were in one large cluster as seen in (d). As such, the first solvation shell and coordination number are ill-defined. In contrast, there is one clear peak in the RDF of the AIMD simulation in (a), as there was no large cluster formation in the simulation as seen in (b).

I also provide experimental coordination number data from a recent study by Leverick et al. for comparison.[9] However, note that these experimental coordination numbers are obtained from deconvoluted Raman spectra rather than direct distance measurements as in my study. Due to the different calculation methods, I expect well-equilibrated AIMD simulations to reproduce the general association/dissociation trends from the experimental work but not necessarily the exact coordination values.

2.3 Results and Discussion

The first two subsections on the results of the effect of density and the DFT-D3 correction on the simulation results support the validity of my simulation procedures. The remaining subsections are on the comparison of classical force fields and of *ab initio* molecular dynamics methodologies and illustrate the importance of equilibration method and sampling.

2.3.1 Density Study

2.3.1.1 Comparison of Extrapolated and Experimental Densities

The extrapolated and experimentally measured densities for the six solvent–salt systems studied are shown in Table 1. For all systems, the magnitude of the difference between the extrapolated and experimental densities was under 7%, and the average difference was 2.6%. This motivated my simulations at 10% above and below the extrapolated densities (described in the following section) to test the effect of the exact densities used in the simulations.

Salt	Solvent	Measured Experimental Densities in g/mL	Extrapolated Densities in g/mL	Percent Error of Extrapolated vs. Experimental
LiTFSI	MeCN	0.95	0.89	−6.2%
	DMSO	1.18	1.14	−4.0%
	DME	0.96	0.92	−4.4%
LiTFA	MeCN	0.85	0.86	+0.6%
	DMSO	1.14	1.14	+0.0%
LiTfO	MeCN	0.89	0.88	−0.4%
Average Magnitude of Difference				2.6%

Table 1: Comparison of measured experimental densities and extrapolated densities for different solvent–salt systems with a ratio of 3 salt molecules to 50 solvent molecules.

2.3.1.2 Effect of Density on Solvent–Salt Association/Dissociation Behavior

To verify that my extrapolated densities are sufficiently accurate to reproduce the physical association/dissociation behavior in the solvent–salt systems studied, I performed classical MD simulations with the OPLS force field for the solvent–LiTFSI systems with densities 10% above and below the extrapolated densities. The results are shown in Table 2. When the density was increased or decreased by 10%, I observed no difference in association/dissociation behavior, and the numerical coordination numbers differed by at most 0.1. I can thus conclude that any deviations of my extrapolated density from the true experimental density of the systems are unlikely to have an effect on the association/dissociation behavior of the systems.

Salt	Solvent	Density in g/mL [a]	Li–N (MeCN) / Li–O (DME and DMSO) in Solvent	Li–O in Salt	Total Li Coordination [b]	Li-Salt Associated or Dissociated?
LiTFSI	MeCN	0.80	4.4	0.4	4.8	D
		0.89	4.5	0.4	4.9	D
		0.98	4.6	0.4	5.0	D
	DMSO	1.02	5.1	0.1	5.2	D
		1.14	5.2	0.1	5.2	D
		1.25	5.4	0.0	5.4	D
	DME	0.83	4.1	0.7	4.9	A
		0.92	4.2	0.6	4.9	A
		1.01	4.0	0.8	4.8	A

Table 2: Effect of density on coordination of Li^+ ions with N and O atoms in solvents and salts for classical MD *NVT* simulations using OPLS with 50 solvent and 3 LiTFSI salt molecules. (a) Densities 10% above and below the extrapolated density were used, and no change in association/dissociation behavior was observed. (b) Total coordination numbers were calculated separately and therefore may not exactly equal the sum of the Li–solvent and Li–salt coordination numbers due to rounding.

I then performed one additional test for the MeCN–LiTFSI system by performing one AIMD simulation at the densities 10% above and below the extrapolated density. The coordination number results and the comparison to the coordination numbers for the extrapolated density are shown in Table 3. Again, the overall association/dissociation behavior was unchanged for the system, and the numerical coordination numbers found were within the variation of the three runs performed at the extrapolated density. This further supports my assertion that a density difference between simulation and experiment is not the reason for any difference in the coordination behavior.

Salt	Solvent	Density in g/mL [a]	Li–N (MeCN) in Solvent	Li–O in TFSI	Total Li Coordination	Li-Salt Associated or Dissociated?
		0.80	3.6	0.3	3.9	D
LiTFSI	MeCN	0.89 [b]	3.9	0.1 [c]	4.0	D
		0.98	4.0	0.0	4.0	D

Table 3: Effect of density on coordination of Li^+ ions with N and O atoms in the MeCN–LiTFSI systems for AIMD *NVE* simulations using OPLS equilibration with 50 MeCN and 3 LiTFSI salt molecules. (a) Densities 10% above and below the extrapolated density were used, and no change in association/dissociation behavior was observed. (b) The coordination numbers for the extrapolated density of 0.89 g/mL are averaged over three runs, while the data for the other two densities are from only one run. (c) The Li–O coordination numbers for the three runs at the extrapolated density were 0.0, 0.0, and 0.3, so the coordination numbers observed for the lower and higher density systems are within the variation of the systems at the extrapolated density.

2.3.2 Effect of DFT-D3 Correction

To evaluate whether the zero damping DFT-D3 correction method used in the AIMD simulations had an appreciable effect on the simulation dynamics and thus the calculated coordination numbers, I performed two AIMD simulations without the D3 correction using the pure AIMD temperature ramp equilibration method. I selected the MeCN–LiTFSI and DMSO–LiTFA systems for the test because the association/dissociation behavior for the pure AIMD simulations for these systems did not match experimental behavior, as will be seen in Tables 9 and 10. The results of the DFT-D3 study are shown below in Table 4. In both systems, the overall association/dissociation behavior was the same for the simulations with and without the D3 correction (although coordination between one Li^+ ion and F in TFA was observed in the DMSO–LiTFA simulation without the D3 correction and was not observed in any of the simulations with the D3 correction or in experiments[9]). The exact effect of the D3 correction on

dynamic behavior merits further study, but there is no evidence from my test cases that the D3

correction is responsible for the different association/dissociation behavior observed in

simulations and experiments.

Salt	Solvent	D3 Correction?	Li–N (MeCN) / Li–O (DMSO) in Solvent	Li–O in Salt	Li–F in Salt	Total Li Coordination [a]	Li-Salt Associated or Dissociated?
LiTFSI	MeCN	Yes [b]	3.2	0.7	0.0	3.8	A
		No [c]	3.3	0.7	0.0	3.9	A
LiTFA	DMSO	Yes [b]	3.0	0.8	0.0	3.8	A
		No [c]	2.9	0.7	0.3 [d]	3.9	A

Table 4: Effect of DFT-D3 correction on coordination of Li$^+$ ions with N and O atoms in solvents and salts for AIMD *NVE* simulations equilibrated with an AIMD temperature ramp with 50 solvent and 3 salt molecules. (a) Total coordination numbers were calculated separately and therefore may not exactly equal the sum of the Li–solvent and Li–salt coordination numbers due to rounding. (b) The data for the D3 corrections corresponds to the data in Tables 9 and 10 and is thus the average over three 10 ps simulations for each system. (c) The data without D3 corrections is from one 10 ps production run for the MeCN–LiTFSI system and one 5 ps production run for the DMSO–LiTFA system. (d) In both systems, I saw no significant change is overall association/dissociation behavior when the D3 correction was removed, although I did observe Li–F coordination in the DMSO–LiTFA system without the D3 corrections, which was not observed in any of the simulations with the D3 correction or in experiments.[9]

2.3.3 Comparison of Classical Force Fields

In order to evaluate the dependence of the AIMD results on the method used for equilibration, it

was first necessary to compare different classical force fields. As discussed above, I selected

PCFF+ which was expected to be inaccurate for modeling the solvent–salt systems because it

was not parametrized for such systems[82] and OPLS which was expected to more accurately

model the systems as there has been continuing work to improve its parameterization for similar

electrolyte–salt systems and it is generally more prevalent in the literature.[84–86,131] The comparison of these force fields included *NpT* and *NVT* simulations.

2.3.3.1 Classical Molecular Dynamics NpT Simulations

The results for the classical MD *NpT* simulations for the pure solvent and the solvent–salt systems are given in Tables 5–7. As was hypothesized, simulations using OPLS better reproduced the experimental densities on average than simulations using PCFF+. However, unexpectedly OPLS did not perform better than PCFF+ for every system. For example, the equilibrium density for the pure MeCN system found using OPLS was ~5% smaller than the experimental value, whereas the density found using PCFF+ was only ~1% larger than the experimental one (as seen in Table 5).

Solvent	Experimental Density in g/mL	Density in g/mL and Percent Error vs. Experiment			
		PCFF+		OPLS	
MeCN	0.786	0.796	+1.3%	0.749	–4.7%
DMSO	1.100	1.040	–5.5%	1.097	–0.3%
DME	0.868	0.832	–4.1%	0.864	–0.5%
Average Magnitude of Error		**3.6%**		**1.8%**	

Table 5: Equilibrium solvent densities for MeCN, DMSO, and DME calculated from classical MD *NpT* simulations of 300 solvent molecules using LAMMPS compared with experimentally known densities.

Salt	Solvent	Extrapolated Densities in g/mL	Measured Experimental Densities in g/mL	PCFF+		
				Density in g/mL	Percent Error vs. Extrapolated	Percent Error vs. Measured
LiTFSI	MeCN	0.89	0.95	0.99	+10.7%	+3.9%
	DMSO	1.14	1.18	1.16	+2.1%	–2.0%
	DME	0.92	0.96	0.93	+1.1%	–3.3%
LiTFA	MeCN	0.86	0.85	0.88	+2.8%	+3.4%
	DMSO	1.14	1.14	1.09	–4.0%	–4.0%
LiTfO	MeCN	0.88	0.89	0.90	+2.0%	+1.7%
Average Magnitude of Error					3.8%	3.0%

Table 6: Equilibrium densities for different solvent–salt systems from classical MD *NpT* simulations of 50 solvent molecules and 3 salt molecules with the PCFF+ force field compared with the extrapolated and experimental densities.

Salt	Solvent	Extrapolated Densities in g/mL	Measured Experimental Densities in g/mL	OPLS		
				Density in g/mL	Percent Error vs. Extrapolated	Percent Error vs. Measured
LiTFSI	MeCN	0.89	0.95	0.90	+0.7%	–5.6%
	DMSO	1.14	1.18	1.19	+4.8%	+0.6%
	DME	0.92	0.96	0.96	+4.4%	–0.2%
LiTFA	MeCN	0.86	0.85	0.83	–3.1%	–2.4%
	DMSO	1.14	1.14	1.15	+1.3%	+1.3%
LiTfO	MeCN	0.88	0.89	0.86	–2.5%	–2.9%
Average Magnitude of Error					2.8%	2.1%

Table 7: Equilibrium densities for different solvent–salt systems from classical MD *NpT* simulations of 50 solvent molecules and 3 salt molecules with the OPLS force field compared with the extrapolated and experimental densities.

2.3.3.2 Classical Molecular Dynamics NVT *Simulations*

The coordination number results for the classical MD *NVT* simulations for the solvent–salt

systems are given in Table 8. Experimental values from Leverick et al. are provided for

comparison.[9] The final column of Table 8 indicates association or dissociation, with association

defined as an average coordination number between the Li^+ ion and N or O in the salt counter

anion of ≥ 0.5. The PCFF+ force field resulted in the correct association behavior in only one of

the six systems investigated (only MeCN–LiTFA), while the OPLS force field resulted in the

correct behavior in four of the six cases (all except DME–LiTFSI and DMSO–LiTFA). The

OPLS force field was marginal in one of the two cases where the simulation behavior did not

match experiment with a coordination number of 0.6 for Li–O in TFSI in the DME–LiTFSI

system when experiments showed dissociation. In all but one of the cases where simulation

behavior did not match the experimental behavior for either force fields (the exception being the

PCFF+ force field with the MeCN–LiTfO system), the Li^+ ions in the simulations were on

average associated with a salt counter anion, while they were on average dissociated in the

experiments. This suggests that both the PCFF+ and OPLS force fields have too strong an

interaction between the Li^+ ions and counter anions in some systems. However, neither force

field always results in association between the Li^+ ions and counter anions for every system, so

this problem must be related to the parametrization of individual molecules.

Salt	Solvent	Method / Force Field	Li–N (MeCN) / Li–O (DME and DMSO) in Solvent	Li–O in Salt	Li–N in Salt (TFSI only)	Total Li Coordination [a]	Li-Salt Associated or Dissociated? [b]
LiTFSI	MeCN	**Experiment** [c]	**4.3**	**0.3**	**0.0** [d]	**4.6**	**D**
		PCFF+	1.2	2.7	1.9	5.8	A
		OPLS	4.5	0.4	0.0	4.9	D
	DMSO	**Experiment** [c]	**4.3**	**0.0**	**0.0** [d]	**4.3**	**D**
		PCFF+	3.6	1.9	1.1	6.6	A
		OPLS	5.2	0.1	0.0	5.2	D
	DME	**Experiment** [c]	**4.4**	**0.2**	**0.0** [d]	**4.6**	**D**
		PCFF+	1.1	2.9	1.9	5.9	A
		OPLS	4.2	0.6	0.0	4.9	A
LiTFA	MeCN	**Experiment** [c]	**1.2**	**1.5**		**2.7**	**A**
		PCFF+	2.4	3.1		5.4	A
		OPLS	1.8	3.0		4.8	A
	DMSO	**Experiment** [c]	**4.2**	**0.1**		**4.3**	**D**
		PCFF+	2.8	2.1		4.9	A
		OPLS	4.1	1.3		5.4	A
LiTfO	MeCN	**Experiment** [c]	**1.7**	**1.9**		**3.6**	**A**
		PCFF+	5.6	0.2		5.8	D
		OPLS	2.8	2.7		5.4	A

Table 8: Coordination numbers for Li^+ ion with N and O atoms in solvents and salts for classical MD *NVT* simulations with 50 solvent and 3 salt molecules averaged over three simulations for each system. (a) Total coordination numbers were calculated separately and therefore may not exactly equal the sum of the Li–solvent and Li–salt coordination numbers due to rounding. (b) The final column indicates association or dissociation, with association defined as an average coordination number for the Li^+ ion and N or O in the salt counter anion of ≥ 0.5. (c) Experimental values from Leverick et al. are provided for comparison.[9] (d) Coordination between Li and N in TFSI was not reported in the experimental work as it was never observed.

Taken as a whole, the classical MD results indicate that the OPLS force field better reproduces

experimentally known properties such as density and coordination number than the PCFF+ force

field does. This provided a good opportunity to test the dependence of AIMD results on the choice of classical force field used for equilibration.

2.3.4 Comparison of *Ab Initio* Molecular Dynamics Methodologies

The coordination number results for the AIMD simulations with different equilibration methods are shown in Tables 9–11. Of the six systems investigated, the AIMD with the PCFF+ classical equilibration reproduced the same association/dissociation behavior as the experimental results in only one of the six cases (only MeCN–LiTFA). The AIMD with the OPLS classical equilibration reproduced the same behavior as experiments in four of the six cases (all except DME–LiTFSI and DMSO–LiTFA). The AIMD with purely AIMD initialization reproduced the same association/dissociation behavior as the experimental results in three of the six cases (matching for DMSO–LiTFSI, MeCN–LiTFA, and MeCN–LiTfO), although two of the cases (MeCN–LiTFSI and DMSO–LiTFA) with different behavior were marginal (coordination numbers with the salt of ~0.7 and ~0.8 when the experiment showed dissociation). This was also true of the two cases (DME–LiTFSI and DMSO–LiTFA) where the results for OPLS initialization did not match the experimental results (coordination numbers with the salt of ~0.7 when the experiment showed dissociation). In these marginal cases, it is possible that my sample was not large enough and that averaging over more than three initial configurations would result in association/dissociation behavior more closely matching experiment. However, for the OPLS cases, the OPLS classical MD results for the same systems also did not match experiment, so it is also possible that the disagreement in the AIMD results is due to physically unrealistic starting configurations from the classical MD.

Salt	Solvent	Equilibration Method	Force Field	Li–N (MeCN) / Li–O (DME and DMSO) in Solvent	Li–O in TFSI	Total Li Coordination [a]	Li-Salt Associated or Dissociated? [b]
LiTFSI	MeCN	Experiment [c]		4.3	0.3	4.6	D
		Classical MD	PCFF+	2.1	1.8	3.9	A
			OPLS	3.9	0.1	4.0	D
		AIMD		3.2	0.7	3.8	A
	DMSO	Experiment [c]		4.3	0.0	4.3	D
		Classical MD	PCFF+	3.0	0.9	3.9	A
			OPLS	3.7	0.2	4.0	D
		AIMD		3.8	0.1	3.9	D
	DME	Experiment [c]		4.4	0.2	4.6	D
		Classical MD	PCFF+	1.8	2.3	4.1	A
			OPLS	3.3	0.7	4.1	A
		AIMD		3.2	1.2	4.3	A

Table 9: Coordination numbers for Li^+ ion with N and O atoms in different solvents and the $TFSI^-$ anion for AIMD simulations with 50 solvent and 3 salt molecules averaged over three simulations for each system. (a) Total coordination numbers were calculated separately and therefore may not exactly equal the sum of the Li–solvent and Li–salt coordination numbers due to rounding. (b) The final column indicates association or dissociation, with association defined as an average coordination number for the Li^+ ion and O in the salt counter anion of ≥ 0.5. (c) Experimental values from Leverick et al. are provided for comparison.[9] Coordination between Li and N in TFSI is not reported as it was never observed in either the experimental work or AIMD simulations.

Salt	Solvent	Equilibration Method	Force Field	Li–N (MeCN) / Li–O (DMSO) in Solvent	Li–O in TFA	Total Li Coordination [a]	Li-Salt Associated or Dissociated? [b]
LiTFA	MeCN	**Experiment** [c]		**1.2**	**1.5**	**2.7**	**A**
		Classical MD	PCFF+	1.5	2.3	3.8	A
			OPLS	1.6	2.2	3.8	A
		AIMD		2.9	1.0	3.9	A
	DMSO	**Experiment** [c]		**4.2**	**0.1**	**4.3**	**D**
		Classical MD	PCFF+	2.6	1.3	3.9	A
			OPLS	3.2	0.7	3.8	A
		AIMD		3.0	0.8	3.8	A

Table 10: Coordination numbers for Li^+ ion with N and O atoms in different solvents and the TFA^- anion for AIMD simulations with 50 solvent and 3 salt molecules averaged over three simulations for each system. (a) Total coordination numbers were calculated separately and therefore may not exactly equal the sum of the Li–solvent and Li–salt coordination numbers due to rounding. (b) The final column indicates association or dissociation, with association defined as an average coordination number for the Li^+ ion and O in the salt counter anion of ≥ 0.5. (c) Experimental values from Leverick et al. are provided for comparison.[9]

Salt	Solvent	Equilibration Method	Force Field	Li–N (MeCN) in Solvent	Li–O in TfO	Total Li Coordination [a]	Li-Salt Associated or Dissociated? [b]
LiTfO	MeCN	**Experiment** [c]		**1.7**	**1.9**	**3.6**	**A**
		Classical MD	PCFF+	3.7	0.2	4.0	D
			OPLS	1.6	2.3	3.9	A
		AIMD		3.3	0.7	3.9	A

Table 11: Coordination numbers for Li^+ ion with N and O atoms in MeCN and the TfO^- anion for AIMD simulations with 50 solvent and 3 salt molecules averaged over three simulations for each system. (a) Total coordination numbers were calculated separately and therefore may not exactly equal the sum of the Li–solvent and Li–salt coordination numbers due to rounding. (b) The final column indicates association or dissociation, with association defined as an average coordination number for the Li^+ ion and O in the salt counter anion of ≥ 0.5. (c) Experimental values from Leverick et al. are provided for comparison.[9]

From the results shown in these tables, I can conclude that the choice of equilibration method clearly plays a crucial role in the AIMD simulations. This may appear, on the surface, to be an obvious statement that has been well known for decades.[134,135] However, the magnitude and nature of this dependence are often ignored, and it is instead assumed that many paths to a starting AIMD configuration could be "good enough" and that any prior unphysical correlations would quickly disappear, especially with a quick AIMD *NVT* annealing run. My results show this is not the case for these properties and materials. The use of PCFF+ for equilibration led to worse results than either of the other methods, corresponding to its poor performance in the classical MD simulations. In contrast, OPLS equilibration results outperformed even the AIMD using pure AIMD equilibration. This is likely because the classical MD equilibration runs were much longer than the AIMD equilibration runs, which allowed the systems to better find a physically accurate initial configuration; in the short simulation times available for the AIMD production runs, the initial randomly generated configuration had a large impact on the system behavior. Additionally, the overall association/dissociation behavior for the AIMD simulations with either classical equilibration method matched the association/dissociation for the classical *NVT* simulations with the same force field exactly. Thus, choosing a force field well suited to a given system is critical for equilibrating the initial configuration for AIMD simulations. This is because of the small number of association/dissociation events that occur in the short timescale of a typical AIMD simulation. The coordination environments and corresponding RDF plots and coordination numbers for the three Li^+ ions in one MeCN–LiTFSI simulation are shown in Figure 5. Within the ~10 ps of this simulation, no association/dissociation events occurred. However, the different ions had different coordination environments, which emphasizes the

importance of sampling using different initial configurations and multiple Li^+ ions within each configuration.
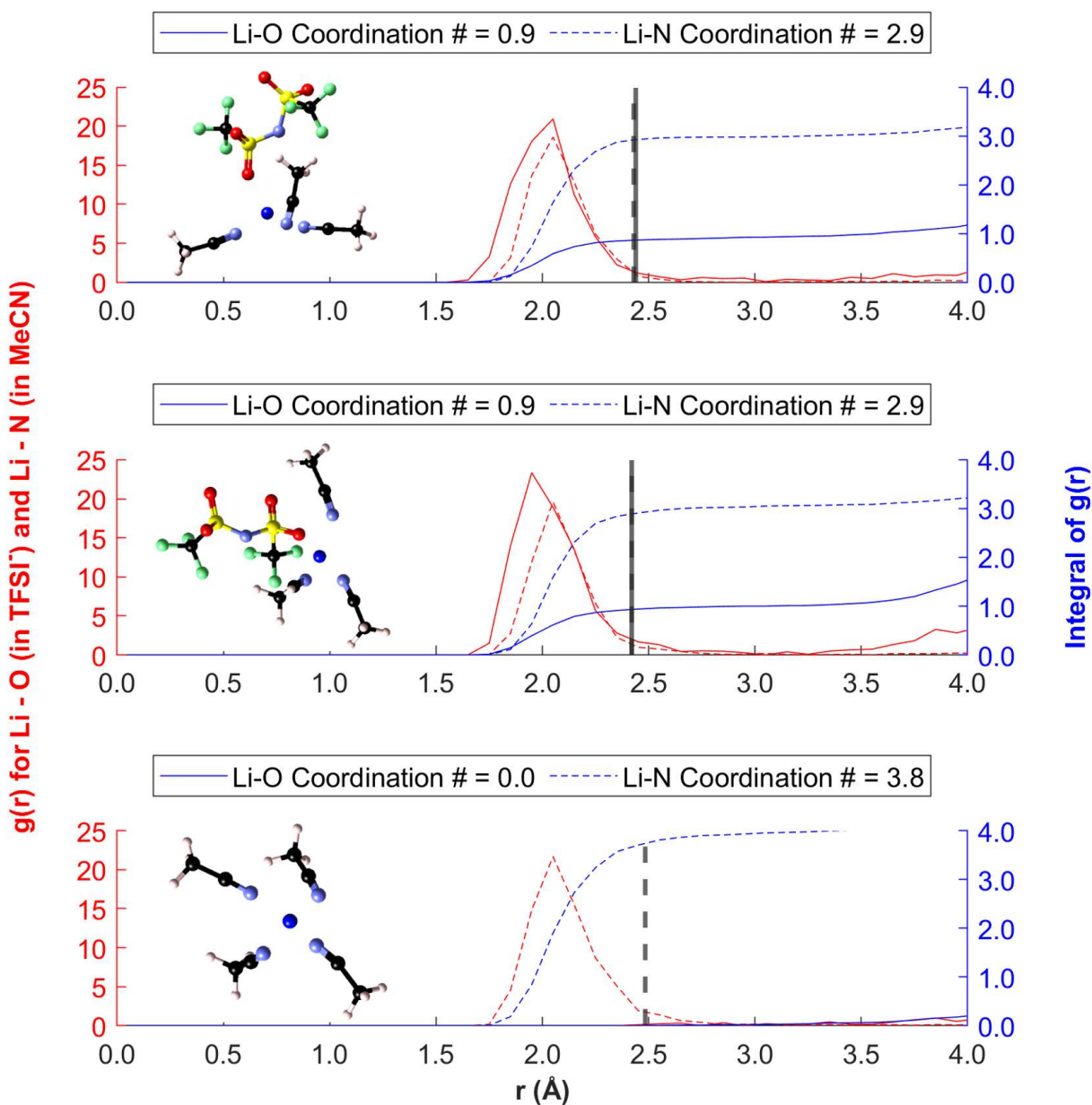
Figure 5: Plots of the radial distribution function and its integral for the Li coordination to O in TFSI⁻ anions and for the Li coordination to N in solvent molecules for each of the three Li⁺ ions in one of the simulations of 50 MeCN molecules and 3 LiTFSI molecules using AIMD with AIMD initialization. Also shown are the first coordination shells of the lithium ions at the end of the simulation. The RDFs are averages over the length of the simulation, but no significant variation was observed over time. N in the TFSI⁻ anions was not present in the first coordination shell of any of the Li⁺ ions. Both the plots and the figures show that the first solvation shell of two of the Li⁺ ions was similar (coordinated to one TFSI⁻ anion and three solvent molecules), whereas the first solvation shell of the third Li⁺ ion was markedly different (coordinated to four solvent molecules).

51

To further examine the relative importance of simulation time and using multiple initial configurations, I performed a few longer AIMD simulations. The coordination number over time for three ~40 ps simulations of MeCN–LiTFSI systems are shown in Figure 6. Simulations of around this length are common for production runs in the literature,[18,20–22,26] and often only one or two simulations are performed for each system.[20,21,26,27] However, in two of the long simulations, two of the three Li^+ ions did not undergo any association or dissociation event, and in the third case, none of the Li^+ ions underwent any association or dissociation event. Additionally, in each simulation, at least one ion remained dissociated for the entire simulation, while one ion remained associated to the same $TFSI^-$ anion(s). Thus, the lack of association/dissociation events was not because all the ions were trapped in the most energetically favorable state. The small number of exchange events in the Li^+-ion coordination shells is also similar to what was observed with the reorganization of water in the previously mentioned AIMD study of Li coordination in an aqueous LiCl solution: because water reorganization is slow compared to the timescale of the AIMD simulation, full reorganization of the water in the Li^+-ion coordination shells is not possible, and the initial configurations from the classical MD equilibration step bias the AIMD results.[97] The fact that association/dissociation events are relatively rare in my systems further illustrates the importance of both having a well-equilibrated initial configuration and using multiple initial configurations, given that even a simulation of ~40 ps is not long enough for each individual Li^+ ion to sample a statistically significant portion of the phase space.
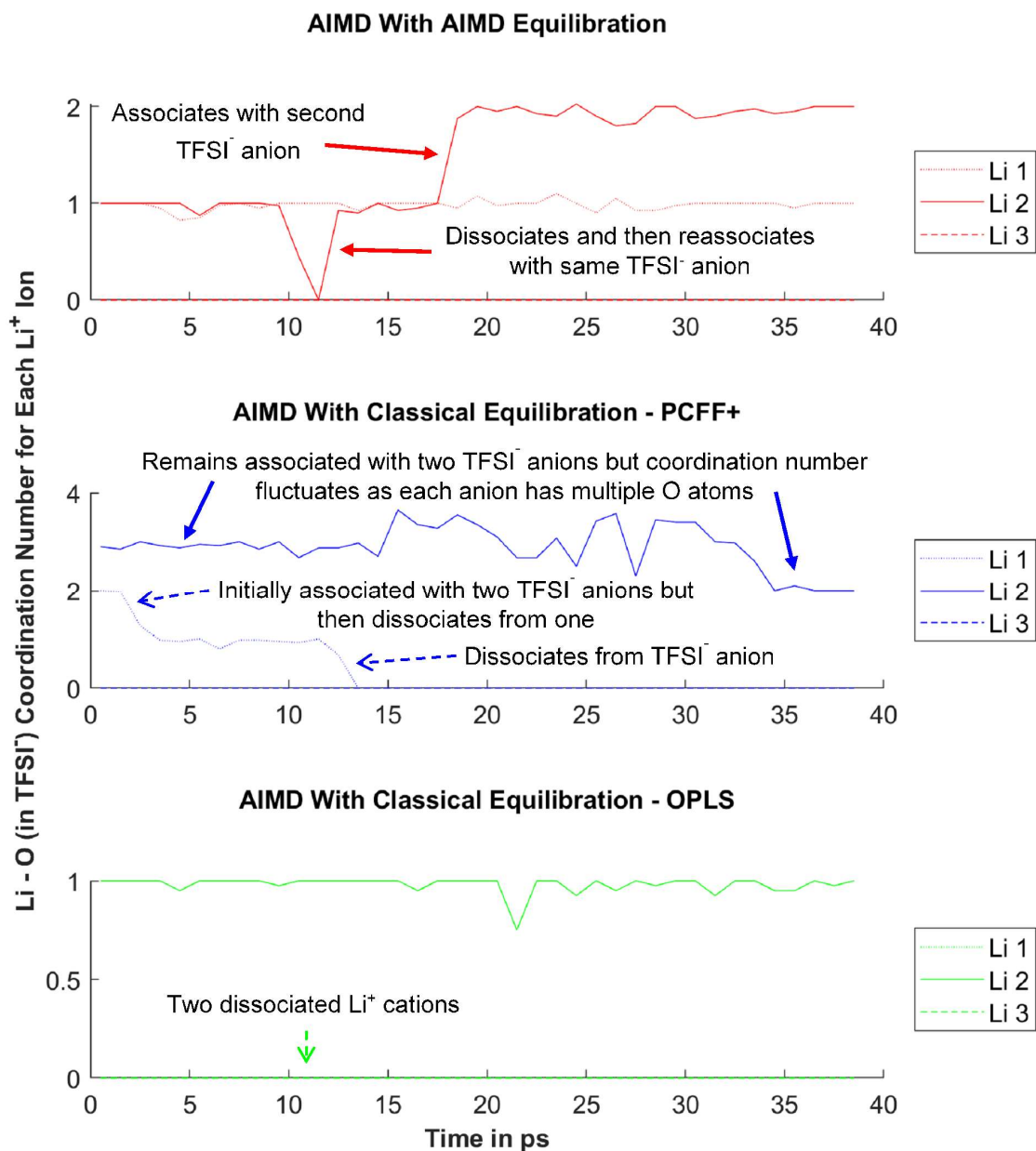
Figure 6: Li–O coordination number over time for three AIMD simulations of MeCN–LiTFSI systems, one with AIMD equilibration, one with classical MD equilibration using the PCFF+ force field, and one with classical MD equilibration using the OPLS force field. Each point of the coordination number data is averaged over 1 ps. In the cases of AIMD and PCFF+ equilibration, two of the three Li^+ ions did not undergo an association or dissociation event. In the case of OPLS equilibration, none of the three Li^+ ions underwent an association or dissociation event. This illustrates the importance of averaging over multiple Li^+ ions and initial configurations instead of just running longer simulations, as even a long AIMD simulation of ~40 ps is not long enough for each individual Li^+ ion to sample a statistically significant portion of the phase space.

To further illustrate the importance of sampling, I computed the dimer existence autocorrelation

functions (DACF) for Li and O in TFSI and for Li and N in MeCN for a classical MD simulation

with the OPLS force field using the TRAVIS analysis program.[136] The DACF of two particles i, j

is defined as the autocorrelation function of $\beta_{i,j}$ where

$$\beta_{i,j} = \begin{cases} 1 \ when \ the \ particles \ remain \ in \ a \ dimer \ state \\ 0 \ when \ the \ dimer \ has \ dissociated \end{cases}$$

with the dimer existence criteria defined as desired.[136] The DACF at a time τ is the probability

that the dimer criteria are still satisfied at time τ and is thus defined as[136]

$$DACF(\tau) = N \cdot \langle \sum_{t=0}^{T-\tau} \beta_{i,j}(t + \tau) \cdot \beta_{i,j}(t) \rangle_{i,j}$$

The results are shown in Figure 7, with an inset showing the DACFs only up to the length of the

long AIMD simulations. The dimer existence criteria used cutoffs of 3 Å and the five nearest

neighbors, although the results were not very sensitive to the choices of criteria. A significant

fraction of the Li–MeCN and Li–TFSI dimers had lifetimes longer than the total AIMD

simulation times of ~40 ps. That, combined with the fact that Li–TFSI dimers were relatively

rare (average coordination number for Li–O of 0.4 for classical MD with OPLS and 0.3 for

experiment[9]), explains why few association/dissociation events were observed in the AIMD

simulations in Figure 6. If the DACFs are fitted to exponential functions of the form

$$Ae^{-\tau/\tau_r}$$

where A is a fitted prefactor, τ is the length of the time interval for the DACF, and τ_r is the mean

residence time of the solvent molecule or anion in the Li^+ coordination shell, I find that the mean

residence time for MeCN in the Li^+ coordination shell is ~50 ps and that the mean residence time

for TFSI$^-$ in the Li$^+$ coordination shell is ~30 ps. These mean residence times are significantly

longer than the timescales of my AIMD production runs (5–10 ps) and on the order of the

timescale of the longer AIMD simulations in Figure 6 (~40 ps), which further explains why I did

not see the Li$^+$-ion coordination environments in all of the AIMD simulations of the same system

equilibrate to the same final steady-state structures; the simulations were simply not long enough

for this equilibration to occur.
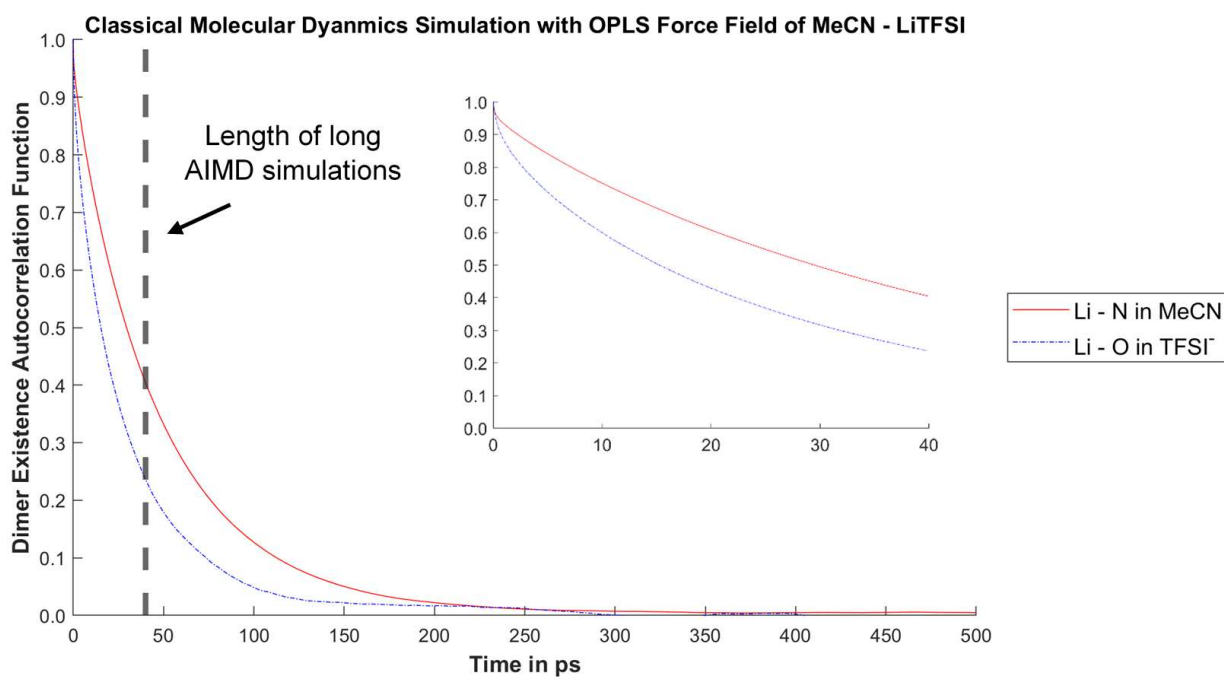
Figure 7: The dimer existence autocorrelation function (DACF) for Li and N in MeCN and for
Li and O in TFSI for a 100 ns classical MD simulation of a MeCN–LiTFSI system calculated
with TRAVIS.[136] Dimers were defined with a cutoff of 3 Å and five nearest neighbors. The inset
shows the DACF for 40 ps, the length of the long AIMD simulations discussed in Figure 6.

Additionally, when I performed similar analysis on the OPLS simulations of the other systems in

this study, the other five systems had longer Li–solvent and Li–salt residence times than the

MeCN–LiTFSI system did, sometimes by more than an order of magnitude. While I cannot be certain of the accuracy of these residence times because the simulations with the OPLS force field do not reproduce experimental behavior in all the systems studied, this is still strong evidence that the AIMD simulations are not long enough for equilibration to occur. As a very rough rule of thumb, it seems reasonable to suggest that an AIMD simulation would have to be several times longer than the longest residence time (slowest process) in the system to be confident that it accurately reproduces experimental results for properties related to the coordination environment. Based on my results, that would suggest a required simulation length of ~200 ps for the MeCN–LiTFSI system and simulation lengths ranging from hundreds of picoseconds to tens of nanoseconds for other small molecule electrolyte systems, which is beyond the timescales available with AIMD.

2.4 Conclusions

I examined the effect of equilibration methodology on AIMD simulations by investigating the Li^+-ion coordination with solvent molecules and counter anions in several common lithium–oxygen battery systems. Much of the previous AIMD literature has largely ignored the effect of equilibration methodology. The AIMD equilibration method is usually a classical MD simulation,[17,20,26,28] often with minimal evaluation of or justification for the choice of force field, and/or the first few picoseconds of the production AIMD simulation.[17,18,21,22,26–28,95] Also, many papers use only one or two initial configurations.[20,21,26,27] The implicit assumption is that a 30–50 ps AIMD simulation is long enough that the initial configuration is of minimal importance and long enough to obtain uncorrelated data. However, I found that the initial equilibration method has a large impact on AIMD trajectories, even for simulations as long as ~40 ps, because

even what is considered a relatively long AIMD simulation is not long enough for individual Li^+

ions to sample a statistically significant portion of the phase space.

As a result, I conclude that two details are critical for accurately calculating properties such as

coordination number from AIMD simulations: (1) using an equilibration method well suited for

the particular system and (2) sampling over several initial configurations. I found that the

association/dissociation behavior for the AIMD simulations closely aligned with the behavior for

the classical MD equilibration runs, as has been reported previously.[97] As a result, a force field

that more accurately reproduced experimental behavior in classical MD simulations, namely

OPLS in this study, was also the equilibration method for AIMD that produced the most accurate

behavior. In contrast, when PCFF+, a force field more poorly suited to these solvent–salt

systems,[82] was used for equilibration, the AIMD coordination behavior matched the

experimental behavior in only one of six systems. In fact, for both OPLS and PCFF+, the overall

association/dissociation behavior for the AIMD simulations exactly matched the

association/dissociation behavior for the corresponding classical MD runs for all six systems

tested. I therefore demonstrated the importance of equilibrating the system using a force field

well suited for it. Additionally, I showed the importance of performing several simulations with

different initial configurations to obtain a good sample of different Li coordination

environments, as individual Li^+ ions may not undergo any association/dissociation events in the

timescale of the simulations.

I am not arguing that AIMD simulations require a perfect potential to equilibrate the system; if a

perfect classical potential exists for a system, there is no need for AIMD simulations. However,

what is required is a potential that can avoid deep wells in the free-energy landscape, such as an

associated ion pair, if these wells would not occur in the corresponding AIMD simulation. If the

AIMD simulation is run for long enough, these artifacts will fade away, but that may require timescales of hundreds of picoseconds or even nanoseconds that are not accessible in a standard AIMD simulation. In contrast, it is not critical that the potential can accurately reproduce features such as bond lengths or angles, as these relax quickly during the AIMD simulation. What is critical is that the potential accurately models features that would take a long time to relax.

An example of a system that may be easier to equilibrate is in the previously cited studies of cation coordination in water.[120,121,123] In these studies, there are no counter anions present; the focus is on the cation–water interactions only, not on the cation–anion association/dissociation. Thus, the only feature DFT needs to capture is the relaxation of the orientational degrees of freedom of the water molecules, which relaxes quickly compared to diffusion-related mechanisms such as dissociation involving bulky anions. Another example well suited to study with AIMD is the interaction of small, monovalent ions dissolved in a low-viscosity solvent, such as a concentrated aqueous Li–Cl solution.[97] Because the timescale of the Li^+–Cl^- interaction is much shorter than the total simulation time (~4.5 ps vs. 30 ps), the AIMD simulation is long enough to allow breakdown of the ion pairing and thus long enough to accurately calculate the coordination between Li^+ and Cl^- ions in the solution, achieving good agreement with experiments.

Overall, my work demonstrates the importance of both equilibration method and sufficient sampling for calculating properties such as coordination number using AIMD simulations. It also shows the importance of documenting this information in articles to enable reproducibility and the importance of using some sort of experimental validation for molecular dynamics studies. Additionally, my results show the inherent difficulty and expense of accurately calculating

experimentally relevant quantities using AIMD simulations. This demonstrates the need for the development of new techniques in the form of either new classical force fields or emerging methods such as machine learning force fields based on the accurate energy and force data provided by AIMD simulations. There are currently significant research efforts in this area,[19,137–139] but further improvements in ease of training from AIMD data, transferability, and usability have the potential to greatly expand the types of systems that can by accurately modeled with molecular dynamics.

3 Lithium Transport Mechanisms

In this study, I investigate how ionic transport mechanisms in lithium-containing electrolytes influence key performance properties of lithium batteries, with a focus on how the choice of solvent affects the transport mechanism. To this end, I develop solvent metrics by combining different properties that can be measured experimentally such as solvent donor number, viscosity, and shear modulus and investigate how these metrics relate to atomistic-scale lithium transport mechanisms in liquid electrolytes. I examine the lithium transport mechanisms, primarily a vehicular transport mechanism with a lithium solvation shell moving through the solvent and a solvent exchange mechanism with net motion caused by solvent molecules entering and exiting the solvation shell, using classical molecular dynamics simulations with the OPLS force field. I utilize diverse small molecule liquid solvents (DEC, DMA, DME, DMF, DMSO, EC, MeCN, MTBE, PC, Py, SL, and THF) and also examine properties of one solvent mixture (EC/MTBE) as a function of solvent composition. I validate the classical force fields used for these solvents by comparing the computed values of the density, viscosity, and ionic conductivity with experimental measurements for the solvent–LiTFSI systems and also examine simulation properties such as diffusion coefficients, coordination numbers, and residence times. The results suggest novel methods for predicting transport properties and designing new solvents.

3.1 Introduction

In the past few decades, there has been a push in the battery community to improve our understanding of battery systems on an atomistic level, and computational methods are a key tool in this process. Examining dynamic processes such as cation transport[17,19] on an atomistic scale

can be difficult experimentally but accessible using classical molecular dynamics (MD) simulations. In this study, I examined transport properties for lithium bis(trifluoromethanesulfonyl)imide (LiTFSI)–solvent systems with twelve different small molecule liquid solvents common in battery applications using classical MD simulations and investigated how these transport properties correlate with other, more easily experimentally measured solvent properties such as donor number, viscosity, and shear modulus at infinite frequency.

In addition to examining fairly standard transport properties such as the Li–solvent and Li–TFSI coordination numbers and residence times, I also utilized an additional, more novel property, the transport ratio, developed by Borodin and Smith[140] and designed to elucidate the atomistic mechanisms by which lithium ions are transported in the different solvents. The transport ratio is a measure of how much a vehicular transport mechanism, where lithium ions move with their solvation shells through the solvent, dominates over a solvent exchange transport mechanism, where there is net movement of lithium ions because solvent molecules exit and reenter the lithium solvation shells. Beyond general interest in understanding the atomistic behavior of the systems, I am interested in the transport mechanisms because vehicular motion is usually faster than transport via solvent exchange. Solvents where the solvent exchange mechanism dominates can have poor lithium ion transport, which can lead to lower ionic conductivity and thus possibly worse overall battery performance including slower charging and discharging rates.[140]

Additionally, as my first study showed the importance of experimentally validating simulation results, I also compared the calculated viscosities, densities, and ionic conductivities for my classical MD simulations directly to experimental measurements.

With the transport properties for the twelve different solvent–LiTFSI systems calculated using classical MD simulations, I then explored whether more experimentally accessible properties such as viscosity or solvent donor number correlate with these transport properties. The goal is to ultimately be able to predict the transport properties of systems, such as the dominant lithium transport mechanism, without needing to perform classical MD simulations. While my work may not yet have this level of predictive power, I have developed a novel tool not to my knowledge previously applied to small molecule solvent systems: solvent metrics. I have examined two such metrics (solvent donor number / solvent–LiTFSI system viscosity and solvent donor number / shear modulus at infinite frequency for the pure solvent) and found correlations between both metrics and the transport ratio.

To further examine how solvent properties affect lithium transport, I also performed classical MD simulations of mixtures of two solvents and investigated how the transport properties varied as a function of solvent composition.

3.2 Methodology

3.2.1 Systems

Each simulation system consisted of 2,000 solvent molecules and 120 lithium bis(trifluoromethanesulfonyl)imide (LiTFSI) molecules. I selected twelve different small molecule solvents that are chemically diverse and parametrized for the OPLS force field; my experimental collaborator also verified that the solvent–LiTFSI systems are liquid at 300 K. LiTFSI was selected as the lithium salt because of its widespread use in battery research.[9,141–143] The solvents used were diethyl carbonate (DEC), dimethylacetamide (DMA), dimethoxyethane (DME), dimethylformamide (DMF), dimethyl sulfoxide (DMSO), ethylene carbonate (EC),

acetonitrile (MeCN), methyl tert-butyl ether (MTBE), propylene carbonate (PC), pyridine (Py), sulfolane (SL), and tetrahydrofuran (THF). The initial amorphous configurations were generated using fftool and packmol,[105,106,108] and the results for three simulations with different random starting configurations were averaged for each solvent–LiTFSI combination. The molecular structure for each solvent molecule and the LiTFSI salt molecule is shown in Figure 8.

(a) Diethyl carbonate (DEC) (b) Dimethylacetamide (DMA) (c) Dimethoxyethane (DME)

(d) Dimethylformamide (DMF) (e) Dimethyl sulfoxide (DMSO) (f) Ethylene carbonate (EC)

(g) Acetonitrile (MeCN) (h) Methyl tert-butyl ether (MTBE) (i) Propylene carbonate (PC)

(j) Pyridine (Py) (k) Sulfolane (SL) (l) Tetrahydrofuran (THF)

(m) Lithium bis(trifluoromethanesulfonyl)imide (LiTFSI)
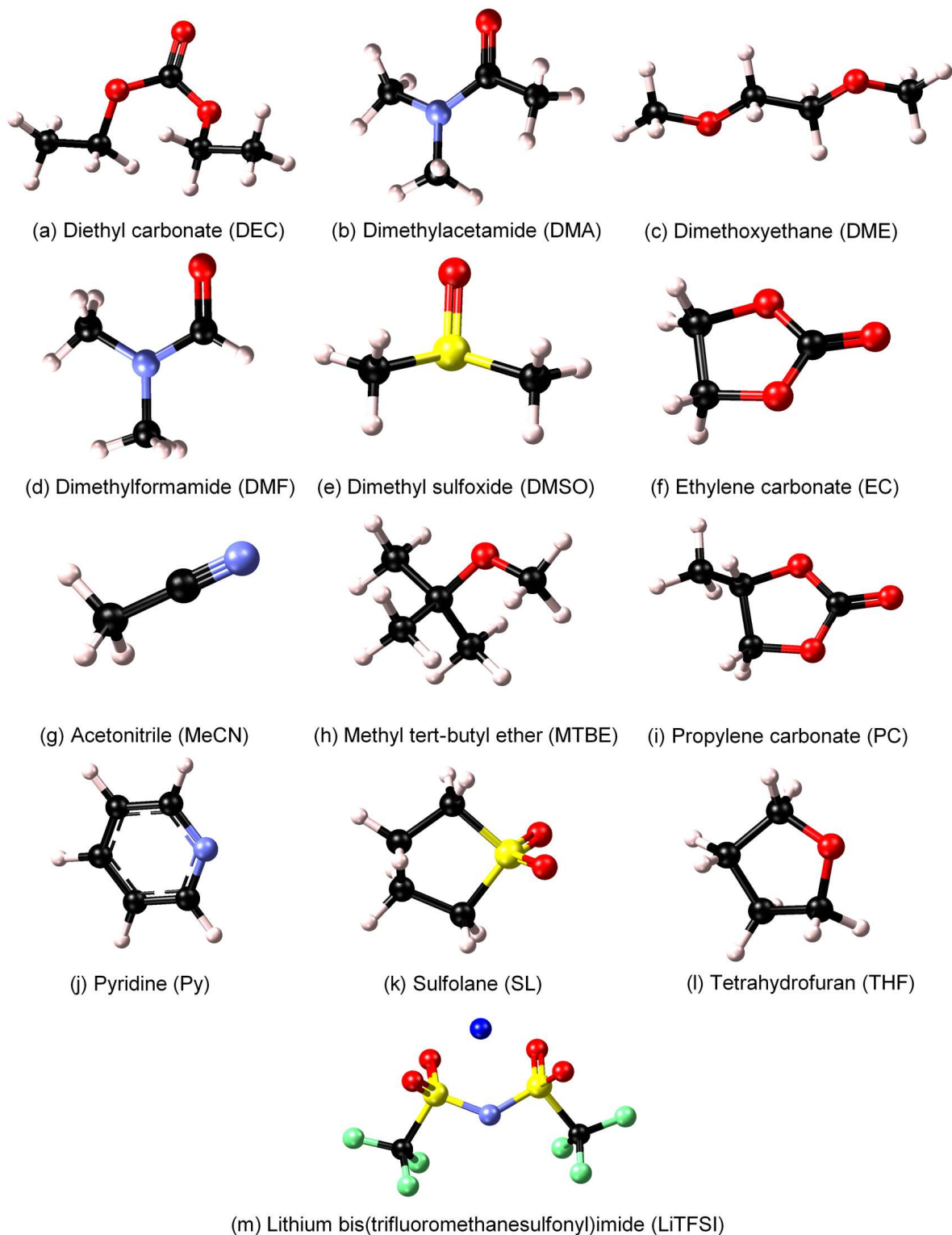
Figure 8: The solvent (a–l) and salt (m) molecules investigated in the study. The atomic color code: carbon – black, fluorine – green, hydrogen – white, lithium – blue, nitrogen – purple, oxygen – red, sulfur – yellow

3.2.2 Classical Molecular Dynamics Methodology

The computational results in this study were obtained using classical MD simulations performed with the LAMMPS code.[122,144] All simulations were performed using the OPLS all-atom force field, which is widely used for the molecules in this study.[84,85,131] The parameters have been assembled from multiple sources, sometimes with small modifications to, for example, ensure that molecules remained neutrally charged.[83,108,129,131,145,146]

Two different types of classical MD simulations were utilized: simulations in the isothermal–isobaric (*NpT*) ensemble and simulations in the canonical (*NVT*) ensemble. The simulations in the *NpT* ensemble were used to find the equilibrium density of each system, and these equilibrium densities were then used to create the initial configurations for the simulations in the canonical (*NVT*) ensemble. Below I will detail each simulation method.

3.2.2.1 NpT *Methodology*

For the simulations in the *NpT* ensemble, the initial random configurations were generated using fftool and packmol at densities extrapolated from the experimentally known densities of LiTFSI and the solvents.[105,106,108,109] The first step was then an equilibration step with minimization using conjugate gradients followed by a short 100 ps classical MD simulation in the *NVT* ensemble with a time step of 0.5 fs and a temperature of 300 K. The cutoff distance for Lennard-Jones and the real-space part of the Coulomb interactions was 12 Å, with long-range Coulomb interactions calculated using the particle–particle–particle–mesh (PPPM) solver with an accuracy of 10^{-5}, and tail corrections were applied. Then, a longer classical MD simulation within the *NpT* ensemble was executed for 5 ns, still with a time step of 0.5 fs, at 300 K, and with other settings unchanged.

3.2.2.2 NVT *Methodology*

For the simulations in the *NVT* ensemble, the initial random configurations were generated using fftool and packmol at the equilibrium densities calculated from the simulations in the *NpT* ensemble.[105,106,108] The first step was again an equilibration step, identical to the equilibration step used for the *NpT* simulations. Then a longer classical MD simulation within the *NVT* ensemble was executed for 10 ns, still with a time step of 0.5 fs, at 300 K, and with other settings unchanged from the *NpT* simulations.

3.2.3 Computational Properties

3.2.3.1 Density

Density was the only property calculated using the simulations in the *NpT* ensemble. The equilibrium density of a solvent–LiTFSI system was defined as the average density of the simulation over the second half of the 5 ns *NpT* production run. This equilibrium density was then averaged over the results of the three simulations for each solvent, but the variation in the density between the independent runs was very small (no variation in the thousandth digit).

3.2.3.2 Viscosity

Viscosity calculations for the simulations in the *NVT* ensemble were performed using the Python LAMMPS Analysis Tools (PyLAT).[147,148] The viscosity was calculated using the stress tensor autocorrelation function and given by

$$\eta = \frac{V}{k_B T} \int_0^\infty \langle \tau_{\alpha\beta}(t) \cdot \tau_{\alpha\beta}(0) \rangle \, dt$$

where η is the viscosity, V is the simulation box volume, k_B is the Boltzmann constant, T is the simulation temperature, and $\tau_{\alpha\beta}(t)$ is the $\alpha\beta$ element of the stress tensor. The detailed calculation methodology implemented by the PyLAT program is documented in Humbert et al.[147] For each simulation, the first nanosecond of data was excluded from the viscosity calculation to allow for equilibration. The final results are the average for the three production runs executed for each system. The reported error is the standard deviation of the viscosities for the three runs, so it reflects the variation between the runs and not an estimate of any possible systemic error due to, for example, the OPLS force field parameters.

3.2.3.3 Diffusion Coefficients and Ionic Conductivity

Diffusion coefficient calculations for Li^+ ions, $TFSI^-$ counter anions, and solvent molecules in the simulations in the *NVT* ensemble were performed using the Mean Square Displacement / Diffusion Coefficients function of the TRAVIS analysis program.[136] To find the diffusion coefficient for one type of particle, the mean square displacement (MSD) for that type of particle is first calculated. The MSD for a type of particle is the square of the average distance a particle has traveled away from its starting point during a time interval of length τ, averaged over all particles of that type and all starting times, and is defined by the equation

$$MSD(\tau) = \langle |\vec{r}_i(t+\tau) - \vec{r}_i(t)|^2 \rangle_{t,i}$$

where $\vec{r}_i(t)$ is the position of the ith particle of the desired type at a time t. The diffusion coefficient is then defined as

$$D = \lim_{\tau \to \infty} \left(\frac{1}{2n} MSD(\tau) \right)$$

for n-dimension motion. n was always 3 in this study. The detailed calculation methodology implemented by the TRAVIS program is documented in Brehm et al.[136] Similarly to the viscosity calculations, the first nanosecond of data was excluded from the calculations, the final results are the average for the three simulations for each system, and the reported error is the standard deviation of the diffusion coefficients for the three runs.

The ionic conductivity for each system was calculated using the Nernst–Einstein equation and the Li$^+$ and TFSI$^-$ diffusion coefficients. The Nernst–Einstein equation is

$$\sigma_{NE} = \frac{e^2}{V k_B T} (N_- z_-{}^2 D_- + N_+ z_+{}^2 D_+)$$

where σ_{NE} is the ionic conductivity, e is the elementary charge, V is the simulation box volume, k_B is the Boltzmann constant, T is the simulation temperature, $N_\pm$ are the number of cations and anions in the simulation (number of Li$^+$ and TFSI$^-$ ions in this study), $z_\pm$ are the charge of the cation and anion (± 1 in this study), and $D_\pm$ are the diffusion coefficients of the cation and anion.[149] The Nernst–Einstein equation relies on the assumption that the ions do not interact, so the equation is only exact in the infinite dilution limit and will break down for highly concentrated systems and systems with a high degree of ion clustering.[149] The systems in this study are not highly concentrated, so this equation should generally be expected to be a good approximation. However, the approximation may still break down for systems with less salt dissociation where the Li$^+$ and TFSI$^-$ ions do not diffuse independently.

3.2.3.4 Coordination Numbers

Coordination numbers represent the average number of solvent molecules or TFSI$^-$ anions in the first solvation shell of a Li$^+$ ion and are a method of quantifying the lithium solvation

environment. The solvent and TFSI coordination numbers were found using the Radial Distribution function of the TRAVIS analysis program.[136] The radial distribution function (RDF, denoted in equations as $g(r)$), is the probability of finding another molecule or ion of a specific type α in a shell at a distance r and with thickness dr from a reference molecule or ion, which in this study is a Li^+ ion. In terms of the local density $\rho_\alpha(r)$ of molecule or ion of type α, the partial RDF for species α is given by

$$g_\alpha(r) = \frac{dn_\alpha(r)}{4\pi\, dr * \rho_\alpha(r)}$$

The coordination number n_α for the first solvation sphere is then defined as the integral of the RDF up to its first minimum r_{min}

$$n_\alpha(r_{min}) = \int_0^{r_{min}} 4\pi r^2 g_\alpha(r)\,\rho_\alpha(r)dr$$

In practice, the exact location of the first minimum of the RDF of a simulation could be ill-defined as it was averaged over different time steps and over the three Li^+ ions in the simulation. As such, I averaged the RDF values into bins 0.05 Å thick (dr), fitted the RDF for the first solvation shell to a Gaussian function, extracted the mean and standard deviation of the fit, and defined the coordination number as the numerical integral of the RDF at three standard deviations above the mean.

As with the other calculations, the first nanosecond of data was excluded from the calculations, the final results are the average for the three simulations for each system, and the reported error is the standard deviation of the diffusion coefficients for the three runs. An example of raw data and the fitted Gaussian for a MeCN–LiTFSI system is shown in Figure 9.
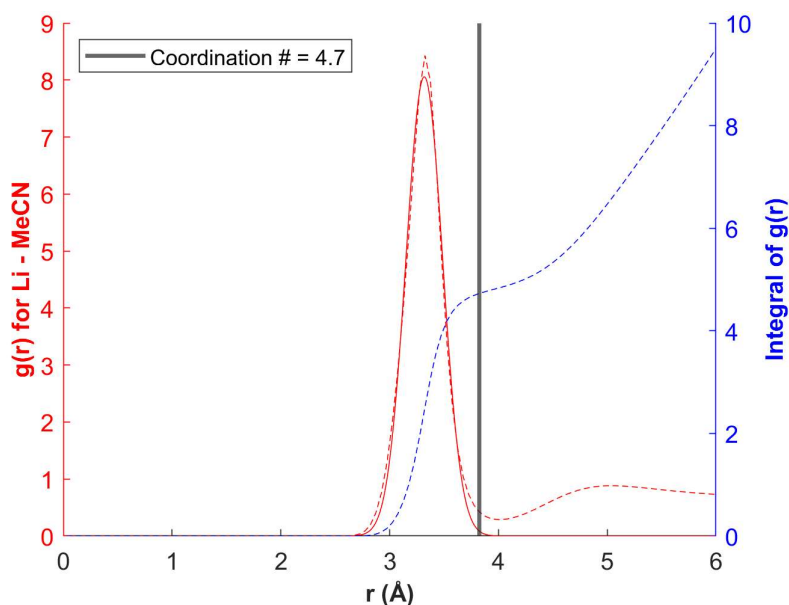
Figure 9: The radial distribution function for MeCN with respect to Li. The red dashed line is the radial distribution function data, the blue dashed line is the numerical integral of the radial distribution function, and the solid red line is the fitted Gaussian function. The grey vertical line indicates three standard deviations above the mean for the Gaussian function, which was also used as a cutoff distance in the residence time calculation. The integral of the radial distribution function at this point is defined as the coordination number.

3.2.3.5 Residence Times

Residence times for solvent molecules and TFSI⁻ anions in the lithium solvation shell were calculated using the Aggregation function of the TRAVIS analysis program.[136] I defined a solvent molecule or TFSI⁻ anion as being within the solvation shell of a Li^+ ion if its center of mass was within a cutoff distance of three standard deviations above the mean of the Gaussian fit to the RDF used in the coordination number calculation and it was one of the six nearest neighbors of the Li^+ ion. The condition of being one of the six nearest neighbors was included because the maximum average total coordination number for lithium in any of the systems was 5.94. Overall, the results were not very sensitive to the choice of cutoff distance or the nearest neighbor constraints. To find the residence time, I first calculated the dimer existence

70

autocorrelation function (DACF). The DACF of two particles i, j is defined as the autocorrelation function of $\beta_{i,j}$ where

$$\beta_{i,j} = \begin{cases} 1 \text{ when the particles remain in a dimer state} \\ 0 \text{ when the dimer has dissociated} \end{cases}$$

with the dimer existence criteria defined as desired, which in this study was when the solvent molecule or TFSI⁻ anion was within the cutoff distance of the Li^+ ion and was one of the six nearest neighbors of the Li^+ ion.[136] The DACF is the probability that the dimer criteria are still satisfied after a time interval of length τ given that the criteria were fulfilled at the start of the interval, averaged over all dimers of the given type and all starting times, and is thus defined as[136]

$$DACF(\tau) = N \cdot \langle \sum_{t=0}^{T-\tau} \beta_{i,j}(t + \tau) \cdot \beta_{i,j}(t) \rangle_{i,j}$$

The mean residence time for solvent molecules or TFSI⁻ anions within the lithium solvation shell can then be found by fitting the DACF to an exponential function of the form

$$Ae^{-\tau/\tau_r}$$

where A is a fitted prefactor, τ is the length of the time interval for the DACF, and τ_r is the mean residence time of solvent molecules or anions in the Li^+ coordination shell. As with the other calculations, the first nanosecond of data was excluded from the calculations, the final results are the average for the three simulations for each system, and the reported error is the standard deviation of the diffusion coefficients for the three runs.

3.2.3.6 Transport Ratio

For ion transport in small molecule liquid systems such as the ones in this study, there are two dominant competing ion transport mechanisms: vehicular motion and solvent exchange.[140] Vehicular motion is when the ion (Li^+ in this study) is transported with its first solvation shell (typically 4–6 solvent molecules and/or $TFSI^-$ anions in this study). Solvent exchange is the net motion of the ion due to the breakup and reformation of its solvation shell, specifically the exchange of solvent molecules between the first solvation shell and the bulk solvent. Another possible ion transport mechanism is anion exchange, which would be when an anion exits the solvation shell and is replaced by another anion; mixed exchanges (a solvent molecule being replaced in the solvation shell by an anion or vice versa) are also possible. However, for the systems in this study, LiTFSI was generally fairly dissociated with few $TFSI^-$ anions in the lithium solvation shells. Thus, vehicular motion and solvent exchange were the dominant transport mechanisms for the Li^+ ions, though a more thorough justification for neglecting contributions from salt exchange will also be discussed in the Results and Discussion section. As mentioned previously, I am interested in the transport mechanisms in part because vehicular motion is usually faster than transport via the solvent exchange. Therefore solvents where vehicular motion is dominant tend to have better lithium ion transport, which can correlate with higher ionic conductivity and thus potentially better battery performance including higher charging and discharging rates.[140]

The transport ratio is a measure of the relative importance of the vehicular and solvent exchange mechanisms of lithium transport and was developed by Borodin and Smith.[140] It first requires calculating the Li–solvent residence time $\tau_{r,Li-solv}$, as was described above. Then the average

72

distance traveled by a Li^+ ion while coordinated with a solvent molecule, L_{res}, is calculated using

$$L_{res} = \sqrt{6 * D_+ * \tau_{r,Li-solv}}$$

L_{res} is equivalent to the square root of the mean square displacement of a Li^+ ion in the average time between solvent exchanges.

The next step in the calculation is to find the average molecular size of a solvent molecule, S_{solv}, which is defined as twice the radius of gyration of the solvent molecule.[140] The average radius of gyration of the solvent molecule can be outputted directly from LAMMPS. L_{res}/S_{solv} will then be the average number of solvent molecule diameters that a Li^+ ion travels between solvent exchanges. A higher value corresponds to the vehicular mechanism being more dominant.[140] Borodin and Smith then argued that the MSD of the Li^+ ion after a time $\tau_{r,Li-solv}$ can be approximately broken up into vehicular and structure components as

$$L_{res}^2 = MSD\left(\tau_{r,Li}\right) \approx MSD\left(\tau_{r,Li-solv}\right)_{vehicular} + MSD\left(\tau_{r,Li-solv}\right)_{structure}$$

and that

$$MSD\left(\tau_{r,Li-solv}\right)_{structure} \approx S_{solv}^2$$

such that

$$L_{res}^2 \approx MSD\left(\tau_{r,Li-solv}\right)_{vehicular} + S_{solv}^2$$

Rearranging this, the vehicular to solvent exchange ratio, which I will hereafter refer to the transport ratio for conciseness, can be defined as[140]

$$Transport\ ratio \equiv \frac{Vehicular}{Solvent\ exchange} = \frac{MSD(\tau_{r,Li-solv})_{vehicular}}{S_{solv}^2} = \left(\frac{L_{res}}{S_{solv}}\right)^2 - 1$$

This analysis assumes that the average displacement of the Li^+ ion during a solvent exchange is equal to the solvent size, S_{solv}.[140] A transport ratio of 1 corresponds to equal contributions to lithium transport from the two mechanisms, and previous studies of EC–LiTFSI systems have found a transport ratio of 1 and observed roughly equal contributions from the vehicular and solvent exchange mechanisms, supporting the validity of the definition of this property.[140,150]

3.3 Results and Discussion

3.3.1 Experimental Validation

I will now discuss the results of the experimental validation using three properties of the solvent–LiTFSI systems: density, viscosity, and ionic conductivity. The experimental methodology is included in the Appendix.

3.3.1.1 Density

The computationally calculated densities for the solvent–LiTFSI systems compared to the experimentally measured densities are shown in Figure 10 and included in Table 12. The agreement between the computational and experimental values is generally quite good, with the maximum percent error for the computational densities being 5.0% for the DME–LiTFSI system. It is not surprising that the DME system most poorly matched the experimental results, as the force field parametrization of DME is primarily designed for larger glyme molecules[131] and was shown in my earlier work using OPLS as an equilibration method for AIMD simulations to not be very well suited for small molecule liquid simulations.
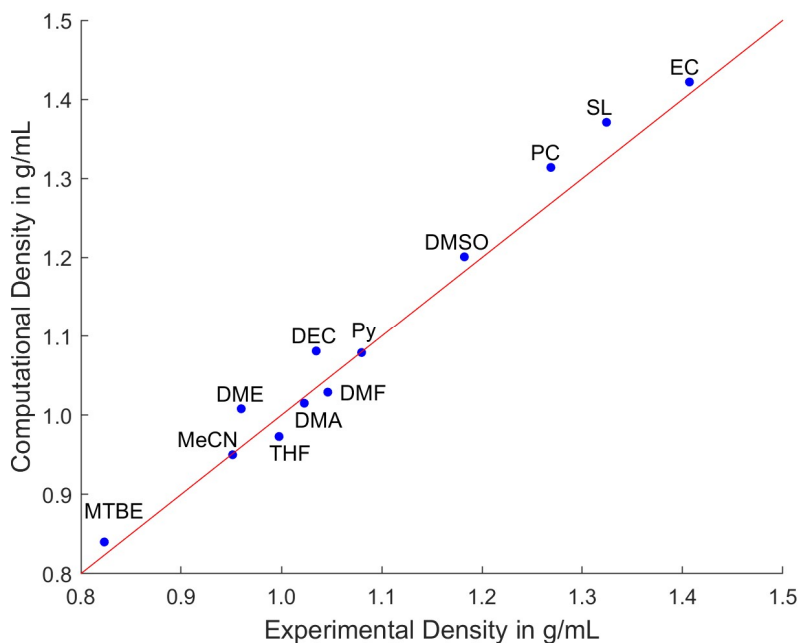
Figure 10: Densities calculated for the solvent–LiTFSI systems by averaging over three *NpT* simulations of 2,000 solvent molecules and 120 LiTFSI molecules vs. measured experimentally for systems with the same concentration. The red line represents perfect agreement.

Solvent	Computational Density in g/mL	Experimental Density in g/mL
DEC	1.081	1.035
DMA	1.015	1.023
DME	1.008	0.960
DMF	1.029	1.046
DMSO	1.201	1.182
EC	1.422	1.407
MeCN	0.950	0.951
MTBE	0.840	0.823
PC	1.314	1.269
Py	1.079	1.080
SL	1.371	1.324
THF	0.973	0.998

Table 12: Computational and experimental densities for solvent–LiTFSI systems.

3.3.1.2 Viscosity

The computationally calculated viscosities for the solvent–LiTFSI systems compared to the experimentally measured viscosities are shown in Figure 11 and included in Table 13. The computational viscosities are all higher than experimental values, which I hypothesize is due to the OPLS force field used. In my first study using OPLS as an equilibration method for AIMD, I observed that simulations with the OPLS force field often resulted in a higher degree of Li–salt association than was seen in experiments. The higher viscosities in this study suggest that OPLS also overestimates the strength of intermolecular interactions between solvent molecules. Apart from this general trend, DME is again an outlier, with the computational viscosity being almost twenty times larger than the experimental viscosity. As mentioned above for the density, this may be due to DME being poorly parametrized for small molecule liquid simulations. I will include results for the DME–LiTFSI system in this study but note that I expect them to be less accurate than for the other systems.
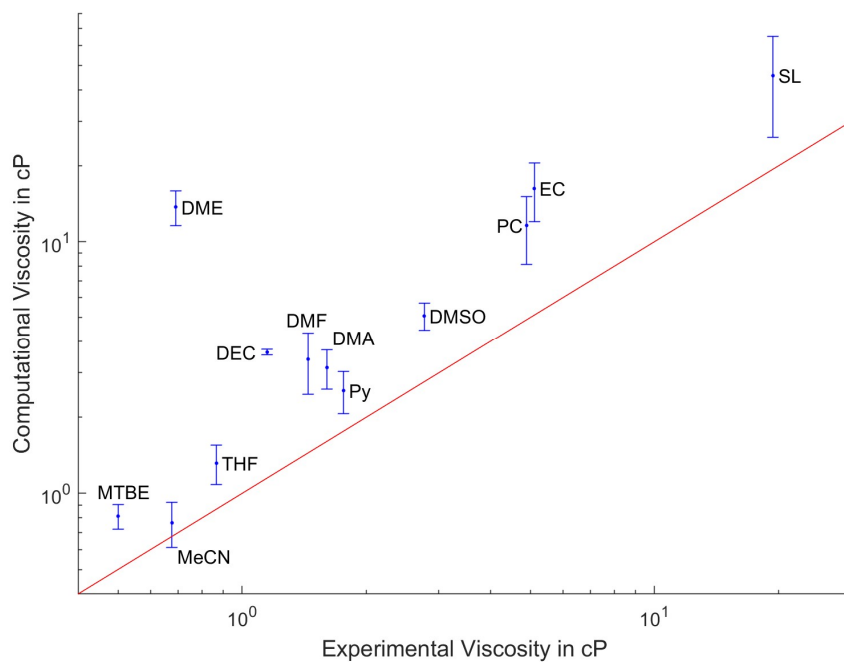
Figure 11: Viscosities for the solvent–LiTFSI systems calculated using three *NVT* simulations of 2,000 solvent molecules and 120 LiTFSI molecules vs. measured experimentally for systems with the same concentration. The red line represents perfect agreement. The error bars represent variation between the different *NVT* simulations.

Solvent	Computational Viscosity in cP	Experimental Viscosity in cP
DEC	3.62 ± 0.09	1.15
DMA	3.1 ± 0.6	1.61
DME	14 ± 2	0.69
DMF	3.4 ± 0.9	1.45
DMSO	5.1 ± 0.6	2.76
EC	16 ± 4	5.11
MeCN	0.8 ± 0.2	0.68
MTBE	0.81 ± 0.09	0.50
PC	12 ± 3	4.90
Py	2.5 ± 0.5	1.76
SL	46 ± 20	19.38
THF	1.3 ± 0.2	0.87

Table 13: Computational and experimental viscosities for solvent–LiTFSI systems, with error reflecting variation between simulations.

3.3.1.3 Ionic Conductivity

The experimentally measured ionic conductivities and computational ionic conductivities calculated using the Nernst–Einstein equation with the Li^+ and $TFSI^-$ diffusion coefficients from the simulations are shown in Figure 12 and included in Table 14. The MTBE–LiTFSI system appears to be an outlier, with the computational ionic conductivity over an order of magnitude higher than the experimental ionic conductivity. However, the low experimental conductivity of the MTBE–LiTFSI system relative to its viscosity suggests a high degree of ion pairing. As discussed in the Methodology section, the Nernst–Einstein equation relies on the assumption that there is no ion clustering in order to extrapolate the ionic conductivity of the system from the diffusion coefficients of the cation and anion. Thus, I hypothesize that this assumption breaks

down for the MTBE–LiTFSI system and that the computational ionic conductivity calculated using the Nernst–Einstein equation is therefore inaccurate. However, the Li^+ and $TFSI^-$ diffusion coefficients themselves could still be more physically accurate, so no strong conclusions about how well parametrized the MTBE solvent is can be drawn from this single result.

Figure 12: Ionic conductivities for the solvent–LiTFSI systems calculated with the Nernst–Einstein equation using Li^+ and $TFSI^-$ diffusion coefficients calculated for three *NVT* simulations of 2,000 solvent molecules and 120 LiTFSI molecules vs. measured experimentally for systems with the same concentration. The red line represents perfect agreement. The error bars represent variation 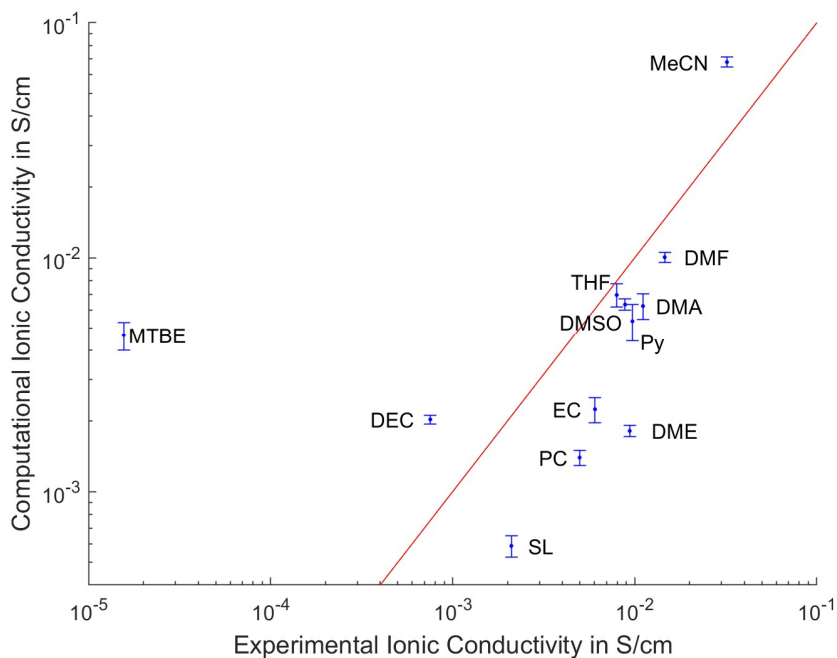between the different *NVT* simulations. I hypothesize the poor agreement between the computational and experimental ionic conductivities for MTBE is due to the breakdown of the approximations underlying the Nernst–Einstein equation.

Solvent	Ionic Conductivity in S/cm	Experimental Ionic Conductivity in S/cm
DEC	$(2.03 \pm 0.09) \times 10^{-3}$	7.5×10^{-4}
DMA	$(6.2 \pm 0.8) \times 10^{-3}$	1.1×10^{-2}
DME	$(1.8 \pm 0.1) \times 10^{-3}$	9.4×10^{-3}
DMF	$(1.01 \pm 0.05) \times 10^{-2}$	1.5×10^{-2}
DMSO	$(6.3 \pm 0.4) \times 10^{-3}$	8.9×10^{-3}
EC	$(2.2 \pm 0.3) \times 10^{-3}$	6.0×10^{-3}
MeCN	$(6.8 \pm 0.3) \times 10^{-2}$	3.2×10^{-2}
MTBE	$(4.7 \pm 0.6) \times 10^{-3}$	1.6×10^{-5}
PC	$(1.4 \pm 0.1) \times 10^{-3}$	5.0×10^{-3}
Py	$(5 \pm 1) \times 10^{-3}$	9.7×10^{-3}
SL	$(5.8 \pm 0.6) \times 10^{-4}$	2.1×10^{-3}
THF	$(6.9 \pm 0.8) \times 10^{-3}$	8.0×10^{-3}

Table 14: Computational and experimental ionic conductivities for solvent–LiTFSI systems, with error reflecting variation between simulations.

3.3.2 Properties, Trends, and Insights Into Lithium Transport Mechanisms

Diffusion coefficients for Li^+ ions, $TFSI^-$ counter anions, and solvent molecules in the different solvent–LiTFSI systems are included in Table 15. Also included again as a point of reference are the computational ionic conductivities calculated from the Li^+ and $TFSI^-$ diffusion coefficient using the Nernst–Einstein equation; these were previously listed with the experimental ionic conductivities in Table 14.

Solvent	Lithium Diffusion Coefficient in cm²/s	TFSI Diffusion Coefficient in cm²/s	Solvent Diffusion Coefficient in cm²/s	Ionic Conductivity in S/cm
DEC	$(5.6 \pm 0.3) \times 10^{-7}$	$(5.7 \pm 0.3) \times 10^{-7}$	$(4.5 \pm 0.2) \times 10^{-6}$	$(2.03 \pm 0.09) \times 10^{-3}$
DMA	$(1.2 \pm 0.7) \times 10^{-6}$	$(1.6 \pm 0.4) \times 10^{-6}$	$(4.25 \pm 0.06) \times 10^{-6}$	$(6.2 \pm 0.8) \times 10^{-3}$
DME	$(3.4 \pm 0.3) \times 10^{-7}$	$(5.2 \pm 0.4) \times 10^{-7}$	$(1.12 \pm 0.03) \times 10^{-6}$	$(1.8 \pm 0.1) \times 10^{-3}$
DMF	$(1.7 \pm 0.1) \times 10^{-6}$	$(2.2 \pm 0.2) \times 10^{-6}$	$(5.68 \pm 0.04) \times 10^{-6}$	$(1.01 \pm 0.05) \times 10^{-2}$
DMSO	$(9 \pm 1) \times 10^{-7}$	$(1.30 \pm 0.08) \times 10^{-6}$	$(2.60 \pm 0.07) \times 10^{-6}$	$(6.3 \pm 0.4) \times 10^{-3}$
EC	$(3.3 \pm 0.2) \times 10^{-7}$	$(4.1 \pm 0.9) \times 10^{-7}$	$(1.41 \pm 0.01) \times 10^{-6}$	$(2.2 \pm 0.3) \times 10^{-3}$
MeCN	$(9.4 \pm 0.8) \times 10^{-6}$	$(9.3 \pm 0.4) \times 10^{-6}$	$(2.19 \pm 0.06) \times 10^{-5}$	$(6.8 \pm 0.3) \times 10^{-2}$
MTBE	$(1.3 \pm 0.2) \times 10^{-6}$	$(1.3 \pm 0.3) \times 10^{-6}$	$(1.51 \pm 0.02) \times 10^{-5}$	$(4.7 \pm 0.6) \times 10^{-3}$
PC	$(2.6 \pm 0.1) \times 10^{-7}$	$(3.1 \pm 0.4) \times 10^{-7}$	$(1.07 \pm 0.05) \times 10^{-6}$	$(1.4 \pm 0.1) \times 10^{-3}$
Py	$(1.1 \pm 0.3) \times 10^{-6}$	$(1.1 \pm 0.3) \times 10^{-6}$	$(6.5 \pm 0.2) \times 10^{-6}$	$(5 \pm 1) \times 10^{-3}$
SL	$(7 \pm 1) \times 10^{-8}$	$(1.9 \pm 0.2) \times 10^{-7}$	$(3.5 \pm 0.2) \times 10^{-7}$	$(5.8 \pm 0.6) \times 10^{-4}$
THF	$(1.4 \pm 0.2) \times 10^{-6}$	$(1.4 \pm 0.2) \times 10^{-6}$	$(1.26 \pm 0.01) \times 10^{-5}$	$(6.9 \pm 0.8) \times 10^{-3}$

Table 15: Computational diffusion coefficients and ionic conductivities, with error reflecting variation between simulations.

While the computational and experimental ionic conductivities were discussed above, the relationship between the computational lithium diffusion coefficients and the computational viscosities for the different systems is shown in Figure 13. There is a general trend of decreasing lithium diffusion coefficient with increasing viscosity, as would be expected given that particles have reduced mobility in more viscous liquids. This is a good check that the simulation results model the expected physical behavior.
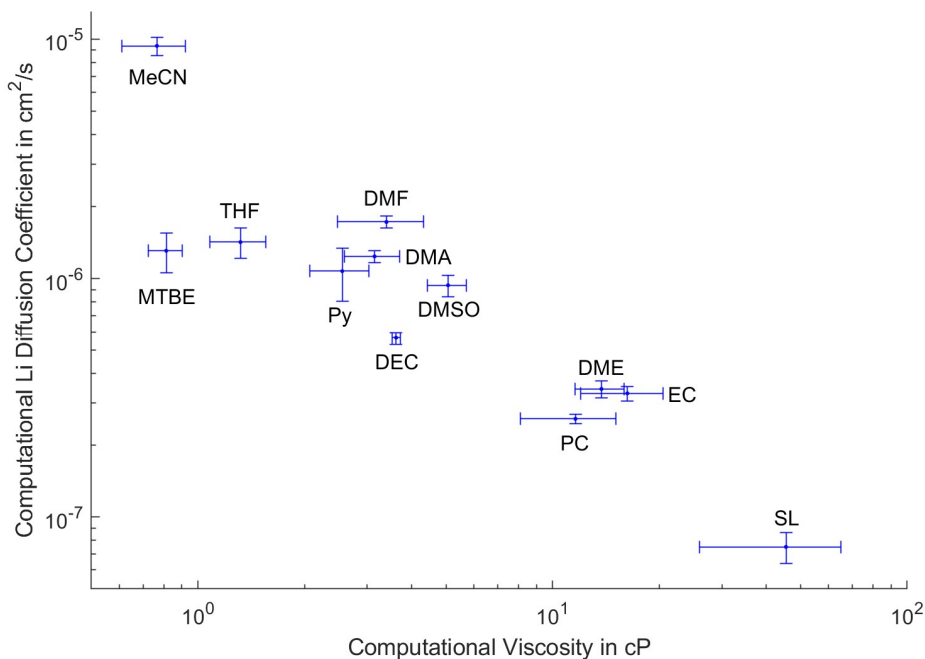
Figure 13: Computational viscosity vs. computational lithium diffusion coefficient. The expected trend of decreasing diffusion coefficient with increasing viscosity is evident.

Another check of the physical accuracy of the simulations was performed using the coordination numbers, which are displayed in Figure 14 and included in Table 16. In my previous work using OPLS for AIMD equilibration and in past studies in the literature, the total lithium coordination number was generally between 4 and 6.[151,152] This was found to be true in two thirds of the systems examined here, as can be seen in Figure 14. The systems where this was not true had lower total coordination numbers, and in all but one of these cases, the Li–TFSI coordination number was high (> 0.7). The TFSI⁻ anion is larger than any of the solvent molecules: TFSI had an average radius of gyration of ~2.57 Å in the simulations, while the average radius of gyration for the solvent molecules varied from 1.17 Å for MeCN to 2.31 Å for DEC (all radii of gyration are included in Table 17). Therefore, it is not surprising that a higher degree of Li–TFSI coordination correlates with a lower overall coordination number, as the TFSI⁻ anion takes up

more physical space in the lithium coordination shell than a solvent molecule does. The only

system with a low overall coordination number but also a low degree of Li–TFSI coordination

was for the DME solvent, which can have either monodentate or bidentate coordination with a

Li$^+$ ion due to its two oxygen molecules. Therefore, fewer total solvent molecules would be

required to surround a Li$^+$ ion with 4 to 6 oxygen atoms compared to other solvents that can only

have monodentate coordination.
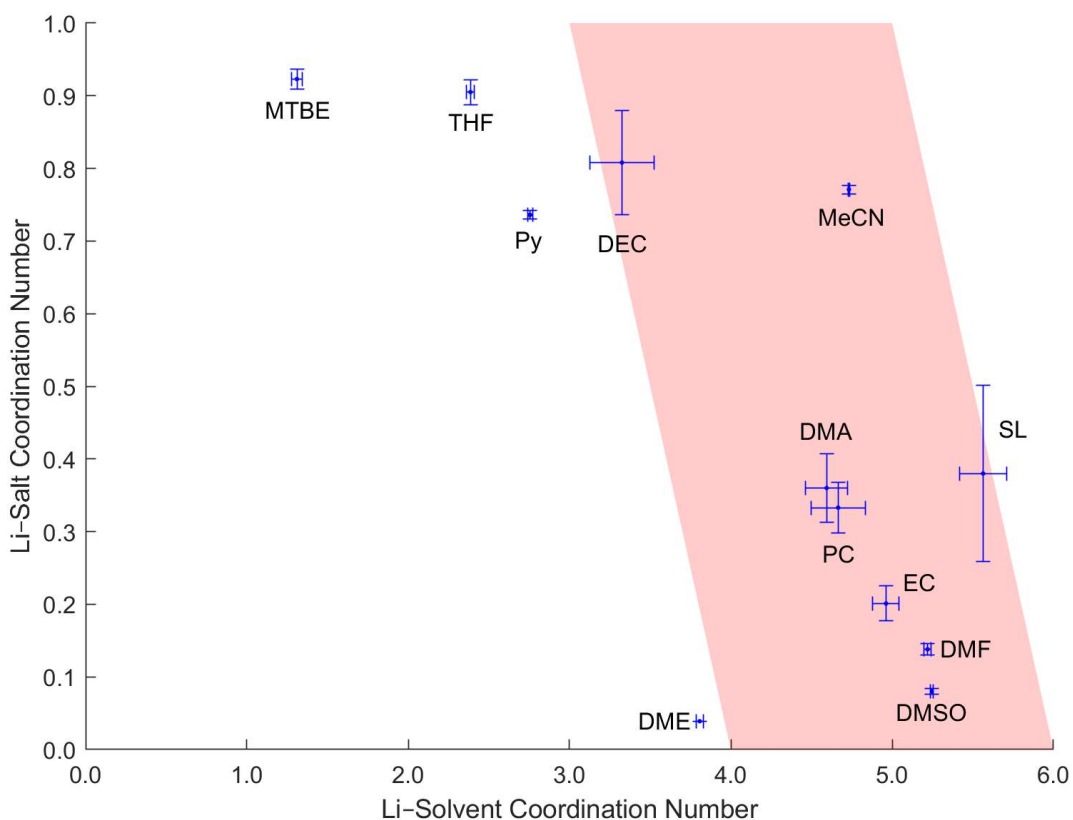
Figure 14: Computational lithium–solvent coordination number vs. computational lithium–salt coordination number. The red region corresponds to a total lithium coordination number of between 4 and 6. Most systems fall in this region, which agrees with past studies and my prior work.[151,152]

Solvent	Li–Solvent Coordination #	Li–TFSI Coordination #	Total Li Coordination # [a]
DEC	3.3 ± 0.2	0.81 ± 0.07	4.1 ± 0.1
DMA	4.6 ± 0.1	0.36 ± 0.05	4.95 ± 0.08
DME	3.81 ± 0.02	0.039 ± 0.004	3.85 ± 0.02
DMF	5.22 ± 0.02	0.138 ± 0.008	5.36 ± 0.01
DMSO	5.246 ± 0.009	0.080 ± 0.004	5.326 ± 0.006
EC	4.96 ± 0.08	0.20 ± 0.02	5.16 ± 0.06
MeCN	4.732 ± 0.003	0.771 ± 0.006	5.503 ± 0.008
MTBE	1.31 ± 0.04	0.92 ± 0.01	2.23 ± 0.03
PC	4.7 ± 0.2	0.33 ± 0.04	5.0 ± 0.1
Py	2.75 ± 0.02	0.736 ± 0.006	3.49 ± 0.01
SL	5.6 ± 0.1	0.4 ± 0.1	5.94 ± 0.02
THF	2.39 ± 0.03	0.90 ± 0.02	3.29 ± 0.02

Table 16: Computational coordination numbers for the first solvation shell of lithium, with error reflecting variation between simulations. (a) Total coordination numbers were calculated separately and therefore may not exactly equal the sum of the Li–solvent and Li–TFSI coordination numbers due to rounding.

Having evaluated the accuracy of the simulation methods, I can now examine what properties influence the lithium transport mechanisms in different systems. The transport ratios for the different Li–solvent systems as well as the remaining properties used in the transport ratio calculation and the Li–TFSI residence times as a comparison point for the Li–solvent residence times are included in Table 17. The Li–TFSI residence times generally have significantly larger variation between runs compared to the Li–solvent residence times due to the lower degree of Li–TFSI coordination compared to Li–solvent coordination, as this results in fewer association/dissociation events to average over for TFSI in the lithium coordination shell.

The residence time results combined with the lower degree of Li–TFSI coordination compared to Li–solvent coordination support my earlier assumption that vehicular motion and solvent

exchange are the dominant mechanisms of lithium transport, with salt exchange (net motion of a Li^+ ion because a $TFSI^-$ counter anion exits or enters the solvation shell of the Li^+ ion) contributing much less. The Li–TFSI residence time is longer than the Li–solvent residence time for most systems, meaning that there are fewer Li–TFSI association/dissociation events than Li–solvent association/dissociation events to contribute to the motion of the Li^+ ions. In the few systems where the Li–TFSI residence time is shorter than the Li–solvent residence time, the Li–TFSI coordination number is low (< 0.4), so there again must be few Li–TFSI dissociation events that can contribute to the motion of the Li^+ ions. As such, the initial assumption that vehicular motion and solvent exchange are the dominant mechanisms seems reasonable, and I can thus proceed to use the transport ratio, which relies on this assumption.

| Solvent	Li–Solvent Residence Time in ns	Li–TFSI Residence Time in ns [a]	Solvent Radius of Gyration	TFSI Radius of Gyration	Transport Ratio
DEC	12.8 ± 0.6	19 ± 1	2.307	2.57	19.4
DMA	2.77 ± 0.09	4 ± 1	1.691	2.57	17.0
DME	7.9 ± 0.2	30 ± 31 [b]	2.028	2.56	8.9
DMF	1.50 ± 0.04	0.5 ± 0.1	1.545	2.57	15.3
DMSO	1.85 ± 0.06	1.2 ± 0.4	1.313	2.56	14.1
EC	3.7 ± 0.3	2.9 ± 0.7	1.439	2.56	7.9
MeCN	0.108 ± 0.000 [c]	0.123 ± 0.001	1.172	2.57	10.0
MTBE	6.8 ± 0.9	17 ± 3	1.670	2.56	47.1
PC	5.5 ± 0.2	8 ± 2	1.679	2.56	6.5
Py	1.8 ± 0.1	7.0 ± 0.7	1.477	2.58	12.1
SL	28 ± 2	15 ± 5	1.674	2.56	10.2
THF	2.1 ± 0.1	13 ± 2	1.364	2.58	22.8

Table 17: Computational residences times, radii of gyration, and transport ratios, with error reflecting variation between simulations. (a) The TFSI calculations have relatively large error compared to the solvent calculations because LiTFSI is fairly dissociated in most of these systems. There are thus fewer TFSI⁻ anions in the lithium solvation shells, and the residence times are averaged over a relatively small number of Li–TFSI dimers. (b) LiTFSI is almost completely dissociated in DME, so there are few TFSI⁻ anions in the lithium solvation shells. Thus, the Li–TFSI residence time has large uncertainty. (c) Results are only reported to 1 ps accuracy given that the trajectory is outputted and saved only every 0.1 ps.

Having established the validity of the transport ratio for these systems, I was interested in novel ways to use the transport ratio and the insights it provides into the atomistic behavior of the systems. Different solvent metrics versus the lithium transport ratio for the different Li–solvent systems are shown in Figures 15 and 16. In both cases, the solvent metric is created by combining different solvent properties that can be fairly straightforwardly measured experimentally and that are expected to relate to the transport mechanism, as will be explained below. The goal is to correlate easy to measure experimental properties with the lithium transport mechanisms in different systems and ultimately predict the dominant lithium transport

mechanism for new systems without needing to perform simulations. As stated earlier, vehicular transport is generally faster than transport via solvent exchange,[140] so understanding the transport mechanisms gives insight into overall performance. In Figure 15, the solvent metric is the solvent donor number in kcal/mol divided by the experimental viscosity of the solvent–LiTFSI system in cP, with the solvent donor numbers taken from the literature.[153,154] The only exception is the donor number for MTBE, which was estimated from donor number values for other ethers. In Figure 16, the solvent metric is the solvent donor number in kcal/mol divided by the shear modulus at infinite frequency for the pure solvent (G^∞) in GPa.

These solvent properties were chosen because they are expected to relate to the transport mechanisms. Solvent donor number is a measure of the ability of a solvent to solvate cations such as the lithium ions, so it should be inversely correlated with transport via the solvent exchange mechanism. In other words, I would expect solvents with a higher solvent donor number to have less transport via the solvent exchange mechanism because the solvent molecules in the lithium solvation shells are more strongly associated with the lithium ions and thus the solvation shells are more stable with fewer exchange events. In contrast, the viscosity is a measure of the internal friction of the system, and the shear modulus is a measure of the stiffness or rigidity of the system. Both of these properties should be inversely correlated with transport via the vehicular motion mechanism. I would expect solvents with higher viscosities or shear moduli to have less transport via the vehicular motion mechanism because the transport of the lithium solvation shells through the bulk solvent is slow. Thus, for the solvent metrics of solvent donor number / viscosity and solvent donor number / shear modulus, higher values of the metric should correspond to higher transport ratios (more vehicular motion and less motion via

solvent exchange), and indeed, in Figures 15 and 16, there is a trend of increasing lithium transport ratio with increasing value of the solvent metric.
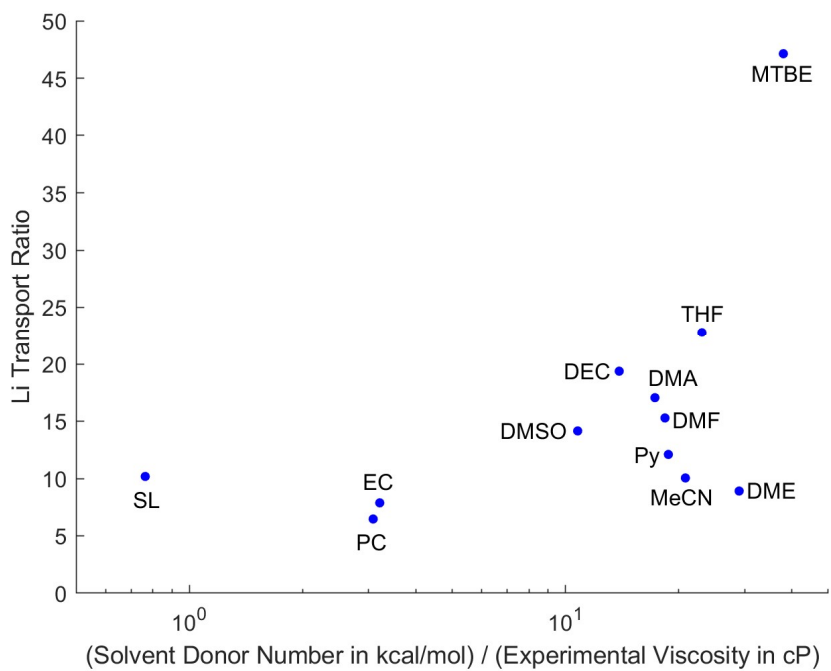
Figure 15: Solvent metric (solvent donor number / viscosity of the solvent–LiTFSI system) vs. computational lithium transport ratio.[153,154]
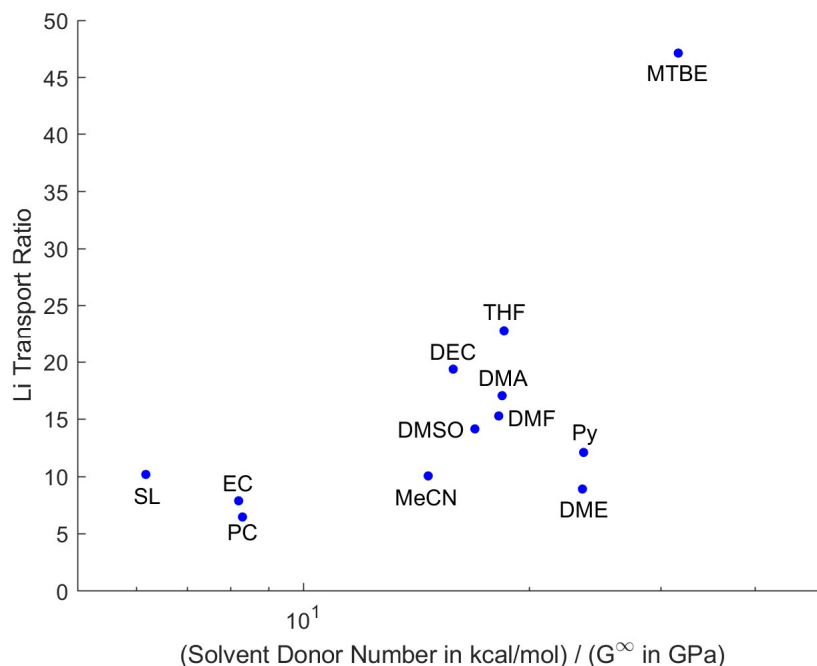
Figure 16: Solvent metric (solvent donor number / shear modulus at infinite frequency for the pure solvent) vs. computational lithium transport ratio.[153,154]

To my knowledge, such a trend between solvent metrics combining different experimentally accessible solvent properties and atomistic ion transport mechanisms has not been previously reported for small molecule liquid systems. I believe it warrants further study, as it could provide a straightforward way to predict atomistic transport properties for new systems without developing a classical MD parametrization for each new solvent molecule. Thus, one method for further examining these trends would be to add additional solvents, which I am interested in doing in the future and encourage others to explore. However, a second method to investigate these trends is to examine mixtures of different solvents. I have therefore examined the behavior of LiTFSI in EC/MTBE systems with different ratios of the two solvents. EC and MTBE were selected because they have very different values of the solvent metric (for both metrics examined) and of the lithium transport ratio. I thus expect properties of the mixtures to vary

strongly as a function of composition. The results of this study are discussed in the following section.

3.3.3 EC/MTBE Solvent Composition Study

In this study, I examined the behavior of LiTFSI in EC/MTBE systems with three different molar ratios for the solvents: 25:75, 50:50, and 75:25. In each case, there were still 2,000 solvent molecules total and 120 LiTFSI molecules, and other simulation properties were unchanged, including running three independent simulations for each system. As one test of my simulations, I examined the viscosity as a function of the solvent composition, and the results are shown in Figure 17. The EC–LiTFSI system has a signficantly higher viscosity than the MTBE–LiTFSI system (a computational viscosity of 16 ± 4 cP for the EC–LiTFSI system vs. a computational viscosity of 0.81 ± 0.09 cP for the MTBE–LiTFSI system; values in Table 13). Thus, I expected the viscosity to increase as the mole fraction of EC increases, and this is indeed what is observed.
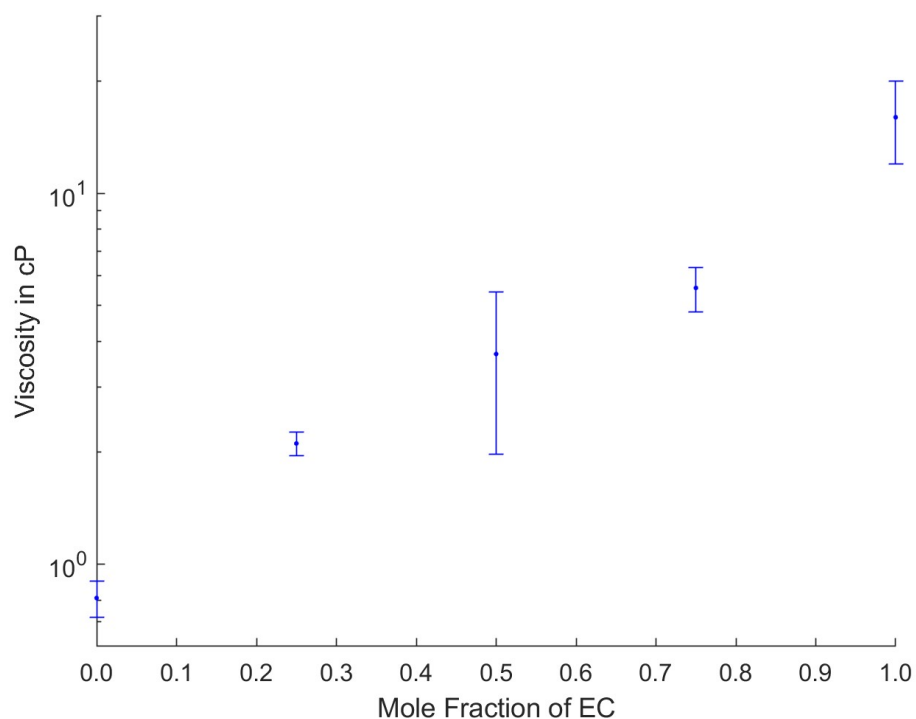
Figure 17: Viscosity as a function of solvent composition for the EC/MTBE–LiTFSI systems.

A more interesting property to examine for insights into the effect of solvent composition is the Li$^+$-ion coordination environment. The Li–EC, Li–MTBE, Li–TFSI, and total coordination numbers as a function of solvent composition are shown in Figure 18. In every system except the one with no EC solvent, EC molecules dominate the lithium solvation shells. Additionally, there are on average more TFSI$^-$ counter anions than MTBE solvent molecules in the lithium solvation shell. This was a very interesting result, as adding even a relatively small fraction of EC to the MTBE solvent drastically changes the lithium solvation environment. I would expect this to significantly affect how lithium is transported, as the two primary lithium transport mechanisms, the vehicular transport mechanism and the solvent exchange mechanism, both depend on the size and stability of the lithium solvation shell. This can be investigated by examining the lithium transport ratio.
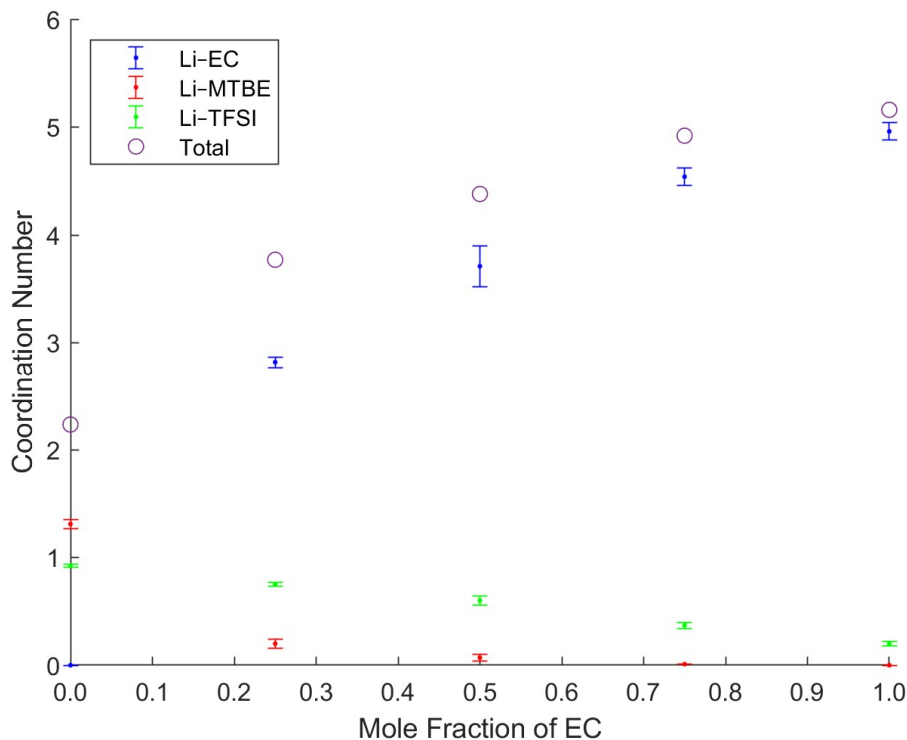
Figure 18: Li–EC, Li–MTBE, Li–TFSI, and total coordination numbers as a function of solvent composition for the EC/MTBE–LiTFSI systems.

The lithium transport ratio is not a perfect descriptor for mixed solvent systems, as it depends on the solvent radius of gyration and the average residence time of a solvent molecule in a lithium solvation shell and does not have a clean way to combine contributions from different solvents. However, in the EC/MTBE systems, lithium is far more likely to be coordinated by EC molecules than by MTBE molecules. Thus, I can calculate the lithium transport ratio using just the EC radius of gyration and average residence time and neglect the MTBE contribution. This is similar to my previously neglecting the contribution of interactions between the Li^+ ions and the $TFSI^-$ counter anions on the lithium transport behavior because the lithium solvation shells are dominated by solvent molecules and not $TFSI^-$ counter anions.

The resulting lithium transport ratio is shown as a function of the solvent composition in Figure 19. Systems with more MTBE and less EC had a higher lithium transport ratio. On the one hand, this was expected as the MTBE–LiTFSI system had a much higher transport ratio than the EC–LiTFSI system did (47.1 vs. 7.9). Also, the viscosity of the EC/MTBE systems decreased as the mole fraction of EC decreased, which should generally lead to increased ion mobility and increased vehicular motion. However, it was still interesting that the lithium transport ratio had such as strong correlation with the EC mole fraction even though the lithium coordination shell was dominated by EC in all of the systems. These results suggest that for the systems with a low fraction of EC, the lithium solvation shell is primarily composed of EC molecules and is fairly stable. However, the solvation shell can move farther before undergoing any association/dissociation events in the EC/MTBE systems than it could in the pure EC solvent because it is moving through a significantly less viscous solvent. Thus, the vehicular transport mechanism is more dominant over the solvent exchange mechanism for the EC/MTBE systems than for the EC system, which corresponds to a higher lithium transport ratio.
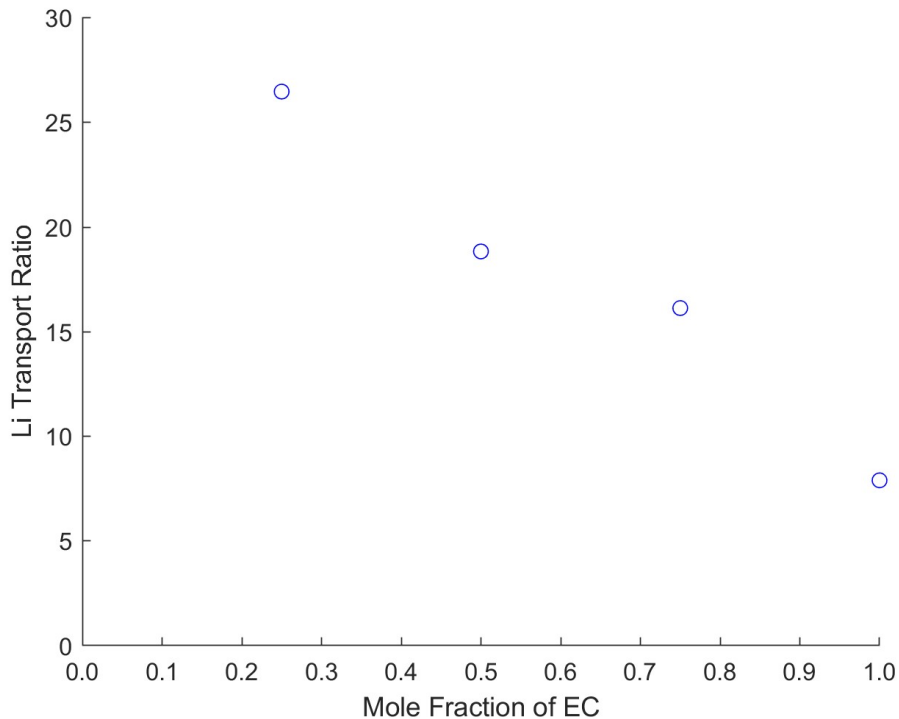
Figure 19: Lithium transport ratio using EC as solvent as a function of solvent composition for the EC/MTBE–LiTFSI systems.

3.4 Conclusions

These results suggest a way to look for combinations of solvents that could facilitate lithium transport while optimizing other solvent properties. I have examined only transport-related properties here, but there can be many other considerations in selecting a solvent ranging from thermal stability to melting point to cost. If a given solvent is considered desirable for one of its non-transport properties, measurements of properties such as its donor number, viscosity, and/or shear modulus at infinite frequency could predict the mechanism by which lithium ions are transported in the system without needing to perform new simulations. Knowing the mechanism then gives an indication of how well the solvent would perform in a battery, as a higher lithium transport ratio (more vehicular transport) often corresponds to overall better transport properties.

If the measurements of the given solvent suggest worse transport properties than desired, my work with the EC/MTBE systems gives guidance for how to select other solvents to mix with the given solvent to change the transport properties. For example, if one solvent has a property such as exceptional thermal stability or resistance to solvent decomposition well suited to a given application but has low ionic conductivity due to less vehicular ionic transport, it could be mixed with a solvent where vehicular transport is more dominant to enable faster overall ionic transport.

More research, which could include adding new solvents or examining more mixtures, is needed to further investigate the trend between the solvent metrics and the transport ratio. Additional solvent metrics using different experimental properties could also be examined. However, I believe that there is much potential in the concept of using a metric that captures different solvent properties to predict atomistic behavior such as transport mechanisms that cannot be easily examined experimentally.

4 Conclusions and Broader Impact

This work in this thesis can broadly be described as using atomistic simulation methods to investigate how ions are transported in small molecule liquid electrolyte systems relevant to battery applications, with a focus on lithium–oxygen batteries. However, my research encompasses two different but complementary goals: (1) evaluating and improving the methods used for these atomistic simulations and (2) then using these methods to extract physical insights into various battery systems.

For the methodology development portion of this thesis, I focused on how *ab initio* molecular dynamics simulations are typically performed in the literature and evaluated whether this methodology produces physically accurate, reproducible results. To this end, I compared two *ab initio* molecular dynamics equilibration methods as well as two different classical force fields for simulating how Li^+ ions are coordinated with solvent molecules and counter anions in several common lithium–oxygen battery systems. By comparing the computational behavior of lithium salts in different solvents with the experimental behavior, I found that equilibration with the classical force field that produced more physically accurate behavior in the classical molecular dynamics simulations also resulted in more physically accurate behavior in the *ab initio* molecular dynamics runs compared to the other equilibration methods, illustrating the importance of equilibration methodology. I also demonstrated the importance of averaging coordination number over multiple starting configurations and Li^+ ions, as the majority of Li^+ ions do not undergo a single association or dissociation event even in what is considered a long *ab initio* molecular dynamics simulation and thus do not sample a statistically significant portion of the phase space.

Overall, these results show the importance of both equilibration method and sufficient independent sampling for extracting experimentally relevant quantities from *ab initio* molecular dynamics simulations. This had not been previously systematically studied in the field, and many *ab initio* molecular dynamics papers exist in the literature with no justification for why their chosen equilibration method is sufficient or even with no discussion of their equilibration methods at all. Thus, my work also demonstrates the importance of documenting information on equilibration and sampling methodology in articles to enable reproducibility.

Additionally, my results showed the inherent difficulty and expense of accurately calculating experimentally relevant quantities using from *ab initio* molecular dynamics simulations. This motivated my using classical molecular dynamics simulations in the second portion of the thesis focused on extracting physical insights into battery systems, as I could calculate more material properties by using classical molecular dynamics than with *ab initio* molecular dynamics simulations. In this work, I examined a variety of transport properties for solvent–LiTFSI systems with twelve different small molecule liquid solvents commonly used in battery. As my previous research had illustrated the importance of using physically accurate simulation methods, I also evaluated the classical molecular dynamics force fields by calculating computational viscosities, densities, and ionic conductivities for each system and comparing them to experimental data. I finally examined whether more experimentally accessible properties such as viscosity or solvent donor number correlate with the atomistic transport properties and developed solvent metrics such as the donor number / viscosity that correlate with atomistic transport properties. To my knowledge, this work is the first time such combined solvent metrics have been utilized for analyzing ionic transport in small molecule liquid solvents. While the trends found in this work may be more indicative than predictive, they are an important step towards

the ultimate goal of predicting atomistic transport properties without the need to perform simulations. This would allow more efficient screening of new candidate solvents or proposed solvent mixtures.

In all, I hope the work in this thesis will shape how future *ab initio* molecular dynamics studies are performed, with the goal of increased physical accuracy, documentation, and reproducibility. The concept of solvent metrics correlated to ionic transport mechanisms developed here also has the potential to greatly aid in the search for improved battery electrolytes, as such metrics could allow for high-throughput screening of potential solvents without needing to develop force field parameters for and then simulate each system. The need for simulations would not disappear, but they could be more targeted towards systems predicted to have optimal transport properties. This will allow us to continue our development of novel battery technologies, such as lithium–oxygen or lithium–air batteries, needed to conquer hard decarbonization problems such as electric aviation.

5 Appendix: Experimental Methodology

While the work in this thesis is purely computational, the research was performed in collaboration with experimentalists who provided experimental data for comparison and validation. The experimental methodologies are included below; the methodology for the AIMD study is adapted from Crabb et al. (2020).[94]

5.1 Experimental Density Methodology for the AIMD Study

High purity dimethyl sulfoxide (DMSO, Sigma Aldrich, anhydrous, $\geq$ 99.9%) and acetonitrile (MeCN, Sigma Aldrich, anhydrous, $\geq$ 99.8%) were purchased and dried over molecular sieves for at least a week before use. 1,2-dimethoxyethane (DME) was purchased from Acros and was degassed and dried using a Glass Contour Solvent Purification System built by SGWater USA, LLC. Lithium bis(trifluoromethanesulfonyl)imide (LiTFSI, 99.99% extra dry grade provided by Solvay) was used as received. Lithium trifluoromethanesulfonate (LiTfO, Sigma Aldrich, 99.995%) and lithium trifluoroacetate (LiTFA, Alfa Aesar, 97%) were dried at 150°C under vacuum for 48 hours and transferred directly to an argon-filled glovebox (MBraun, < 0.1 ppm H_2O, < 0.1 ppm O_2) without exposure to the ambient. All chemicals were stored in an argon-filled glovebox (MBraun, USA) with H_2O and O_2 content of < 0.1 ppm. Electrolytes were prepared by dissolution of the salt and solvent where proportions were determined based on the mass of salt and solvent. Density measurements were performed with an Anton Paar SVM 3001 at 300 K with three repetitions per measurement.

5.2 Experimental Methodology for the Transport Study

As experimental validation of classical force fields is very important, a collaborator measured experimental densities, viscosities, and ionic conductivities for the twelve solvent–LiTFSI systems used in this study to compare with my computational results. The methodology is included below. For each system, the LiTFSI concentration was the same as that of the corresponding computational system (with all systems having a ratio of 3 LiTFSI molecules to 50 solvent molecules).

5.2.1 Chemicals

High purity dimethyl sulfoxide (DMSO, Sigma Aldrich, anhydrous, $\geq$ 99.9%), N,N-dimethylacetamide (DMA, Sigma Aldrich, anhydrous, $\geq$ 99.8%), N,N-dimethylformamide (DMF, Sigma Aldrich, anhydrous, $\geq$ 99.8%), tert-butyl methyl ether (MTBE, Sigma Aldrich, anhydrous, $\geq$ 99.8%), tetrahydrofuran (THF, Sigma Aldrich, anhydrous, $\geq$ 99.9%, inhibitor-free), acetonitrile (MeCN, Sigma Aldrich, anhydrous, $\geq$ 99.8%), pyridine (Py, Sigma Aldrich, anhydrous, 99.8%) and sulfolane (SL, Thermo Scientific, 99%) were purchased and dried over molecular sieves for at least a week before use. 1,2-dimethoxyethane (DME) was purchased from Acros and was degassed and dried using a Glass Contour Solvent Purification System built by SGWater USA, LLC. Propylene carbonate (PC, BASF Selectilyte), ethylene carbonate (EC, BASF Selectilyte) and diethyl carbonate (DEC, BASF Selectilyte) were used as received. Lithium bis(trifluoromethanesulfonyl)imide (LiTFSI, 99.99% extra dry grade provided by Solvay) was used as received. All chemicals were stored in an argon-filled glovebox (MBraun, USA) with H_2O and O_2 content of < 0.1 ppm. Electrolytes were prepared by dissolution of the desired mass of the salt and solvent. The total H_2O content in the solvents was checked using a

C20 compact Karl Fisher coulometer from Mettler Toledo; for the dry solvent, it was < 20 ppm

for ~2 g of sample. 0.5 M LiTFSI solutions in DMSO and DME had water contents < 40 ppm

indicating no significant water contamination of the salt.

5.2.2 Characterization of Solvent–LiTFSI Systems

Ionic conductivity was measured using the complex impedance method in the frequency range of

1 MHz to 400 mHz with 100 mV amplitude using a Bio-Logic SP-300. The electrolyte was

sealed in a cell containing two platinum-black electrodes (conductivity cell CG-511B, TOA

Electronics), and the cell was thermally equilibrated at 300 K in an environmental chamber

(Espec SU-241) until the impedance spectra stabilized (typically ~30 minutes). The cell constant

of the conductivity cells was determined using an aqueous KCl solution of known conductivity

(Ricca Chemical, 1.413 mS/cm at 25°C). Viscosity and density measurements were performed

with an Anton Paar SVM 3001.

6 Resource Acknowledgements

7 References

(1)   Short-Term Energy Outlook - U.S. Energy Information Administration (EIA) https://www.eia.gov/outlooks/steo/.

(2)   Koebrich, S.; Tian, T.; Chen, E. 2017 Renewable Energy Data Book: Including Data and Trends for Energy Storage and Electric Vehicles. 142.

(3)   Joint Research Centre (European Commission); Tarvydas, D.; Tsiropoulos, I.; Lebedeva, N. *Li-Ion Batteries for Mobility and Stationary Storage Applications: Scenarios for Costs and Market Growth*; Publications Office of the European Union: LU, 2018.

(4)   DAYS | arpa-e.energy.gov https://arpa-e.energy.gov/technologies/programs/days.

(5)   Harmon, J. JCESR Renewed for Another Five Years | Argonne National Laboratory. September 18, 2018.

(6)   Yao, P.; Yu, H.; Ding, Z.; Liu, Y.; Lu, J.; Lavorgna, M.; Wu, J.; Liu, X. Review on Polymer-Based Composite Electrolytes for Lithium Batteries. *Front. Chem.* **2019**, *7*.

(7)   Xu, X.; Hui, K. S.; Dinh, D. A.; Hui, K. N.; Wang, H. Recent Advances in Hybrid Sodium–Air Batteries. *Mater. Horiz.* **2019**, *6* (7), 1306–1335. https://doi.org/10.1039/C8MH01375F.

(8)   Córdoba, D.; Rodríguez, H. B.; Calvo, E. J. Singlet Oxygen Formation during the Oxygen Reduction Reaction in DMSO LiTFSI on Lithium Air Battery Carbon Electrodes. *ChemistrySelect* **2019**, *4* (42), 12304–12307. https://doi.org/10.1002/slct.201904112.

(9)   Leverick, G.; Tatara, R.; Feng, S.; Crabb, E.; France-Lanord, A.; Tułodziecki, M.; Lopez, J.; Stephens, R. M.; Grossman, J. C.; Shao-Horn, Y. Solvent- and Anion-Dependent $Li^{+}-O_2^{-}$ Coupling Strength and Implications on the Thermodynamics and Kinetics of $Li–O_2$ Batteries. *J. Phys. Chem. C* **2020**, *124* (9), 4953–4967. https://doi.org/10.1021/acs.jpcc.9b09968.

(10)   November 2021 | TOP500 https://www.top500.org/lists/top500/2021/11/.

(11)   Vázquez-Montelongo, E. A.; Vázquez-Cervantes, J. E.; Cisneros, G. A. Current Status of AMOEBA–IL: A Multipolar/Polarizable Force Field for Ionic Liquids. *Int. J. Mol. Sci.* **2020**, *21* (3), 697. https://doi.org/10.3390/ijms21030697.

(12)   Xie, T.; France-Lanord, A.; Wang, Y.; Shao-Horn, Y.; Grossman, J. C. Graph Dynamical Networks for Unsupervised Learning of Atomic Scale Dynamics in Materials. *Nat. Commun.* **2019**, *10* (1), 2667. https://doi.org/10.1038/s41467-019-10663-6.

(13)   Zhang, Y.; Xiong, R.; He, H.; Pecht, M. G. Lithium-Ion Battery Remaining Useful Life Prediction With Box–Cox Transformation and Monte Carlo Simulation. *IEEE Trans. Ind. Electron.* **2019**, *66* (2), 1585–1597. https://doi.org/10.1109/TIE.2018.2808918.

(14)   Attarian Shandiz, M.; Gauvin, R. Application of Machine Learning Methods for the Prediction of Crystal System of Cathode Materials in Lithium-Ion Batteries. *Comput. Mater. Sci.* **2016**, *117*, 270–278. https://doi.org/10.1016/j.commatsci.2016.02.021.

(15)   Koerstz, M.; Christensen, A. S.; Mikkelsen, K. V.; Nielsen, M. B.; Jensen, J. H. High Throughput Virtual Screening of 230 Billion Molecular Solar Heat Battery Candidates. **2020**. https://doi.org/10.26434/chemrxiv.8003813.v3.

(16)   Guan, P.; Liu, L.; Lin, X. Simulation and Experiment on Solid Electrolyte Interphase (SEI) Morphology Evolution and Lithium-Ion Diffusion. *J. Electrochem. Soc.* **2015**, *162* (9), A1798. https://doi.org/10.1149/2.0521509jes.

(17)   Fu, C.; Xu, L.; Aquino, F. W.; v. Cresce, A.; Gobet, M.; Greenbaum, S. G.; Xu, K.; Wong, B. M.; Guo, J. Correlating Li^+-Solvation Structure and Its Electrochemical Reaction Kinetics with Sulfur in Subnano Confinement. *J. Phys. Chem. Lett.* **2018**, *9* (7), 1739–1745. https://doi.org/10.1021/acs.jpclett.8b00567.

(18)   Ganesh, P.; Jiang, D.; Kent, P. R. C. Accurate Static and Dynamic Properties of Liquid Electrolytes for Li-Ion Batteries from Ab Initio Molecular Dynamics. *J. Phys. Chem. B* **2011**, *115* (12), 3085–3090. https://doi.org/10.1021/jp2003529.

(19)   Jung, S.; Federici Canova, F.; Akagi, K. Characteristics of Lithium Ions and Superoxide Anions in EMI-TFSI and Dimethyl Sulfoxide. *J. Phys. Chem. A* **2016**, *120* (3), 364–371. https://doi.org/10.1021/acs.jpca.5b09692.

(20)   Leung, K.; Nielsen, I. M. B.; Kurtz, I. *Ab Initio* Molecular Dynamics Study of Carbon Dioxide and Bicarbonate Hydration and the Nucleophilic Attack of Hydroxide on CO_2. *J. Phys. Chem. B* **2007**, *111* (17), 4453–4459. https://doi.org/10.1021/jp068475l.

(21)   Ong, M. T.; Verners, O.; Draeger, E. W.; van Duin, A. C. T.; Lordi, V.; Pask, J. E. Lithium Ion Solvation and Diffusion in Bulk Organic Electrolytes from First-Principles and Classical Reactive Molecular Dynamics. *J. Phys. Chem. B* **2015**, *119* (4), 1535–1545. https://doi.org/10.1021/jp508184f.

(22)   Pham, T. A.; Kweon, K. E.; Samanta, A.; Lordi, V.; Pask, J. E. Solvation and Dynamics of Sodium and Potassium in Ethylene Carbonate from Ab Initio Molecular Dynamics Simulations. *J. Phys. Chem. C* **2017**, *121* (40), 21913–21920. https://doi.org/10.1021/acs.jpcc.7b06457.

(23)   Sogawa, M.; Sawayama, S.; Han, J.; Satou, C.; Ohara, K.; Matsugami, M.; Mimura, H.; Morita, M.; Fujii, K. Role of Solvent Size in Ordered Ionic Structure Formation in Concentrated Electrolytes for Lithium-Ion Batteries. *J. Phys. Chem. C* **2019**, *123* (14), 8699–8708. https://doi.org/10.1021/acs.jpcc.9b01038.

(24)   Saitoh, K.; Takai, Y.; Sato, T.; Takuma, M.; Takahashi, Y. Optimization of LIB Electrolyte and Exploration of Novel Compounds via the Molecular Dynamics Method. *Batteries* **2022**, *8* (3), 27. https://doi.org/10.3390/batteries8030027.

(25)   Khetan, A.; Arjmandi, H. R.; Pande, V.; Pitsch, H.; Viswanathan, V. Understanding Ion Pairing in High-Salt Concentration Electrolytes Using Classical Molecular Dynamics Simulations and Its Implications for Nonaqueous $Li–O_2$ Batteries. *J. Phys. Chem. C* **2018**, *122* (15), 8094–8101. https://doi.org/10.1021/acs.jpcc.8b00944.

(26)   Caro, M. A.; Lopez-Acevedo, O.; Laurila, T. Redox Potentials from Ab Initio Molecular Dynamics and Explicit Entropy Calculations: Application to Transition Metals in Aqueous Solution. *J. Chem. Theory Comput.* **2017**, *13* (8), 3432–3441. https://doi.org/10.1021/acs.jctc.7b00314.

(27) Cheng, L.; Redfern, P.; Lau, K. C.; Assary, R. S.; Narayanan, B.; Curtiss, L. A. Computational Studies of Solubilities of LiO_2 and Li_2O_2 in Aprotic Solvents. *J. Electrochem. Soc.* **2017**, *164* (11), E3696. https://doi.org/10.1149/2.0721711jes.

(28) Scheers, J.; Lidberg, D.; Sodeyama, K.; Futera, Z.; Tateyama, Y. Life of Superoxide in Aprotic Li–O_2 Battery Electrolytes: Simulated Solvent and Counter-Ion Effects. *Phys. Chem. Chem. Phys.* **2016**, *18* (15), 9961–9968. https://doi.org/10.1039/C5CP08056H.

(29) Du, Z.; Wood, D. L.; Belharouak, I. Enabling Fast Charging of High Energy Density Li-Ion Cells with High Lithium Ion Transport Electrolytes. *Electrochem. Commun.* **2019**, *103*, 109–113. https://doi.org/10.1016/j.elecom.2019.04.013.

(30) Government of Canada, C. E. R. NEB – Market Snapshot: Average electric vehicle range almost doubled in the last six years https://www.cer-rec.gc.ca/en/data-analysis/energy-markets/market-snapshots/2019/market-snapshot-average-electric-vehicle-range-almost-doubled-in-last-six-years.html.

(31) FOTW# 1167, January 4, 2021: Median Driving Range of All-Electric Vehicles Tops 250 Miles for Model Year 2020 https://www.energy.gov/eere/vehicles/articles/fotw-1167-january-4-2021-median-driving-range-all-electric-vehicles-tops-250.

(32) Bills, A.; Sripad, S.; Fredericks, W. L.; Singh, M.; Viswanathan, V. Performance Metrics Required of Next-Generation Batteries to Electrify Commercial Aircraft. *ACS Energy Lett.* **2020**, *5* (2), 663–668. https://doi.org/10.1021/acsenergylett.9b02574.

(33) Schäfer, A. W.; Barrett, S. R. H.; Doyme, K.; Dray, L. M.; Gnadt, A. R.; Self, R.; O'Sullivan, A.; Synodinos, A. P.; Torija, A. J. Technological, Economic and Environmental Prospects of All-Electric Aircraft. *Nat. Energy* **2019**, *4* (2), 160–166. https://doi.org/10.1038/s41560-018-0294-x.

(34) Alternative Fuels Data Center. Batteries for Hybrid and Plug-In Electric Vehicles https://afdc.energy.gov/vehicles/electric_batteries.html.

(35) Asenbauer, J.; Eisenmann, T.; Kuenzel, M.; Kazzazi, A.; Chen, Z.; Bresser, D. The Success Story of Graphite as a Lithium-Ion Anode Material – Fundamentals, Remaining Challenges, and Recent Developments Including Silicon (Oxide) Composites. *Sustain. Energy Fuels* **2020**, *4* (11), 5387–5416. https://doi.org/10.1039/D0SE00175A.

(36) Schweidler, S.; de Biasi, L.; Schiele, A.; Hartmann, P.; Brezesinski, T.; Janek, J. Volume Changes of Graphite Anodes Revisited: A Combined Operando X-Ray Diffraction and In Situ Pressure Analysis Study. *J. Phys. Chem. C* **2018**, *122* (16), 8829–8835. https://doi.org/10.1021/acs.jpcc.8b01873.

(37) An, S. J.; Li, J.; Daniel, C.; Mohanty, D.; Nagpure, S.; Wood, D. L. The State of Understanding of the Lithium-Ion-Battery Graphite Solid Electrolyte Interphase (SEI) and Its Relationship to Formation Cycling. *Carbon* **2016**, *105*, 52–76. https://doi.org/10.1016/j.carbon.2016.04.008.

(38) Lead Acid Battery Systems - an overview | ScienceDirect Topics https://www.sciencedirect.com/topics/engineering/lead-acid-battery-systems.

(39) Fact #607: January 25, 2010 Energy and Power by Battery Type https://www.energy.gov/eere/vehicles/fact-607-january-25-2010-energy-and-power-battery-type.

(40) Liu, K.; Liu, Y.; Lin, D.; Pei, A.; Cui, Y. Materials for Lithium-Ion Battery Safety. *Sci. Adv.* **2018**. https://doi.org/10.1126/sciadv.aas9820.

(41) BU-808c: Coulombic and Energy Efficiency with the Battery https://batteryuniversity.com/article/bu-808c-coulombic-and-energy-efficiency-with-the-battery.

(42) The Complete Guide to Lithium vs Lead Acid Batteries https://www.power-sonic.com/blog/lithium-vs-lead-acid-batteries/.

(43) Chen, X.; Yao, N.; Zeng, B.-S.; Zhang, Q. Ion–Solvent Chemistry in Lithium Battery Electrolytes: From Mono-Solvent to Multi-Solvent Complexes. *Fundam. Res.* **2021**, *1* (4), 393–398. https://doi.org/10.1016/j.fmre.2021.06.011.

(44) Lamb, J.; Orendorff, C. J.; Roth, E. P.; Langendorf, J. Studies on the Thermal Breakdown of Common Li-Ion Battery Electrolyte Components. *J. Electrochem. Soc.* **2015**, *162* (10), A2131–A2135. https://doi.org/10.1149/2.0651510jes.

(45) Lavi, O.; Luski, S.; Shpigel, N.; Menachem, C.; Pomerantz, Z.; Elias, Y.; Aurbach, D. Electrolyte Solutions for Rechargeable Li-Ion Batteries Based on Fluorinated Solvents. *ACS Appl. Energy Mater.* **2020**, *3* (8), 7485–7499. https://doi.org/10.1021/acsaem.0c00898.

(46) Zhang, S. S. Insight into the Gassing Problem of Li-Ion Battery. *Front. Energy Res.* **2014**, *2*.

(47) Berhaut, C. L.; Dedryvère, R.; Timperman, L.; Schmidt, G.; Lemordant, D.; Anouti, M. A New Solvent Mixture for Use of LiTDI as Electrolyte Salt in Li-Ion Batteries. *Electrochimica Acta* **2019**, *305*, 534–546. https://doi.org/10.1016/j.electacta.2019.02.097.

(48) Ströbel, M.; Kiefer, L.; Birke, K. P. Investigation of a Novel Ecofriendly Electrolyte-Solvent for Lithium-Ion Batteries with Increased Thermal Stability. *Batteries* **2021**, *7* (4), 72. https://doi.org/10.3390/batteries7040072.

(49) 6 electric aviation companies to keep on your radar | Greenbiz https://www.greenbiz.com/article/6-electric-aviation-companies-keep-your-radar.

(50) Ma, K. H., Tammy. Electric Aviation Could Be Closer Than You Think https://www.scientificamerican.com/article/electric-aviation-could-be-closer-than-you-think/.

(51) Eviation's Maiden Flight Could Usher in Electric Aviation Era https://spectrum.ieee.org/eviations-maiden-flight-to-usher-in-era-of-electric-aviation.

(52) Home | Airflow https://www.airflow.aero/.

(53) Beta Technologies ALIA https://evtol.news/beta-technologies-alia.

(54) FAQ | Heart Aerospace.

(55) Borrás, J. Hybrid Electric Aircraft Builder Electra Secures Series A Funding from Lockheed Martin. *Electrek*, 2022.

(56) Electric flight | Airbus https://www.airbus.com/en/innovation/zero-emission/electric-flight.

(57) Alcock, C. Wright Takes BAe 146 Fast-Track to Electric Airliner Market https://www.ainonline.com/aviation-news/air-transport/2021-11-04/wright-takes-bae-146-fast-track-electric-airliner-market.

(58) Universal Hydrogen | Fueling Carbon-Free Flight https://hydrogen.aero/.

(59) First Practical Zero Emission Aviation Powertrain | USA & UK https://www.zeroavia.com.

(60) Lithium batteries https://www.doitpoms.ac.uk/tlplib/batteries/batteries_lithium.php.

(61) Jet Fuel | Glossary | Marquard & Bahls https://www.marquard-bahls.com/en/news-info/glossary/detail/term/jet-fuel-german-kerosin.html.

(62) Decarbonization in Aviation: 4 Ways the Industry Is Moving Forward. *National Aviation Academy*, 2021.

(63) Reichmann, K. Why Industry Experts Are Saying Decarbonization Efforts in the Aviation Industry Are Different This Time Around. *Aviation Today*. July 19, 2021.

(64) With Ultralight Lithium-Sulfur Batteries, Electric Airplanes Could Finally Take Off https://spectrum.ieee.org/with-ultralight-lithiumsulfur-batteries-electric-airplanes-could-finally-take-off.

(65) Vetter, D. How This Tesla-Busting Battery Could Be The 'Holy Grail' For Electric Flight https://www.forbes.com/sites/davidrvetter/2022/02/01/how-this-tesla-busting-battery-could-be-the-holy-grail-for-electric-flight/.

(66) Lithium-Air Battery - an overview | ScienceDirect Topics https://www.sciencedirect.com/topics/engineering/lithium-air-battery.

(67) Massé, R. C.; Liu, C.; Li, Y.; Mai, L.; Cao, G. Energy Storage through Intercalation Reactions: Electrodes for Rechargeable Batteries. *Natl. Sci. Rev.* **2017**, *4* (1), 26–53. https://doi.org/10.1093/nsr/nww093.

(68) Girishkumar, G.; McCloskey, B.; Luntz, A. C.; Swanson, S.; Wilcke, W. Lithium−Air Battery: Promise and Challenges. *J. Phys. Chem. Lett.* **2010**, *1* (14), 2193–2203. https://doi.org/10.1021/jz1005384.

(69) Aetukuri, N. B.; McCloskey, B. D.; García, J. M.; Krupp, L. E.; Viswanathan, V.; Luntz, A. C. Solvating Additives Drive Solution-Mediated Electrochemistry and Enhance Toroid Growth in Non-Aqueous Li–O_2 Batteries. *Nat. Chem.* **2015**, *7* (1), 50–56. https://doi.org/10.1038/nchem.2132.

(70) Abraham, K. M. A Brief History of Non-Aqueous Metal-Air Batteries. *ECS Trans.* **2019**, *3* (42), 67–71. https://doi.org/10.1149/1.2838193.

(71) Miao, R.; Yang, J.; Xu, Z.; Wang, J.; Nuli, Y.; Sun, L. A New Ether-Based Electrolyte for Dendrite-Free Lithium-Metal Based Rechargeable Batteries. *Sci. Rep.* **2016**, *6* (1), 21771. https://doi.org/10.1038/srep21771.

(72)   Bocharova, V.; Sokolov, A. P. Perspectives for Polymer Electrolytes: A View from Fundamentals of Ionic Conductivity. *Macromolecules* **2020**, *53* (11), 4141–4157. https://doi.org/10.1021/acs.macromol.9b02742.

(73)   de Klerk, N. J. J.; Wagemaker, M. Space-Charge Layers in All-Solid-State Batteries; Important or Negligible? *ACS Appl. Energy Mater.* **2018**, *1* (10), 5609–5618. https://doi.org/10.1021/acsaem.8b01141.

(74)   Uddin, M.-J.; Cho, S.-J. Reassessing the Bulk Ionic Conductivity of Solid-State Electrolytes. *Sustain. Energy Fuels* **2018**, *2* (7), 1458–1462. https://doi.org/10.1039/C8SE00139A.

(75)   Numerical Integration of Newton's Equation of Motion https://www.compadre.org/PICUP/resources/Numerical-Integration/.

(76)   Brooks, B. R.; Bruccoleri, R. E.; Olafson, B. D.; States, D. J.; Swaminathan, S.; Karplus, M. CHARMM: A Program for Macromolecular Energy, Minimization, and Dynamics Calculations. *J. Comput. Chem.* **1983**, *4* (2), 187–217. https://doi.org/10.1002/jcc.540040211.

(77)   Christen, M.; Hünenberger, P. H.; Bakowies, D.; Baron, R.; Bürgi, R.; Geerke, D. P.; Heinz, T. N.; Kastenholz, M. A.; Kräutler, V.; Oostenbrink, C.; Peter, C.; Trzesniak, D.; van Gunsteren, W. F. The GROMOS Software for Biomolecular Simulation: GROMOS05. *J. Comput. Chem.* **2005**, *26* (16), 1719–1751. https://doi.org/10.1002/jcc.20303.

(78)   Wang, J.; Wolf, R. M.; Caldwell, J. W.; Kollman, P. A.; Case, D. A. Development and Testing of a General Amber Force Field. *J. Comput. Chem.* **2004**, *25* (9), 1157–1174. https://doi.org/10.1002/jcc.20035.

(79)   van Duin, A. C. T.; Dasgupta, S.; Lorant, F.; Goddard, W. A. ReaxFF: A Reactive Force Field for Hydrocarbons. *J. Phys. Chem. A* **2001**, *105* (41), 9396–9409. https://doi.org/10.1021/jp004368u.

(80)   4.3. Parallel algorithms — LAMMPS documentation https://docs.lammps.org/Developer_parallel.html.

(81)   Maple, J. R.; Dinur, U.; Hagler, A. T. Derivation of Force Fields for Molecular Mechanics and Dynamics from *Ab Initio* Energy Surfaces. *Proc. Natl. Acad. Sci.* **1988**, *85* (15), 5350–5354. https://doi.org/10.1073/pnas.85.15.5350.

(82)   Sun, H. COMPASS: An Ab Initio Force-Field Optimized for Condensed-Phase ApplicationsOverview with Details on Alkane and Benzene Compounds. *J. Phys. Chem. B* **1998**, *102* (38), 7338–7364. https://doi.org/10.1021/jp980939v.

(83)   Anderson, P. M.; Wilson, M. R. Developing a Force Field for Simulation of Poly(Ethylene Oxide) Based upon *Ab Initio* Calculations of 1,2-Dimethoxyethane. *Mol. Phys.* **2005**, *103* (1), 89–97. https://doi.org/10.1080/00268970412331293811.

(84)   Kubisiak, P.; Eilmes, A. Solvation of Mg_2^+ Ions in Mg(TFSI)$_2$–Dimethoxyethane Electrolytes—A View from Molecular Dynamics Simulations. *J. Phys. Chem. C* **2018**, *122* (24), 12615–12622. https://doi.org/10.1021/acs.jpcc.8b02460.

(85) Lei, Y.; Li, H.; Han, S. An All-Atom Simulation Study on Intermolecular Interaction of DMSO–Water System. *Chem. Phys. Lett.* **2003**, *380* (5), 542–548. https://doi.org/10.1016/j.cplett.2003.09.064.

(86) Price, M. L. P.; Ostrovsky, D.; Jorgensen, W. L. Gas-Phase and Liquid-State Properties of Esters, Nitriles, and Nitro Compounds with the OPLS-AA Force Field. *J. Comput. Chem.* **2001**, *22* (13), 1340–1352. https://doi.org/10.1002/jcc.1092.

(87) Jorgensen, W. L.; Maxwell, D. S.; Tirado-Rives, J. Development and Testing of the OPLS All-Atom Force Field on Conformational Energetics and Properties of Organic Liquids. *J. Am. Chem. Soc.* **1996**, *118* (45), 11225–11236. https://doi.org/10.1021/ja9621760.

(88) Hohenberg, P.; Kohn, W. Inhomogeneous Electron Gas. *Phys. Rev.* **1964**, *136* (3B), B864–B871. https://doi.org/10.1103/PhysRev.136.B864.

(89) Kohn, W.; Sham, L. J. Self-Consistent Equations Including Exchange and Correlation Effects. *Phys. Rev.* **1965**, *140* (4A), A1133–A1138. https://doi.org/10.1103/PhysRev.140.A1133.

(90) Baseden, K. A.; Tye, J. W. Introduction to Density Functional Theory: Calculations by Hand on the Helium Atom. *J. Chem. Educ.* **2014**, *91* (12), 2116–2123. https://doi.org/10.1021/ed5004788.

(91) Kohn, W.; Becke, A. D.; Parr, R. G. Density Functional Theory of Electronic Structure. *J. Phys. Chem.* **1996**, *100* (31), 12974–12980. https://doi.org/10.1021/jp960669l.

(92) Carloni, P.; Rothlisberger, U.; Parrinello, M. The Role and Perspective of Ab Initio Molecular Dynamics in the Study of Biological Systems. *Acc. Chem. Res.* **2002**, *35* (6), 455–464. https://doi.org/10.1021/ar010018u.

(93) Kirchner, B.; di Dio, P. J.; Hutter, J. Real-World Predictions from Ab Initio Molecular Dynamics Simulations. In *Multiscale Molecular Methods in Applied Chemistry*; Kirchner, B., Vrabec, J., Eds.; Topics in Current Chemistry; Springer: Berlin, Heidelberg, 2012; pp 109–153. https://doi.org/10.1007/128_2011_195.

(94) Crabb, E.; France-Lanord, A.; Leverick, G.; Stephens, R.; Shao-Horn, Y.; Grossman, J. C. Importance of Equilibration Method and Sampling for *Ab Initio* Molecular Dynamics Simulations of Solvent–Lithium-Salt Systems in Lithium-Oxygen Batteries. *J. Chem. Theory Comput.* **2020**, *16* (12), 7255–7266. https://doi.org/10.1021/acs.jctc.0c00833.

(95) Leung, K.; Budzien, J. L. *Ab Initio* Molecular Dynamics Simulations of the Initial Stages of Solid–Electrolyte Interphase Formation on Lithium Ion Battery Graphitic Anodes. *Phys. Chem. Chem. Phys.* **2010**, *12* (25), 6583–6586. https://doi.org/10.1039/B925853A.

(96) Muralidharan, A.; Chaudhari, M. I.; Pratt, L. R.; Rempe, S. B. Molecular Dynamics of Lithium Ion Transport in a Model Solid Electrolyte Interphase. *Sci. Rep.* **2018**, *8* (1), 10736. https://doi.org/10.1038/s41598-018-28869-x.

(97) Petit, L.; Vuilleumier, R.; Maldivi, P.; Adamo, C. Ab Initio Molecular Dynamics Study of a Highly Concentrated LiCl Aqueous Solution. *J. Chem. Theory Comput.* **2008**, *4* (7), 1040–1048. https://doi.org/10.1021/ct800007v.

(98) Petit, L.; Vuilleumier, R.; Maldivi, P.; Adamo, C. Molecular Dynamics Study of the Coordination Sphere of Trivalent Lanthanum in a Highly Concentrated LiCl Aqueous

Solution: A Combined Classical and Ab Initio Approach. *J. Phys. Chem. B* **2008**, *112* (34), 10603–10607. https://doi.org/10.1021/jp8017106.

(99) Hassanali, A. A.; Cuny, J.; Verdolino, V.; Parrinello, M. Aqueous Solutions: State of the Art in *Ab Initio* Molecular Dynamics. *Philos. Trans. R. Soc. Math. Phys. Eng. Sci.* **2014**, *372* (2011), 20120482. https://doi.org/10.1098/rsta.2012.0482.

(100) Timko, J.; De Castro, A.; Kuyucak, S. *Ab Initio* Calculation of the Potential of Mean Force for Dissociation of Aqueous Ca–Cl. *J. Chem. Phys.* **2011**, *134* (20), 204510. https://doi.org/10.1063/1.3595261.

(101) Du, H.; Rasaiah, J. C.; Miller, J. D. Structural and Dynamic Properties of Concentrated Alkali Halide Solutions: A Molecular Dynamics Simulation Study. *J. Phys. Chem. B* **2007**, *111* (1), 209–217. https://doi.org/10.1021/jp064659o.

(102) Impey, R. W.; Madden, P. A.; McDonald, I. R. Hydration and Mobility of Ions in Solution. *J. Phys. Chem.* **1983**, *87* (25), 5071–5083. https://doi.org/10.1021/j150643a008.

(103) Horwitz, G.; Rodríguez, C.; Factorovich, M.; Corti, H. R. Maximum Electrical Conductivity of Associated Lithium Salts in Solvents for Lithium–Air Batteries. *J. Phys. Chem. C* **2019**, *123* (19), 12081–12087. https://doi.org/10.1021/acs.jpcc.9b00864.

(104) Kwabi, D. G.; Bryantsev, V. S.; Batcho, T. P.; Itkis, D. M.; Thompson, C. V.; Shao-Horn, Y. Experimental and Computational Analysis of the Solvent-Dependent O_2/Li^+-O_2^- Redox Couple: Standard Potentials, Coupling Strength, and Implications for Lithium–Oxygen Batteries. *Angew. Chem. Int. Ed.* **2016**, *55* (9), 3129–3134. https://doi.org/10.1002/anie.201509143.

(105) Martínez, J. M.; Martínez, L. Packing Optimization for Automated Generation of Complex System's Initial Configurations for Molecular Dynamics and Docking. *J. Comput. Chem.* **2003**, *24* (7), 819–825. https://doi.org/10.1002/jcc.10216.

(106) Martínez, L.; Andrade, R.; Birgin, E. G.; Martínez, J. M. PACKMOL: A package for building initial configurations for molecular dynamics simulations. *J. Comput. Chem.* **2009**, *30* (13), 2157–2164. https://doi.org/10.1002/jcc.21224.

(107) *MedeA–3.0 and MedeA–2.0*; Materials Design, Inc: San Diego, CA, 2017.

(108) *Fftool*; Padua Group, 2021.

(109) Molinari, N.; Mailoa, J. P.; Kozinsky, B. Effect of Salt Concentration on Ion Clustering and Transport in Polymer Solid Electrolytes: A Molecular Dynamics Study of PEO–LiTFSI. *Chem. Mater.* **2018**, *30* (18), 6298–6306. https://doi.org/10.1021/acs.chemmater.8b01955.

(110) Seo, D. M.; Borodin, O.; Han, S.-D.; Boyle, P. D.; Henderson, W. A. Electrolyte Solvation and Ionic Association II. Acetonitrile-Lithium Salt Mixtures: Highly Dissociated Salts. *J. Electrochem. Soc.* **2012**, *159* (9), A1489. https://doi.org/10.1149/2.035209jes.

(111) Blöchl, P. E. Projector Augmented-Wave Method. *Phys. Rev. B* **1994**, *50* (24), 17953–17979. https://doi.org/10.1103/PhysRevB.50.17953.

(112) Kresse, G.; Hafner, J. *Ab Initio* Molecular Dynamics for Liquid Metals. *Phys. Rev. B* **1993**, *47* (1), 558–561. https://doi.org/10.1103/PhysRevB.47.558.

(113) Kresse, G.; Hafner, J. *Ab Initio* Molecular-Dynamics Simulation of the Liquid-Metal–Amorphous-Semiconductor Transition in Germanium. *Phys. Rev. B* **1994**, *49* (20), 14251–14269. https://doi.org/10.1103/PhysRevB.49.14251.

(114) Kresse, G.; Furthmüller, J. Efficiency of Ab-Initio Total Energy Calculations for Metals and Semiconductors Using a Plane-Wave Basis Set. *Comput. Mater. Sci.* **1996**, *6* (1), 15–50. https://doi.org/10.1016/0927-0256(96)00008-0.

(115) Kresse, G.; Furthmüller, J. Efficient Iterative Schemes for *Ab Initio* Total-Energy Calculations Using a Plane-Wave Basis Set. *Phys. Rev. B* **1996**, *54* (16), 11169–11186. https://doi.org/10.1103/PhysRevB.54.11169.

(116) Kresse, G.; Joubert, D. From Ultrasoft Pseudopotentials to the Projector Augmented-Wave Method. *Phys. Rev. B* **1999**, *59* (3), 1758–1775. https://doi.org/10.1103/PhysRevB.59.1758.

(117) Grimme, S.; Antony, J.; Ehrlich, S.; Krieg, H. A Consistent and Accurate *Ab Initio* Parametrization of Density Functional Dispersion Correction (DFT-D) for the 94 Elements H-Pu. *J. Chem. Phys.* **2010**, *132* (15), 154104. https://doi.org/10.1063/1.3382344.

(118) Perdew, J. P.; Burke, K.; Ernzerhof, M. Generalized Gradient Approximation Made Simple. *Phys. Rev. Lett.* **1996**, *77* (18), 3865–3868. https://doi.org/10.1103/PhysRevLett.77.3865.

(119) Perdew, J. P.; Burke, K.; Ernzerhof, M. Generalized Gradient Approximation Made Simple [Phys. Rev. Lett. 77, 3865 (1996)]. *Phys. Rev. Lett.* **1997**, *78* (7), 1396–1396. https://doi.org/10.1103/PhysRevLett.78.1396.

(120) Lightstone, F. C.; Schwegler, E.; Hood, R. Q.; Gygi, F.; Galli, G. A First Principles Molecular Dynamics Simulation of the Hydrated Magnesium Ion. *Chem. Phys. Lett.* **2001**, *343* (5), 549–555. https://doi.org/10.1016/S0009-2614(01)00735-7.

(121) White, J. A.; Schwegler, E.; Galli, G.; Gygi, F. The Solvation of Na^+ in Water: First-Principles Simulations. *J. Chem. Phys.* **2000**, *113* (11), 4668–4673. https://doi.org/10.1063/1.1288688.

(122) Plimpton, S. Fast Parallel Algorithms for Short-Range Molecular Dynamics. *J. Comput. Phys.* **1995**, *117* (1), 1–19. https://doi.org/10.1006/jcph.1995.1039.

(123) Lightstone, F. C.; Schwegler, E.; Allesch, M.; Gygi, F.; Galli, G. A First-Principles Molecular Dynamics Study of Calcium in Water. *ChemPhysChem* **2005**, *6* (9), 1745–1749. https://doi.org/10.1002/cphc.200500053.

(124) Canongia Lopes, J. N.; Deschamps, J.; Pádua, A. A. H. Modeling Ionic Liquids Using a Systematic All-Atom Force Field. *J. Phys. Chem. B* **2004**, *108* (6), 2038–2047. https://doi.org/10.1021/jp0362133.

(125) Canongia Lopes, J. N.; Deschamps, J.; Pádua, A. A. H. Modeling Ionic Liquids Using a Systematic All-Atom Force Field. *J. Phys. Chem. B* **2004**, *108* (30), 11250–11250. https://doi.org/10.1021/jp0476996.

(126) Canongia Lopes, J. N.; Pádua, A. A. H. Molecular Force Field for Ionic Liquids Composed of Triflate or Bistriflylimide Anions. *J. Phys. Chem. B* **2004**, *108* (43), 16893–16898. https://doi.org/10.1021/jp0476545.

(127) Canongia Lopes, J. N.; Padua, A. A. H. Molecular Force Field for Ionic Liquids III: Imidazolium, Pyridinium, and Phosphonium Cations; Chloride, Bromide, and Dicyanamide Anions. *J. Phys. Chem. B* **2006**, *110* (39), 19586–19592. https://doi.org/10.1021/jp063901o.

(128) Canongia Lopes, J. N.; Pádua, A. A. H.; Shimizu, K. Molecular Force Field for Ionic Liquids IV: Trialkylimidazolium and Alkoxycarbonyl-Imidazolium Cations; Alkylsulfonate and Alkylsulfate Anions. *J. Phys. Chem. B* **2008**, *112* (16), 5039–5046. https://doi.org/10.1021/jp800281e.

(129) *CL&P Force Field for Ionic Liquids*; Padua Group, 2021.

(130) Shimizu, K.; Almantariotis, D.; Gomes, M. F. C.; Pádua, Agílio. A. H.; Canongia Lopes, J. N. Molecular Force Field for Ionic Liquids V: Hydroxyethylimidazolium, Dimethoxy-2-Methylimidazolium, and Fluoroalkylimidazolium Cations and Bis(Fluorosulfonyl)Amide, Perfluoroalkanesulfonylamide, and Fluoroalkylfluorophosphate Anions. *J. Phys. Chem. B* **2010**, *114* (10), 3592–3600. https://doi.org/10.1021/jp9120468.

(131) Tsuzuki, S.; Shinoda, W.; Matsugami, M.; Umebayashi, Y.; Ueno, K.; Mandai, T.; Seki, S.; Dokko, K.; Watanabe, M. Structures of [Li(Glyme)]$^+$ Complexes and Their Interactions with Anions in Equimolar Mixtures of Glymes and Li[TFSA]: Analysis by Molecular Dynamics Simulations. *Phys. Chem. Chem. Phys.* **2014**, *17* (1), 126–129. https://doi.org/10.1039/C4CP04718D.

(132) Humphrey, W.; Dalke, A.; Schulten, K. VMD: Visual Molecular Dynamics. *J. Mol. Graph.* **1996**, *14* (1), 33–38. https://doi.org/10.1016/0263-7855(96)00018-5.

(133) Kohlmeyer, A. *G(r) GUI Plugin*.

(134) Ballone, P.; Andreoni, W.; Car, R.; Parrinello, M. Equilibrium Structures and Finite Temperature Properties of Silicon Microclusters from *Ab Initio* Molecular-Dynamics Calculations. *Phys. Rev. Lett.* **1988**, *60* (4), 271–274. https://doi.org/10.1103/PhysRevLett.60.271.

(135) Tuckerman, M.; Laasonen, K.; Sprik, M.; Parrinello, M. *Ab Initio* Molecular Dynamics Simulation of the Solvation and Transport of Hydronium and Hydroxyl Ions in Water. *J. Chem. Phys.* **1995**, *103* (1), 150–161. https://doi.org/10.1063/1.469654.

(136) Brehm, M.; Kirchner, B. TRAVIS - A Free Analyzer and Visualizer for Monte Carlo and Molecular Dynamics Trajectories. *J. Chem. Inf. Model.* **2011**, *51* (8), 2007–2023. https://doi.org/10.1021/ci200217w.

(137) Chan, H.; Narayanan, B.; Cherukara, M. J.; Sen, F. G.; Sasikumar, K.; Gray, S. K.; Chan, M. K. Y.; Sankaranarayanan, S. K. R. S. Machine Learning Classical Interatomic Potentials for Molecular Dynamics from First-Principles Training Data. *J. Phys. Chem. C* **2019**, *123* (12), 6941–6957. https://doi.org/10.1021/acs.jpcc.8b09917.

(138) Gu, G. H.; Noh, J.; Kim, I.; Jung, Y. Machine Learning for Renewable Energy Materials. *J. Mater. Chem. A* **2019**, *7* (29), 17096–17117. https://doi.org/10.1039/C9TA02356A.

(139) Wang, J.; Olsson, S.; Wehmeyer, C.; Pérez, A.; Charron, N. E.; de Fabritiis, G.; Noé, F.; Clementi, C. Machine Learning of Coarse-Grained Molecular Dynamics Force Fields. *ACS Cent. Sci.* **2019**, *5* (5), 755–767. https://doi.org/10.1021/acscentsci.8b00913.

(140) Borodin, O.; Smith, G. Li$^+$ Transport Mechanism in Oligo(Ethylene Oxide)s Compared to Carbonates. *J. Solut. Chem.* **2007**, *36*, 803–813. https://doi.org/10.1007/s10953-007-9146-1.

(141) Bouchet, R.; Lascaud, S.; Rosso, M. An EIS Study of the Anode Li/PEO-LiTFSI of a Li Polymer Battery. *J. Electrochem. Soc.* **2003**, *150* (10), A1385. https://doi.org/10.1149/1.1609997.

(142) Parimalam, B. S.; Lucht, B. L. Reduction Reactions of Electrolyte Salts for Lithium Ion Batteries: LiPF$_6$, LiBF$_4$, LiDFOB, LiBOB, and LiTFSI. *J. Electrochem. Soc.* **2018**, *165* (2), A251. https://doi.org/10.1149/2.0901802jes.

(143) Hu, J. J.; Long, G. K.; Liu, S.; Li, G. R.; Gao, X. P. A LiFSI–LiTFSI Binary-Salt Electrolyte to Achieve High Capacity and Cycle Stability for a Li–S Battery. *Chem. Commun.* **2014**, *50* (93), 14647–14650. https://doi.org/10.1039/C4CC06666A.

(144) Thompson, A. P.; Aktulga, H. M.; Berger, R.; Bolintineanu, D. S.; Brown, W. M.; Crozier, P. S.; in 't Veld, P. J.; Kohlmeyer, A.; Moore, S. G.; Nguyen, T. D.; Shan, R.; Stevens, M. J.; Tranchida, J.; Trott, C.; Plimpton, S. J. LAMMPS - a Flexible Simulation Tool for Particle-Based Materials Modeling at the Atomic, Meso, and Continuum Scales. *Comput. Phys. Commun.* **2022**, *271*, 108171. https://doi.org/10.1016/j.cpc.2021.108171.

(145) Mukherji, S.; Avula, N. V. S.; Balasubramanian, S. Refined Force Field for Liquid Sulfolane with Particular Emphasis to Its Transport Characteristics. *ACS Omega* **2020**, *5* (43), 28285–28295. https://doi.org/10.1021/acsomega.0c04243.

(146) William L. Jorgensen Research Group - OPLS-AA/M for Proteins http://zarbi.chem.yale.edu/oplsaam.html.

(147) Humbert, M. T.; Zhang, Y.; Maginn, E. J. PyLAT: Python LAMMPS Analysis Tools. *J. Chem. Inf. Model.* **2019**, *59* (4), 1301–1305. https://doi.org/10.1021/acs.jcim.9b00066.

(148) *PyLAT*; Maginn Research Group, 2022.

(149) France-Lanord, A.; Grossman, J. C. Correlations from Ion Pairing and the Nernst-Einstein Equation. *Phys. Rev. Lett.* **2019**, *122* (13), 136001. https://doi.org/10.1103/PhysRevLett.122.136001.

(150) Borodin, O.; Smith, G. D. LiTFSI Structure and Transport in Ethylene Carbonate from Molecular Dynamics Simulations. *J. Phys. Chem. B* **2006**, *110* (10), 4971–4977. https://doi.org/10.1021/jp056249q.

(151) Olsher, Uriel.; Izatt, R. M.; Bradshaw, J. S.; Dalley, N. Kent. Coordination Chemistry of Lithium Ion: A Crystal and Molecular Structure Review. *Chem. Rev.* **1991**, *91* (2), 137–164. https://doi.org/10.1021/cr00002a003.

(152) Brouillette, D.; Irish, D. E.; Taylor, N. J.; Perron, G.; Odziemkowski, M.; Desnoyers, J. E. Stable Solvates in Solution of Lithium Bis(Trifluoromethylsulfone)Imide in Glymes and Other Aprotic Solvents: Phase Diagrams, Crystallography and Raman Spectroscopy. *Phys. Chem. Chem. Phys.* **2002**, *4* (24), 6063–6071. https://doi.org/10.1039/B203776A.

(153) Gutmann Acceptor and Donor Number http://www.stenutz.eu/chem/solv21.php.

(154) Sekhon, S. S.; Arora, N.; Singh, H. P. Effect of Donor Number of Solvent on the Conductivity Behaviour of Nonaqueous Proton-Conducting Polymer Gel Electrolytes. *Solid State Ion.* **2003**, *160* (3), 301–307. https://doi.org/10.1016/S0167-2738(03)00167-X.

(155) Towns, J.; Cockerill, T.; Dahan, M.; Foster, I.; Gaither, K.; Grimshaw, A.; Hazlewood, V.; Lathrop, S.; Lifka, D.; Peterson, G. D.; Roskies, R.; Scott, J. R.; Wilkins-Diehr, N. XSEDE: Accelerating Scientific Discovery. *Comput. Sci. Eng.* **2014**, *16* (5), 62–74. https://doi.org/10.1109/MCSE.2014.80.